

**EFFECTS OF WEATHERING ON THE SURFACE AND CHEMICAL
PROPERTIES OF CHRYSOTILE ASBESTOS: IMPLICATIONS FOR
MANAGEMENT OF NATURALLY OCCURRING ASBESTOS AND
CARBON DIOXIDE SEQUESTRATION IN ULTRAMAFIC MINE
TAILINGS**

by

Emma Holmes

B.Sc., The University of British Columbia, 2010

A THESIS SUBMITTED IN PARTIAL FULFILLMENT OF
THE REQUIREMENTS FOR THE DEGREE OF

MASTER OF SCIENCE

in

THE FACULTY OF GRADUATE STUDIES

(Soil Science)

THE UNIVERSITY OF BRITISH COLUMBIA
(Vancouver)

November, 2012

© Emma Holmes, 2012

Abstract

This study focuses on the surface properties of chrysotile asbestos and the effects that naturally occurring acids and different environments, specifically stream and mine tailing environments, have in altering the surface chemistry. Surface reactions are likely the governing factors affecting chrysotile, both as a toxicant and as a carbon sequestration material. This information is important for concerns related to naturally occurring chrysotile asbestos in the environment and carbon dioxide sequestration in chrysotile tailings. FESEM, XRD, ATR FTIR, zeta potential, aqua regia digestion, ICP-MS, and ToF-SIMS were used to examine the bulk and surface properties of chrysotile asbestos. Oxalic acid and hydrochloric acid are effective at removing the magnesium brucite layer, and associated trace metals, and reducing the surface charge of chrysotile asbestos. Fibers treated with these acids are likely less hazardous from a human health perspective. Carbonic acid, a weaker acid, is much less effective at altering the surface properties of chrysotile. Natural weathering in stream and mine tailing environments altered the surface properties of chrysotile asbestos, but the extent remains unknown. It appears that the slow dissolution of magnesium is the rate-limiting step for the mineral carbonation process. The results of zeta potential analysis, a surface specific technique measured on a bulk sample, are supported by ToF-SIMS analysis, a very fine scale surface specific technique measuring a small area of one fiber. Zeta potential analysis is less expensive and time consuming to carry out than is ToF-SIMS and measures the surface characteristics of a larger sample which enables it to better account for the variability within a sample. Covering naturally occurring asbestos deposits with acid producing organic matter could enhance the weathering of chrysotile and likely reduce its toxicity over time, while also acting as a barrier, preventing the fibers from becoming airborne and posing an inhalation hazard. Treating chrysotile mine tailings with naturally occurring acids will release more magnesium, potentially increasing the rate of carbon sequestration.

Preface

This work is composed of four body chapters. A version of chapter 2 has been published. Holmes, Wilson, Schreier, and Lavkulich (2010). Processes affecting surface and chemical properties of chrysotile: Implications for reclamation of asbestos in the natural environment. *Canadian Journal of Soil Science*. 92:229-242. I conducted the research discussed in chapter 2 occurring after 2009 and wrote most of the manuscript. Analysis was done with the assistance of Julie Wilson, Maureen Soon, Mary Fletcher, Hans Schreier, and Les Lavkulich. Samples prior to 2009 were collected by Drs. Hans Schreier and Les Lavkulich.

Chapters 3, 4, and 5 were initiated and supervised by Drs. Les Lavkulich and Gregory Dipple. Sumas watershed suspended sediment samples were collected by Drs. Les Lavkulich and Hans Schreier. Cassiar mine tailings were collected by Dr. Gregory M. Dipple. XRD analysis was done with the assistance of Dr. Mati Raudsepp and Jenny Lai. Zeta Potential was performed by Beini Xu. ToF-SIMS was performed by Drs. Tae Kyong John Kim and Philip Wong. Sally Finora assisted with ATR FTIR analysis. Maureen Soon assisted with ICP-MS, and Derrick Horne assisted with FESEM.

Table of Contents

Abstract.....	i
Preface.....	ii
Table of Contents	iii
List of Figures.....	v
List of Tables	viii
List of Abbreviations	x
List of Symbols	xi
Acknowledgements	xiii
Dedication	xv
Chapter 1 : Introduction	1
1.1 Study Overview	1
1.2 Chrysotile Asbestos	2
1.3 Asbestos	4
1.4 Health Effects of Asbestos	5
1.5 Naturally Occurring Asbestos	8
1.6 Strategies for Reducing the Toxicant Effect of NOA.....	9
1.7 Atmospheric CO ₂ Sequestration Using Chrysotile Mine Tailings	10
1.8 Serpentine Dissolution	11
1.9 Objectives.....	13
1.10 Site Descriptions.....	13
Chapter 2 : Long-term rock and sediment analysis in the Sumas River Watershed, including acid treatment of asbestos contaminated sediment and soil to simulate natural processes.....	18
2.1 Introduction	18
2.2 Sampling Locations.....	18
2.3 Materials and Methods	19
2.4 Results and Discussion.....	21
2.5 Conclusions	29
Chapter 3 : The Effect of Simple Organic Acids on the Bulk and Surface Properties of Chrysotile Asbestos	31

3.1	Introduction	31
3.2	Materials and Methods	31
3.3	Results and Discussion	34
3.4	Conclusions	57
Chapter 4 : Bulk and Surface Properties of Environmentally Exposed Chrysotile Samples		58
4.1	Introduction	58
4.2	Materials and Methods	58
4.3	Results and Discussion	62
4.4	Conclusions	78
Chapter 5 : Conclusions and Recommendations		79
References		81
Appendix		88

List of Figures

Figure 1.1. Diagram of the structure of chrysotile formed of several scrolls. Each scroll consists of a connected double layer made up of brucite-like units on the outer surface and silicate tetrahedra units in the inner surface. Taken from Crummet (2005).	3
Figure 1.2. FESEM image of chrysotile bundles magnified 3000 times.	4
Figure 1.3. Number of discharge events greater than $15\text{m}^3/\text{sec}$ by decades for the Sumas River (adapted from Holmes et al. 2012).	14
Figure 1.4. Location of the Sumas River watershed.	15
Figure 1.5. Left: Location of Cassiar, BC with Prince George as a reference point (UNBC). Right: The tailings pile at Cassiar mine (Wilson 2005).	16
Figure 2.1 Map of the Sumas River watershed including sediment sampling stations.	19
Figure 2.2. Total Ni in Sumas River fine bed sediments collected in 1993, 1994, and 2009. 23	
Figure 2.3. Total Cr in Sumas River fine bed sediments collected in 1993, 1994, and 2009. 24	
Figure 3.1. FESEM image depicting a bundle of untreated chrysotile fibers magnified 3000X.	41
Figure 3.2. FESEM image depicting a bundle of carbonic acid treated chrysotile fibers magnified 3000X.	42
Figure 3.3. FESEM image depicting a bundle of hydrochloric acid treated chrysotile fibers magnified 3000X.	43

Figure 3.4. FESEM image depicting a bundle of oxalic acid treated chrysotile fibers magnified 3000X.	44
Figure 3.5. Zeta Potential values for untreated and acid treated chrysotile samples. Error bars represent standard deviation values. (n=5).	45
Figure 3.6. The Mg:Si of untreated and acid treated chrysotile fibers. Error bars represent the standard deviation. (n=5). No standard deviation data for oxalic acid treated fibers.	48
Figure 3.7. ToF-SIMS image of the surface area (=1600 μ m ² ; X=400 μ m, Y=400 μ m) of an untreated fiber. Green = Mg, Blue =Si, and Red = Al.	49
Figure 3.8. ToF-SIMS image of the depth view of an untreated chrysotile fiber. Surface area = 1600 μ m ² ; X=400 μ m, Y=400 μ m and depth of analysis (Z) is 2 nm. The Z axis is blown up ~ 10,000X to make features visible. Green = Mg, Blue = Si, and Red = Al.	50
Figure 3.9. ToF-SIMS images of the magnesium and silica ions on the surface of the untreated and acid treated chrysotile fibers. Surface area = 1600 μ m ² ; X=400 μ m, Y=400 μ m and depth of analysis (Z) is 2 nm.	51
Figure 3.10. Mg:Si vs. Zeta Potential for untreated and acid treated chrysotile fibers. Error bars represent standard deviation for Mg:Si and Zeta Potential. (n=5). No Mg:Si standard deviation data for the oxalic acid treatment.	53
Figure 3.11. Mg (ppm) of the bulk mineral after acid treatment vs. Mg:Si for untreated and acid treated chrysotile fibers. Error bars represent standard deviation of the Mg:Si values. (n=5). No Mg:Si standard deviation data for the oxalic acid treatment.	54
Figure 3.12. Mg (ppm) vs. Zeta Potential for untreated and acid treated chrysotile fibers. Error bars represent standard deviation of the Zeta Potential values. (n=5).	55

Figure 3.13. pH vs. Mg:Si for untreated and acid treated chrysotile fibers. Error bars represent standard deviation of the Mg:Si values. (n=5). No Mg:Si standard deviation data for the oxalic acid treatment. 56

Figure 4.1. Map of Sumas River Watershed, including sampling sites..... 59

Figure 4.2. ToF-SIMS images of the magnesium and silica ions on the surface of the chrysotile fibers found in suspended sediment from the Sumas River watershed. Surface area = $1600 \mu\text{m}^2$; X=400 μm , Y=400 μm and depth of analysis (Z) is 2 nm..... 71

Figure 4.3. ToF-SIMS images of the magnesium and silica ions on the surface of chrysotile fibers from Cassiar mine tailings. Surface area = $1600 \mu\text{m}^2$; X=400 μm , Y=400 μm and depth of analysis (Z) is 2 nm..... 72

Figure 4.4. Mg:Si vs. Zeta Potential for suspended sediment samples from the Sumas River watershed and mine tailing samples from Cassiar, BC. Error bars represent standard deviation for Mg:Si and Zeta Potential values. (n=5)..... 74

Figure 4.5. Mg (ppm) vs. Mg:Si for suspended sediment samples from the Sumas River watershed and mine tailing samples from Cassiar mine, BC. Error bars represent standard deviation for Mg:Si values. (n=5)..... 75

Figure 4.6. Mg (ppm) vs. Zeta Potential for suspended sediment samples from the Sumas River watershed and mine tailing samples from Cassiar mine, BC. Error bars represent standard deviation for Zeta Potential values. (n=5)..... 76

Figure 4.7. pH vs. Mg:Si for suspended sediment samples from the Sumas River watershed and mine tailing samples from Cassiar, BC. Error bars represent standard deviation for Mg:Si values. (n=5). 77

List of Tables

Table 2.1. Average percentage and concentration of metals in serpentine bedrock and Sumas River sediments (HF digestion).	22
Table 2.2. Total recoverable metal concentrations in sediments and soils from the Sumas River watershed (aqua regia digestion). (n=2).....	25
Table 2.3. Total metal concentrations extracted from soil and sediment samples taken from the Sumas River watershed after treatment with different organic acid (n=2).	28
Table 3.1. Summary of XRD peaks for untreated and acid treated chrysotile samples. M=major peak, Mi=minor peak (<50% major peak), and T=trace peak (<10% major peak).35	
Table 3.2. Summary of ATR-FTIR spectra for untreated and acid treated chrysotile fibers. 37	
Table 3.3. Summary of the ICP elemental analysis data for untreated digested chrysotile and the effluent from chrysotile acid treatments. (bdl = below detection limit). (n=2).	39
Table 4.1. Summary of XRD peaks for suspended sediment samples from the Sumas River watershed and mine tailings from Cassiar, BC. M = major peak, Mi = minor peak (<50 % of major peak), and T = trace (<10 % major peak).	63
Table 4.2. Summary of ATR-FTIR spectra for Swift Creek suspended sediment from the Sumas River watershed and mine tailings from Cassiar, BC.	65
Table 4.3. Summary of the ICP elemental analysis data for suspended sediment samples from the Sumas River watershed and mine tailings from Cassiar, BC.	67

Table 4.4. Comparison of the Zeta Potential and Mg:Si values of the suspended sediment, mine tailing, and acid treated chrysotile samples. Standard deviation values are provided. (n=5). (nd = no data). 69

List of Abbreviations

ATR FTIR	Attenuated Total Reflectance Fourier Transform Infrared
BC	British Columbia
FESEM	Field Emission Scanning Electron Microscope
ICP-MS	Inductively Coupled Plasma Mass Spectroscopy
NOA	Naturally Occurring Asbestos
NOM	Natural Organic Matter
US EPA	United States Environmental Protection Agency
ToF-SIMS	Time of Flight Secondary Ion Mass Spectroscopy
XRD	X-Ray Diffraction

List of Symbols

Al	Aluminum
Ap	A soil mineral surface layer that has been disturbed by human activities
Bm	A soil mineral layer that is characterized by having little development.
CH ₃ ⁺	Methene
cm	Centimeter
Co	Cobalt
CO ₂	Carbon dioxide
CO ₃	Carbonate
Cr	Chromium
eV	Electron volt
H	Hydrogen
H ₂ O	Water
HCl	Hydrochloric acid
HF	Hydroflouric acid
HNO ₃	Nitric acid
g	grams
KeV	Kilo-electron volt
Kg	Kilogram
Kj	Kilojoule
Km	Kilometer
KRS5	Thallium Bromoiodide
Kv	Killivolt
m	Meter
mA	Milliampere
Mg	Milligram
Mg:Si	Magnesium to silica ratio
mL	Millilitres
Mol	Moles
MT	Million tonnes
nA	Nanoampere

Ni	Nickel
nm	Nanometers
O	Oxygen
OH ⁻	Hydroxide
pKa	Acid dissociation constant
ppm	Parts per million
s	Seconds
Si	Silica
μm	Micrometer
IICb	A soil mineral parent material horizon that has been buried under more recent depositions

Acknowledgements

This research was funded by a Natural Sciences and Engineering Research Council of Canada Alexander Graham Bell Canada Graduate Scholarship.

I would like to thank Dr. Les Lavkulich for his endless encouragement and support. Your mentorship has been invaluable to me. Thank-you Dr. Greg Dipple and Dr. Hans Schreier for all your help while serving on my graduate committee.

Thank you to Maja Krzic and Sandra Brown for integrating me into the soil science community and providing me with so much support. Thank-you Mati Raudsepp, Maureen Soon, Sally Finora, Mary Fletcher, Jenny Lai, John Kim, Philip Wong, Beini Xu, Trudy Naugler and Derrick Horne for your assistance with lab work and analysis.

Thanks to all my fellow students and friends who assisted and supported me on my academic journey: Dru Yates, I feel so privileged to have had you as a classmate and friend over the years. Anna Harrison, without your generous help, excel and/or phreeqci frustration might have killed me. Thanks for saving me on so many occasions! Melissa Iverson, your example, support, and encouragement has been invaluable. Julie Wilson, thank-you for all your support and help with sampling and analysis. Greg Rekken and Alisha Hackinen, thank-you for the motivational meetings and friendship breaks. Silja Hundt, thank-you so much for helping me with my figures. Jeff Anderson and Christian Evans, thank-you for being soil nerds. Gladys Oka, Lis as, and Manuela Hayn, thank-you for your help in the lab. Thank you Julia Maddison for the nerdy conversations. Jess Sloss and Jess Banning, thank you for living with me while I worked on this thesis, and for talking me off various ledges on various occasions. Finally a big thank you to: Cassandra Van Dyck, Kate Douglas, Kristine and Bob Ferris, Steve Morrison, Marc Shutzbank, Camil Dumont, Amanda Lenhardt, Amanda Mathys, Danny Seeton, Molly Campbell, and Val Castellanos,

A big big thank you to my family. Mom and Dad, this would not have been possible without your belief in me. I can never thank you enough for your overwhelming financial and loving

support that enabled me to figure out what I want to be when I grow up, and take the steps to achieve it. Rob, Ellie, and Tristan Holmes – thank-you for being the best siblings in the world. Katie Holmes, thank-you for feeding and clothing your poor student cousin. Thanks to the rest of my large and loving family who has been so supportive over the years: Jill, Denny, Brett, and Derek Lowes, Anne, Mike, Meghan, and Douglas Leary; Kim, Heather, and Allison Harker; Mike, Jan, Jill, Peter, Doris, and Brian Holmes; Bob, Peggy, Jan, Al, Kate, and James Galbraith.

Dedication

This thesis is dedicated to Doris Holmes. Much love.

Chapter 1 : Introduction

1.1 Study Overview

Chrysotile is an asbestiform serpentine mineral with more than 3000 industrial applications (Choi & Smith 1972). As a result, it has been mined and utilized extensively. Major health issues such as lung cancer, mesothelioma, and asbestosis are associated with occupational exposure to chrysotile asbestos (LaDou et al. 2010). More recently, environmental exposure to chrysotile fibers is being realized as a potential health threat (Favero-Longo et al. 2009), but not much is known about the toxicity of naturally occurring asbestos (NOA).

A more positive aspect of chrysotile is that, along with other magnesium silicate minerals, it naturally sequesters atmospheric CO₂ and offers a significant capacity to permanently store CO₂ in an environmentally benign and geologically stable form. As a result of fine grain size, chrysotile mine tailings undergo accelerated weathering, increasing their ability to sequester carbon. This has made chrysotile mine tailings a natural choice of study for researchers interested in accelerating the natural mineral carbonation processes in order to reduce the concentration of green house gases in the atmosphere and combat the effects of climate change.

Chrysotile changes chemically when exposed to environments that are oxidizing and at standard earth surface temperatures and pressures, in the presence of water, and in an atmosphere with elevated CO₂ levels (White & Brantley 1995). These weathering reactions and chemical alterations are surface driven. Understanding the processes that occur to these minerals and the changes in surface composition provides the basis of predicting the reaction processes and rates of change during weathering. This information is important for a range of considerations, including concerns related to naturally occurring chrysotile asbestos in the environment and carbon dioxide sequestration in chrysotile tailings.

This study focuses on the surface properties of chrysotile asbestos and the effects that environmental agents have in altering the surface chemistry. I explored the effects of bio-geomorphic weathering on chrysotile fibers by simulating these weathering processes in the laboratory with simple acids, and examining the effects of in-situ weathering in

streams and mine tailing. I used X-Ray Diffraction (XRD) to determine mineral composition, Field Emission Scanning Electron Microscopy (FESEM) for surface imaging, Zeta potential for surface charge determination, Aqua Regia and Inductively Coupled Plasma Mass Spectrometry (ICP-MS) for bulk total elemental analysis, Attenuated Total Reflectance Fourier Transform Infrared Spectroscopy (ATR FTIR) for surficial elemental analysis, and Time of Flight Secondary Ion Mass Spectrometry (ToF-SIMS) for surficial chemical analysis.

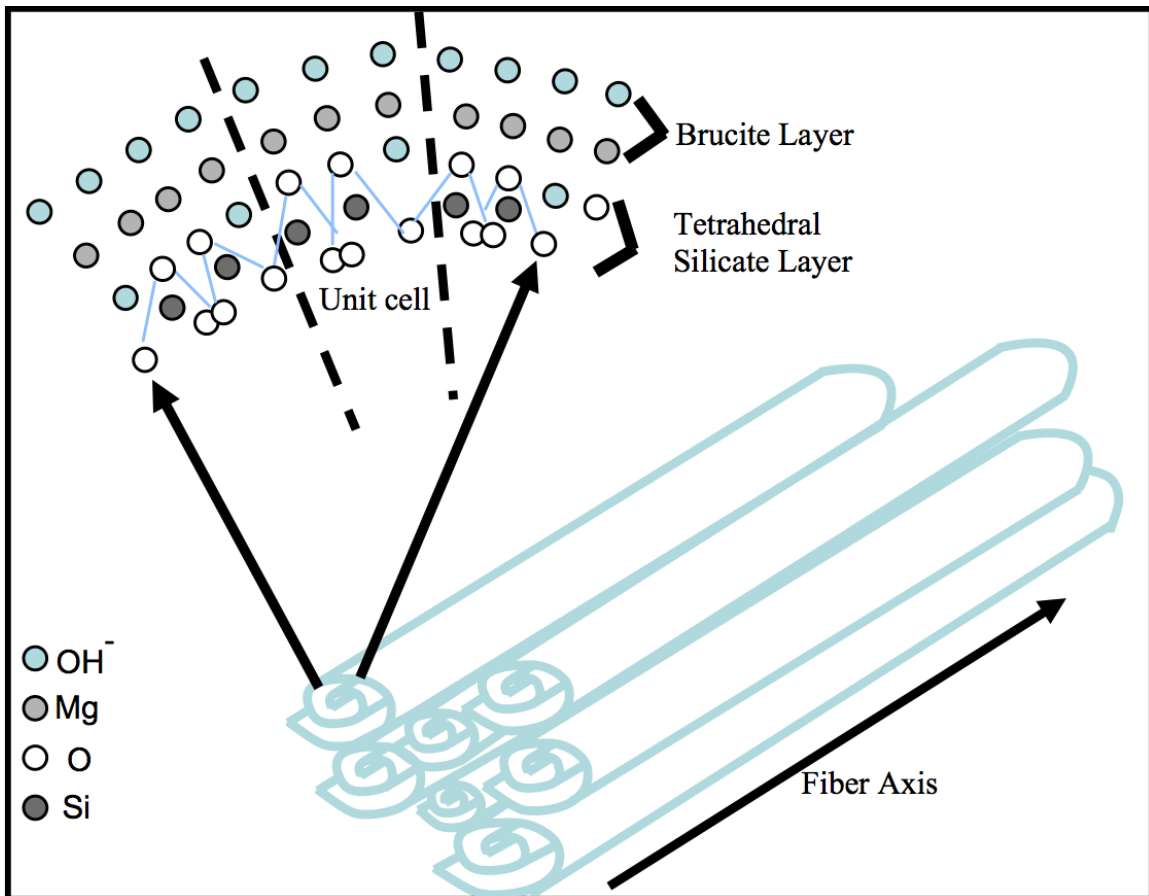
1.2 Chrysotile Asbestos

Chrysotile is a fibrous silicate mineral in the serpentine group. Serpentine rocks are formed by the reaction of ultramafic minerals with water near the earth's surface. Serpentine rocks are distributed globally and occur on all continents (Roberts & Proctor 1991). They are easily weathered, have a low hardness of 3.5-5.5 (Moh's scale), and thus are fairly soft and malleable. The three serpentine polymorphs; antigorite, lizardite, and chrysotile, share the same general chemical formula of $Mg_3(Si_2O_5)(OH)_4$ and a 1:1 silicate structure, composed of one silicate layer and one octahedral layer. The silicate layer is a hexagonal net of silicon-oxygen tetrahedral, in which three of the four ions are linked. The other layer is a brucite octahedral layer dominated with magnesium ions. Each magnesium ion is in coordination with four hydroxides and two oxides. Three hydroxides lie on the particle surface, while the fourth hydroxide lies below the surface with the two oxides that form the apices of the underlying silica tetrahedral (Bales 1984). Each layer is electrically neutral and adjacent layers are held together by van der Waals forces (Klein & Hurlbut 1977) and possibly hydrogen bonding (Bales 1984).

Lizardite and antigorite display a planar, non asbestos, structure. In chrysotile, heavy metals, such as chromium, nickel, iron, and cobalt can occur as substitutional cations for magnesium in the octahedral layer (Morgan 1997). As a result, the b axis of the octahedral sheet is much larger than the b axis in the tetrahedral sheet (Ross et al. 2008), resulting in the larger octahedral brucite sheet curling over the smaller tetrahedral sheet, thus generating the characteristic tubular morphology of asbestos (Cheshire & Guven 2005) (Mizukami et al. 2007). Chrysotile fibers can be thought of as about 40

layers of alternating brucite and silica tetrahedral units that roll up into concentric tubes (Bales 1984) as illustrated in Figure 1.1.

Figure 1.1. Diagram of the structure of chrysotile formed of several scrolls. Each scroll consists of a connected double layer made up of brucite-like units on the outer surface and silicate tetrahedra units in the inner surface. Taken from Crummet (2005).



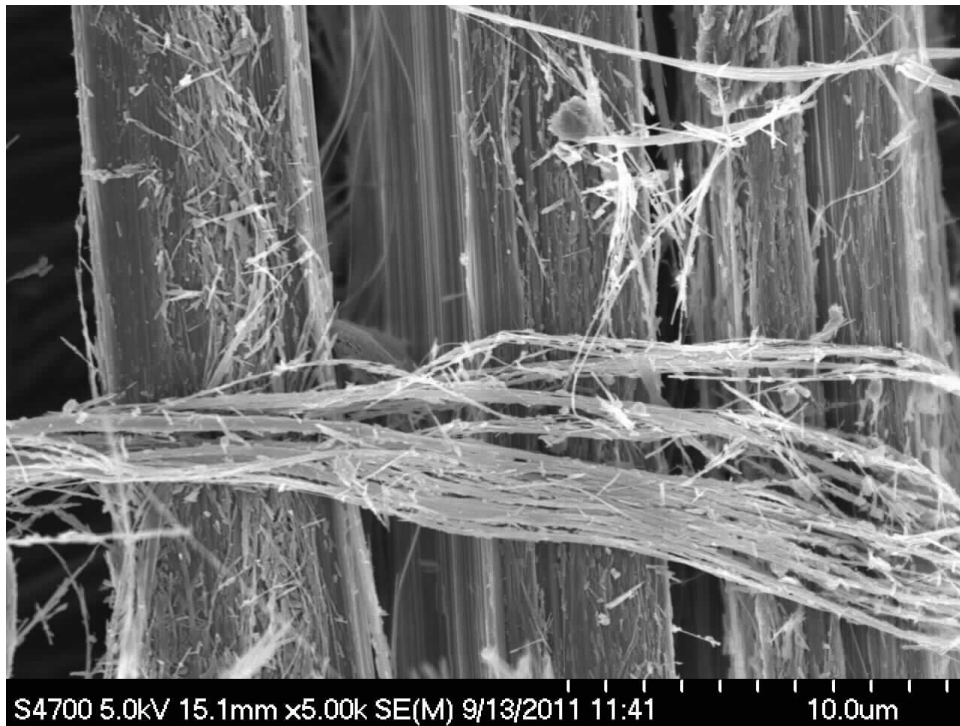
The tubular diameter of chrysotile is 2-30 nm, the length is 200 nm-2 μm (Yang 2010), and the radius of the hollow center is 2.5-4 nm (Titulaer et al. 1993). In addition to the common central capillary in each fibril, the spaces between adjacent fibrils may either be voids (channels) or partially filled channels. The filling material is a non-crystalline hydrated magnesium silicate (Langer & Nolan 1994). The brucite layer is approximately 0.48nm thick (Braterman et al. 2004) and the silica tetrahedral layer is approximately

1nm thick (Titulaer et al. 1993). The external surface of chrysotile is typically the magnesium octahedral layer.

1.3 Asbestos

Asbestiform minerals have a morphologic form or habit of crystallization as polyfilamentous fiber bundles (Figure 1.2). They are a particularly rare form of fibrous mineral because most minerals crystallize in more isometric shapes. Asbestos is the term used to describe a group of six commercial minerals that have an asbestiform habit that imparts the following properties: long fibrous shape, high tensile strength, low thermal electrical conductivity, high absorbency, high mechanical stability, resistance to acids and bases (Ross et al. 2008).

Figure 1.2. FESEM image of chrysotile bundles magnified 3000 times.



Chrysotile, the only serpentine form of asbestos, is the most abundant making up 90 – 95 % of commercial asbestos. It is the only phyllosilicate (layered silicate) mineral characterized by repeating magnesium and silicon layers that roll up into a tube. The

other five types of asbestos belong to the amphibole group: amosite, crocidolite, anthophyllite, tremolite, and actinolite. These forms of asbestos are inosilicates (chain silicates) that form repeating chains made up of silica and oxides of iron, magnesium, calcium, and sodium (Bales 1984). Non-asbestos forms of these minerals exist that lack both the desirable industrial properties and the toxicant effect. Each form of asbestos can be distinguished from one another by their chemical composition and structure. Other asbestiform minerals exist, but rarely occur in sufficient abundance to be of commercial importance (Ross et al. 2008).

Asbestos use in human cultures has been dated back to 2500 BC. Its early uses were for strengthening materials, such as ceramics. In the late 19th century, the total world production of asbestos was fairly low at approximately 25,000 metric tons (Ross 1981). At this time, asbestos was becoming increasingly popular because its unique properties provided the insulation required for steam technology. This led to the formation of an international asbestos trading company, the reopening of existing asbestos mines in Italy, and the exploitation of chrysotile mines in Canada. The supply was vast, and new uses of asbestos were developed to take advantage of its strength, heat resistance, and flexibility (Virta 2006). Cumulative worldwide production reached 181 million metric tons in 2003 (Virta 2006).

1.4 Health Effects of Asbestos

It is generally accepted by the scientific community that the inhalation of asbestos fibers is a human health hazard that can result in lung cancer, asbestosis - a chronic inflammatory disease affecting the lungs, and mesothelioma - a highly fatal cancer of the chest cavity (LaDou et al. 2010). However, the specific mechanism that results in the toxic effect of asbestos, and the differences in toxicity among different types of asbestos, is heavily debated in the scientific literature.

Size, shape and surface area of fibers have long been linked to the toxic effect of asbestos (Ross 1981). The fibrous shape of asbestos allows it to bypass the filtration system that prevents non-fibrous particles from entering the lung. The smaller the fiber, the greater the surface area and thus potential for surface reactivity. However, fibers

smaller than 5 nm are cleared at a similar rate as non-fibrous fibers and likely present little to no risk to human health (ATSDR 2003)

The role of asbestos surface properties in initiating negative health effects in animals and the environment has become increasingly recognized (Bernstein & Hoskins 2006; Favero-Longo et al. 2009; Fubini et al. 1997). Biopersistence, as well as surface chemistry, surface reactivity, surface charge, exposure of crystal planes, and surface coating are all related to asbestos fiber toxicology (Oberdörster et al. 2007). The potential for carcinogenicity depends on the type of asbestos in question and its specific biopersistence in the environment and the lung, as well as surface composition and charge.

Chrysotile is much less ecopersistent than other types of asbestos. Dilute acids remove the soluble brucite layer and eventually destroy the fibrous structure (Langer & Nolan 1994). Chrysotile has a short half-life of 0.3 – 11 days in the lung and thus rapidly alters and is cleared from the lung (Bernstein & Hoskins 2006). The half-life of amphibole asbestos fibers in the lung is 500 to infinite days, causing it be cleared from the lung much more slowly than chrysotile (Bernstein & Hoskins 2006).

The non-fibrous silica dust that is produced from chrysotile dissolution can be cleared by lung mechanisms. However, like any mineral dust, high concentrations of chronic exposure can interfere with the lungs clearance mechanism and result in disease or cancer. Chronic inhalation of silica leads to silicosis (Gilberti et al. 2008).

There is considerable evidence suggesting trace metals play an active role in asbestos related cancer development (Dixon et al. 1970; Foresti et al. 2009). Fenton activity associated with iron and other transition metals such as chromium, results in the generation of highly reactive hydroxyl radicals (Prousek 2007) which are correlated with asbestos pathogenicity (Turci et al. 2007). Chrysotile in particular contains relatively large amounts of nickel, chromium, and iron. Studies have shown that the toxicity of chrysotile fibers is removed when greater than 80 % of magnesium is removed (Monchaux et al. 1981). Heavy metals, such as iron and chromium, substitute for magnesium in the brucite layer. Thus, the loss of negative health effects after magnesium leaching could be because these metals are removed along with the magnesium brucite layer. Turcie (et al. 2007) inactivated the surface of chrysotile asbestos by modifying the

coordinate state of iron through substantial removal of magnesium ions, resulting in significant reduction of Fenton reactivity.

Toxicity of solids is not predictable from chemical composition and structure alone due to surface reactivity, which determines the reactions at the particle – biological medium interface. Due to incongruent dissolution, surface transition metals, and adsorption of toxicants, such as polyaromatic hydrocarbon on to the fiber surfaces, fibers can have several surface sites with very different chemical properties (Fubini et al. 1997).

Surface charge, as measured by zeta potential, is an important determinant of asbestos toxicity (Mossman 1983). Light & Wei (1977) found that surface charge is directly related to hemolytic, or cell killing, activity of fibers. The greater the positive charge, the greater the fiber toxicity. Mossman (1983) found that asbestos induced cell damage is initiated at the plasma membrane and fiber surface and that for certain interactions the reactivity is related to surface charge. Surface reactivity contributes to the health effects of fibers, due to the production of reactive oxygen species and reactive nitrogen species. As well, the fibers ability to adsorb biological molecules also affects its toxicity (Jaurand et al. 2009). Surface charge is correlated with surface composition. Unweathered fibers with the brucite layer intact typically have a positive surface charge, while weathered fibers with a silica dominated surface have a negative surface charge (Bales 1984).

Chrysotile makes up approximately 95 % the worlds' asbestos product (Mossman 1983), and thus, it seems likely that it is the reason for the majority of the negative health effects related to asbestos inhalation, despite its low ecopersistence in both the environment and lungs. A study that supports this theory, conducted by Dement & Brown (1994) found that the highest risks of asbestos-related lung cancer was observed in a textile manufacturing industry in which 100 % chrysotile was used.

However, the amphibole hypothesis puts forth the idea that minor amphibole contamination present in some forms of chrysotile could be the cause of disease and cancer experienced by chrysotile mine workers and their families. In population studies, the percentage of chrysotile fibers found in lungs has been surprisingly low considering chrysotile is the major source of asbestos exposure for the general population (Pooley 1976). Forty-seven workers employed in the Canadian chrysotile mining industries had

nearly equal concentrations of chrysotile fibers and tremolite fibers in their lungs, despite much higher exposure to chrysotile (Rowlands et al. 1982). Stayner (et al. 1996) conducted lung burden studies and found no convincing evidence to support the amphibole hypothesis. Toxicological and epidemiologic studies provided strong evidence that chrysotile is associated with an increased risk of lung cancer and mesothelioma (Stayner et al. 1996). Smith and Wright (1996) found no evidence that chrysotile is less hazardous than amphibole, although there is still scientific support of the amphibole hypothesis (Langer and Nolan 1997; Mossman and Gee 1990). Cyphert et al. (2012) found that in rats, chrysotile asbestos from the Sumas River watershed in Washington was more toxic than amphibole asbestos from Libby, Montana.

It is important to note that there appears to be no increased cancer risk associated with ingestion of asbestos into the gastrointestinal tract (World Health Organization 2003). This could be due to the interaction between the asbestos fibers and strong stomach acids, which are capable of breaking down the fibers and altering their surface properties, making them non-toxic.

1.5 Naturally Occurring Asbestos

The potential hazards and associated public health issues related to exposure of NOA from in-place asbestos deposits has recently gained regulatory and media attention, especially in in the United States (Lee et al. 2008). Although large asbestos deposits are rare, small non-economic occurrences are more common and pose a potential public health concern. NOA poses a health concern when released into the environment, which can occur when rocks and soils containing asbestos are disturbed by crushing, weathering, and various human activities such as mining, excavation, development, recreational activities on unpaved roads, etc.

It is unlikely asbestos exposure levels due to NOA will be as high as those in the asbestos mining and manufacturing industries, however, even if it is from natural sources, asbestos can still poses a serious health concern if released into the atmosphere. Currently there is no consensus around the health risks related to NOA (Lee et al. 2008).

Pan et al. (2005) found that the risk of developing mesothelioma was directly related to an individuals proximity to a source of ultramafic rock, and for every 10 km

between an individual's home and the nearest NOA source, their risk of developing mesothelioma dropped by 6.3 %. However, this study has been questioned because Pan et al. (2005) did not conduct any sampling or measure background asbestos levels near the study groups residence (Lee et al. 2008), or account for immigration or emigration (Harper 2008). In Libby Montanta, occupational and environmental exposure to amphibole asbestos has resulted in lung cancer and mesothelioma in workers and residents of the immediate town and surrounding communities (Cyphert et al. 2012).

It is been postulated that NOA is less hazardous than commercial asbestos because time spent in the weathering environment can potentially alter the surface properties of the fibers, thus reducing their potential toxicity (Favero-Longo et al. 2009). The effect of weathering on the surface properties of NOA fibers is largely unexplored. There is little data available on weathered fibers that have been modified by physical and environmental forces. Hazard evaluation of NOA needs to take into account environmental modifications of toxicity-related physio-chemical features.

The review by Schreier (1989) provides insight into the attributes of asbestos in the natural environment. Its unique shape coupled with its common occurrence as packets of fibrils have significant effects on its transport by both water and wind. The packets decrease the apparent density and the elongated shape allows the asbestos to move greater distances than similar minerals that do not share this configuration. This may be beneficial in that the longer the packets are in transport, the greater the potential for the fibers to weather, and potentially become less toxic (Gloag 1981). However, the particular arrangements allow the particles to be more buoyant than their specific gravity would suggest, thus contributing to their greater dispersal potential.

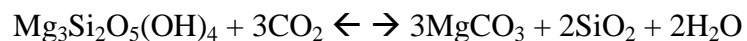
1.6 Strategies for Reducing the Toxicant Effect of NOA

Chelating, resulting from soil microorganism activity, has been proposed as a bioremediation strategy for fibers in soils; however, the process is slow (Turci et al. 2007). Monchaux et al. (1981) found rats injected with untreated chrysotile had dramatically higher incidences of pleural mesothelioma than those injected with hydrochloric or oxalic acid treated chrysotile. These studies suggest that naturally occurring acids, including those found in streams and soil environments, may ameliorate

the toxic characteristics of the fibers. Weathering due to naturally occurring acids in the stream and soil environment modifies the fiber surfaces and potentially ameliorates the negative health effects of chrysotile asbestos (Holmes et al. 2012). Favero-Longo (et al. 2009) found that mimicked weathering of chrysotile fibers did not eliminate its fibrous nature, but it did reduce free radical generation via Fenton-like activity, potentially reducing the toxicity.

1.7 Atmospheric CO₂ Sequestration Using Chrysotile Mine Tailings

Fossil fuel consumption has resulted in a significant increase in greenhouse gases in the atmosphere over the past century. According to Hansen et al. (2008), we must reduce atmospheric CO₂ concentrations from their current levels of 395 ppm down to 350 ppm “if humanity wishes to preserve a planet similar to that on which civilization developed to which life on Earth is adapted”. One proposed carbon sequestration method is the capture and storage of CO₂ into stable mineral forms. Mineral sequestration can provide unlimited capacity to permanently store CO₂ in an environmentally benign form if researchers can find a way to increase the reaction rate in a cost and energy effective manner (Krevor & Lackner 2011). Mineral carbonation by silicate minerals is a naturally occurring process that sequesters an estimated hundred million tons of carbon per year (Seifritz 1990). It occurs when divalent cations, namely magnesium and calcium, react with carbon dioxide to form carbonates (Goldberg et al. 2001). Below is a simplified equation of a mineral carbonation reaction between a serpentine mineral and carbon dioxide that results in the precipitation of magnesite, a stable magnesium carbonate mineral.



Carbonates have a lower energy state than carbon dioxide, and thus mineral carbonation is thermodynamically favorable, which is why it occurs naturally (Goldberg et al. 2001). The above reaction above would release 64 KJ/mol of energy in the form of heat (Fauth et al. 2002).

Dissolution kinetics of magnesium silicate minerals are rate-limiting (Hänchen et al. 2008). The slow rate of silicate dissolution is the reason why high yields of carbonate production in short time periods have only been achieved with the relatively reactive olivine, and only after the dissolution is enhanced through the energy-intensive grinding stage (Gerdemann et al. 2007). The reaction can also be limited by lack of available carbon. Mineral carbon sequestration research involves mimicking and speeding up the natural process by increasing the rate of silicate dissolution and ensuring adequate CO₂ levels.

Magnesium-rich minerals, such as serpentine, are favored as feedstock sequestration minerals due to their vast abundance over several continents, their high availability in minable deposits, and their relatively high magnesium content (Bearat et al. 2002). Grinding the silicate minerals to increase their reactivity and thus dissolution is responsible for 75 % of the mineral carbonation processes total energy inputs, and the main reason for high cost estimates (Gerdemann et al. 2007; Huijgen et al. 2007). Chrysotile mine tailings already have a fine grain size which causes accelerated weathering, increasing the rate magnesium is released from the silicate framework and thereby allowing for rapid carbonate development (Wilson et al. 2009). This makes them a natural choice for CO₂ sequestration research.

1.8 Serpentine Dissolution

Serpentine dissolution rates are kinetically limited in low temperature environments, and have been the subject of much research and controversy (Putnis 2009). Determining the factors that control the rate of silicate dissolution is essential for speeding up the rate at which chrysotile fibers are weathered and ameliorated, and to predict the extent that CO₂ mineralization of serpentine mine tailings may proceed.

Chrysotile dissolution is a multi-step process involving both redistribution of components of diffusion and chemical reactions at the solid-liquid interface (Bales 1984). Brucite dissolution is transport limited and silica dissolution is reaction rate limited, meaning chrysotile dissolution could be either transport or reaction rate limited (Bales 1984). The rate of dissolution may be controlled by: (i) the reaction of the unaltered mineral at the mineral solution interface; (ii) the diffusion rate of ions through a leached

surface layer; or (iii) the rate of diffusion of ions through a precipitated surface layer (Gronow 1987).

When exposed to aqueous solutions, most silicate minerals undergo incongruent dissolution at low temperatures (Gronow 1987) and in field conditions (Loughan 1969) meaning they release ions into solution out of proportion with their solid composition (Putnis 2009). Such non-stoichiometric dissolution results in chemically and structurally altered 'leached' surface layers relative to the bulk mineral (Putnis 2009). This occurs because some components are selectively removed from the solid due to their increased solubility, and the depleted layer becomes concentrated in the other mineral components, and then may become structurally reorganized by a solid state mechanism (Putnis 2009). However, under certain conditions and time frames, magnesium silicates can approach congruent dissolution. Congruent chrysotile dissolution was reached in 2 months at a temp of 90°C and in 9 months at a temp of 25 °C (Luce et al. 1972).

Luce (et al. 1972) present a model for the dissolution of magnesium silicate minerals which can explain the short-term incongruency and long-term near congruency. Diffusion coefficients for magnesium are greater than for silicon, leading to initial incongruent dissolution over moderate time periods. There is a rapid exchange of surface magnesium ions with hydrogen ions. Once the surface brucite layer is leached, the rate of dissolution decreases because silica is less soluble than the brucite layer and is thus the rate controlling factor (Morgan 1997). The exchange kinetics following the initial leaching of the surface brucite layer are consistent with either of two rate controlling mechanisms: the exposure of fresh magnesium by the removal/dissolution of silica, or by the diffusion of magnesium ions through the silicate layer (Gronow 1987).

Because the near-surface partially leached region in the mineral is more depleted in magnesium relative to silicon, its dissolution will cause the ratio of silicon to magnesium in solution to rise toward the stoichiometric ratio if the system is closed. Hence, over a very long time period, dissolution of silica and magnesium dissolved is proportional, meaning congruent dissolution. This dissolution model explains McClelland's (1950) general observation that with increasing time, the rate of release of two ions in the same mineral tends to approach the stoichiometric ratio in the

unweathered mineral. In low pH solutions, dissolution rates are fast and congruent dissolution is reached much sooner than in neutral pH solutions (Luce et al. 1972).

Hume & Rimstidt (1992) “shrinking fiber” model supports the theory that the structural brucite dissolves first, thus exposing a silica rich leached layer, which dissolves at a lower rate and is thus the rate controlling step.

In general, dissolution of 10 % of the silica results in magnesium depletion of ~ 50 %. Silica dissolution of 20 % corresponds to a magnesium dissolution of >70 %. However, in Cassiar chrysotile, more silica has to be dissolved to achieve the same magnesium depletion found in chrysotile fibers from other regions, likely due to the poorly formed interfibrillar amorphous matrix characteristic of Cassiar chrysotile (Morgan 1997).

1.9 Objectives

The objectives of this study are to:

- 1) Assess the effects of laboratory simulations of naturally occurring acids on the surface chemistry and composition of chrysotile minerals.
- 2) Determine the surface chemistry and composition of chrysotile asbestos a) from the Sumas mountain landslide and Sumas River sediment in Northern Washington and Southern British Columbia b) chrysotile tailings from Cassiar, a commercial mine in BC.
- 3) Discuss the significance of chrysotile surface properties in relation to potential human health concerns and carbon dioxide sequestration.

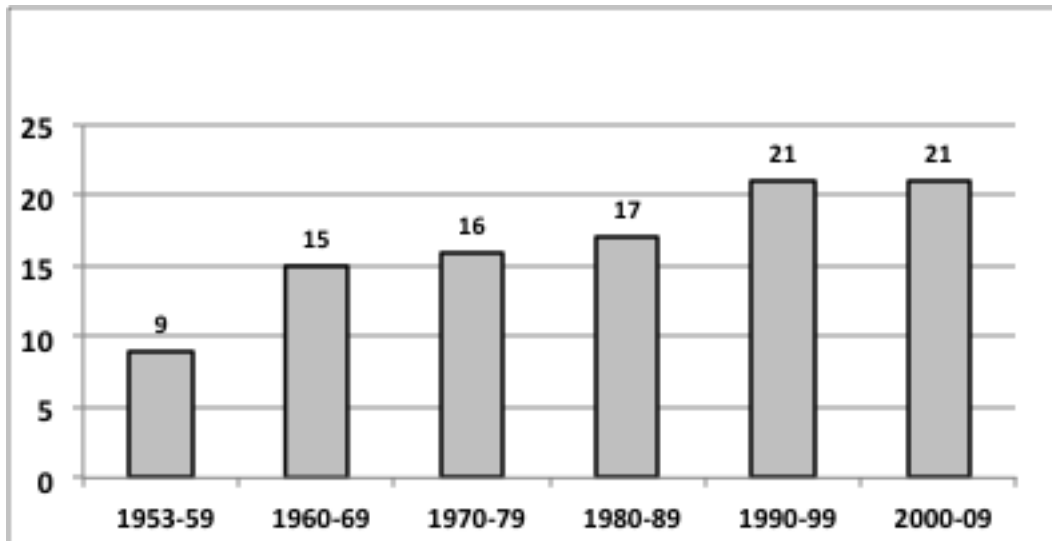
1.10 Site Descriptions

1.10.1 Sumas Watershed

A natural landslide of serpentine material containing chrysotile asbestos at the headwaters of Swift Creek in Washington, USA, a tributary to the Sumas River in southwestern British Columbia, Canada, is contaminating the river and floodplain. Mass wasting and physical and chemical weathering of serpentine bedrock results in sediments entering Swift Creek and being transported downstream (Bayer & Linneman 2011).

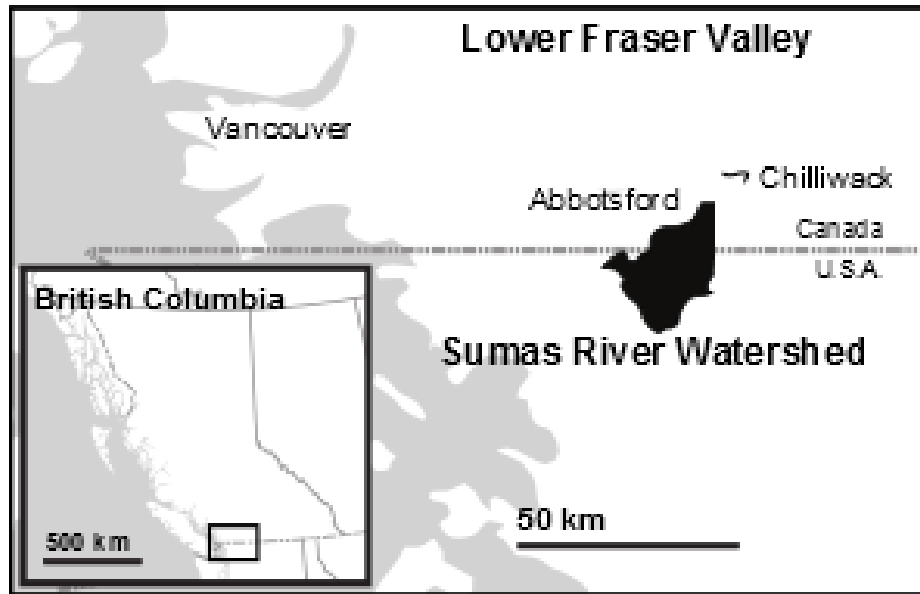
Flooding of agricultural fields due to storm events is a frequent occurrence and each event leaves a layer of very fine sediments that consist of up to 8 % by volume chrysotile asbestos (EPA 2009), with nickel and chromium concentrations up to 1500 and 400 mg kg⁻¹, respectively (Smith et al. 2007) . The number of storm events with discharge rates greater than 15 m³s⁻¹, the minimum discharge that can produce flooding, is outlined in Figure 1.3, and shows that high discharge events are increasing.

Figure 1.3. Number of discharge events greater than 15m³/sec by decades for the Sumas River (adapted from Holmes et al. 2012).



The Sumas River (Figure 1.4) originates in northwestern Washington State and flows in a northeast direction into British Columbia and enters the Fraser River at the confluence of the Vedder Canal, near Chilliwack. The Swift Creek landslide (48°54'54" N, 122°16'07" W) is located east of the town of Nooksack, WA on the western flank of Sumas Mountain. The headwater area of the Sumas River watershed is forested with some logging operations, while the lowland in British Columbia is home to intensive agricultural land, dominated by dairy and poultry enterprises. The topography of the majority of the watershed is level to very gently rolling.

Figure 1.4. Location of the Sumas River watershed.



There is concern the deposited chrysotile asbestos and its subsequent inhalation may be a health hazard to the regional rural population. The US EPA conducted bulk soil and activity-based sampling to determine the potential risk to individuals exposed to asbestos as a result of working or living around the asbestos contaminated flood deposits. They found the soil and sediment contained significant amounts of asbestos, and that disturbance of these materials due to typical activities, such as excavating the dredged sediment or mowing a lawn, could result in exposure greater than what is considered acceptable under Federal guidelines (Wroble 2010). In rat studies, Cyphert (et al. 2012) found Sumas chrysotile taken from near the landside to be toxic, suggesting there may be cause for concern for local residents. There degree of modification by natural processes along the Sumas River and floodplain, and effect this has on the toxicity of the fibers is poorly understood.

1.10.2 Mine tailings

The Cassiar chrysotile mine is located in Northern British Columbia (Figure 1.5). Seventeen MT on mine tailings were produced during the chrysotile asbestos mines 39-year operational lifetime, which ended in 1992. The tailings are primarily composed of

short-fiber chrysotile and cobbles of massive serpentine with minor magnetite, clinocllore, and occasional quartz and carbonates (Wilson 2006).

Figure 1.5. Left: Location of Cassiar, BC with Prince George as a reference point (UNBC). Right: The tailings pile at Cassiar mine (Wilson 2005).



The mineral carbonation research group at UBC has been examining the mineral carbonation process in ultramafic mine tailings at Cassiar mine. Carbon dioxide uptake into the tailings is outpaced by the rate of carbon fixation, implying that a lack of available carbon is slowing down the reaction, thereby limiting carbon dioxide sequestration (Wilson et al. 2010). There is need for a better understanding of what happens to the surface properties of chrysotile mine tailings. Another concern regarding mineral carbonation using tailings is that carbonate crusts form on the surfaces of tailings. This can prevent further dissolution of chrysotile, and thus slow or halt the process of

carbon sequestration. As well, knowledge of the chrysotile tailings surface over time, and whether a silica surface develops due to faster magnesium dissolution compared to the silica layer, is of relevance for long-term sequestration projects. The rate at which the sequestration reaction can occur is dependent on the surface chemistry.

Chapter 2 : Long-term rock and sediment analysis in the Sumas River Watershed, including acid treatment of asbestos contaminated sediment and soil to simulate natural processes.

2.1 Introduction

Research in the Sumas watershed by the UBC Soil Science group began in 1975. Concerns regarding asbestos contamination by the US EPA lead to a continuation of research in the area with a focus on chrysotile reclamation in 2009 and 2010. This chapter presents work, published in the Canadian Journal of Soil Science (Holmes et al. 2012), characterizing the bulk chemistry of rock, soil, and sediment samples that were collected over a period of 35 years. In addition, samples collected in 2010 were treated with dilute acids to simulate the effect naturally occurring acids have on chrysotile fibers.

2.2 Sampling Locations

Eight locations were sampled for bed sediment below the landslide area towards the mouth of the Sumas river (Figure 2.1). Distance from the landslide to the furthest sampling station at McDonald Park is approximately 50 km. Distances from the landslide to the Canada-US border, and from the border to McDonald Park, are 25 km. Marshall Creek and Arnold Slough are tributaries unaffected by the serpentine landslide, and were used as control sites.

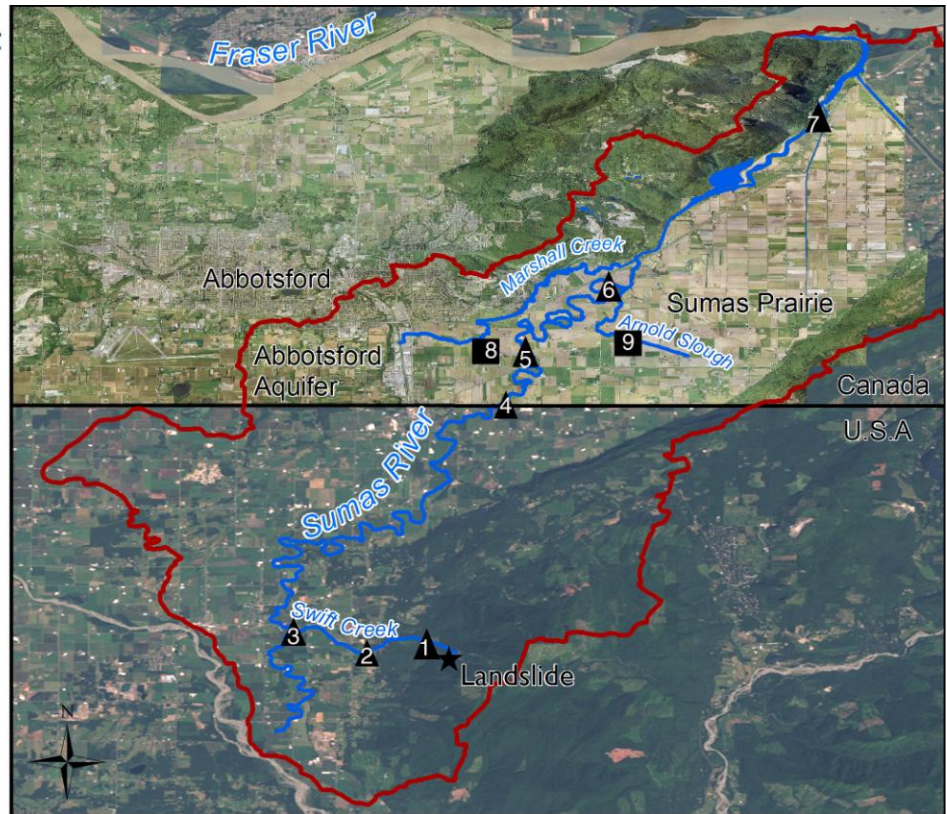
Figure 2.1 Map of the Sumas River watershed including sediment sampling stations.

**Sumas River Watershed:
Sampling Sites**

- ▲ Swift Creek
- ▲ Swift Creek Middle
- ▲ Tuxido Farm
- ▲ Border
- ▲ School
- ▲ Hougan Park
- ▲ MacDonald Park
- 8 Marshall Creek
- 10 Arnold Slough
- 🔴 Sumas River watershed
- International border
- Sumas River and tributaries
- ★ Landslide

Data sources: 2008 digital orthophoto and spatial data provided by the City of Abbotsford; Landsat True Colour Composite, Acquired July, 2000 from: Geomatic Canada, Centre for Topographic Information.

0 2.5 5 10 Km

2.3 Materials and Methods

2.3.1 Sediment samples

Bed sediment was collected as grab samples at each station in 1975, 1983, 1984, 1993, 1994, 1998 and 2009. The 1975, 1983, 1984, 2009 and 2010 samples were collected in winter after storm events. The 1993 and 1994 samples were collected in September and August, respectively. The 2010 samples were collected in April. The samples were stored in acid-washed 250 mL Nalgene bottles that had already been thoroughly rinsed with stream water. The samples were stored on ice in a cooler during transportation to the laboratory.

Samples were wet sieved and the <63 μm fraction was separated and digested. Samples collected prior to 1985 were digested using hydrofluoric acid (Lim & Jackson 1982) and analyzed for trace metals using an inductively coupled argon emission spectrograph (Varian, Vistapro). Subsequent samples were digested using a variation of Aqua Regia method 200.2 for sediments, an acid soluble metal technique for analysis of

total recoverable elements (Martin et al. 1991). Approximately 0.5 g of dried sample was combined with 10 ml of aqua regia and heated. The solution was filtered through a Whatman #42 filter, brought to volume with 5 % nitric acid and stored in plastic bottles. Samples were analyzed for total elements using inductively coupled plasma atomic emission spectroscopy (Varian 725-ES).

2.3.2 Soil and rock samples

In April 2010, Ap (0-15 cm), Bm (15-20 cm) and IICb (20+ cm) horizons were sampled from each of two pits on either side of the Sumas River at the international border. Samples were taken to represent recent soil development (Typic Regosol) and recently buried soil (Cumulic Humic Regosol). In 1980, 1 kg of bedrock was taken from the site of the landslide, crushed and stored in an airtight container. Aqua regia analysis (Martin et al. 1991) was performed on soil and historical rock samples. Samples were analyzed for total elements using inductively coupled plasma atomic emission spectroscopy (Varian 725-ES).

2.3.3 Organic acid treatment

Soil and sediment samples collected in 2010 were treated with dilute acids to simulate weathering of naturally occurring organic acids in stream and soil environments. To assess elemental composition of the fibers, 1 g samples each of soil and sediment sample were weighed and subjected to four different organic acid treatments: carbonic acid (prepared by bubbling CO₂ gas slowly into 500 mL of distilled water until a constant pH was reached); solution of acetic acid (pH = 2.8); citric acid (pH = 2.4) and oxalic acid (pH = 1.9)

Each 1 g sample was treated with 25 ml of acid and shaken for two hours using a reciprocal shaker at 60 cycles per minute and left to stand overnight for 16 hours. Sample solutions were decanted and filtered through Whatman #42 filter paper. The filtrate was collected in a 100 mL volumetric flask, made to volume with 5 % nitric acid and stored in plastic bottles in preparation for ICPMS analysis (Varian 725-ES).

2.3.4 Data Analysis

For acid extraction analysis, one third of the samples were replicated (Soil and Plant Analysis Council 1999). All replicate values were within 10 % of the original value. The absolute values of samples over time and from different locations were compared to one another to gain information related to the elemental composition of the sediment, rock and soil affected by natural processes and laboratory acid weathering.

2.4 Results and Discussion

2.4.1 Sediment and soil analysis

Table 2.1 provides data on the original characterization of the serpentine bedrock and the Sumas River sediments at the border location. Sediment samples were collected following major flood events in 1975 and during winter 1983-1984. Results are representative of serpentine asbestos materials in the region with calcium: magnesium ratios below 0.1, and high nickel ($>1850 \text{ mg kg}^{-1}$) and chromium ($>460 \text{ mg kg}^{-1}$) concentrations (Schreier 1989). Metal concentrations were numerically different between original bedrock and sediments from the flood events and numerically similar among the various sediment samples. Magnesium and nickel concentrations were slightly numerically higher in the original bedrock than in the eroded and deposited sediment and chromium was two fold higher in sediments than original source material. Biogeomorphic processes likely affected chemical composition of the serpentine chrysotile sediment as sediment was transported in the aqueous environment.

Table 2.1. Average percentage and concentration of metals in serpentine bedrock and Sumas River sediments (HF digestion).

Sample	No. of Samples	Magnesium %	Chromium mg kg⁻¹	Nickel mg kg⁻¹	Zinc mg kg⁻¹
Bedrock	3	26.9	230	2720	55
1975 Flood Deposit	5	22.2	505	2120	43
1983 Flood Deposit	5	18.3	648	1940	45
1984 Flood Deposit	5	19.4	480	1860	47
1983-84 Bed Sediment	6	21.9	465	1960	39

A more comprehensive analysis of sediments was conducted during the 1993-1994 and 2009 periods, on a full set of sediment samples from the headwaters of the Sumas to the confluence with the Fraser River. There was a gradual numerical decline in nickel and chromium concentrations in bed sediments from the headwaters to the confluence (Figures 2.2 and 2.3); however, metal concentrations at the downstream MacDonald location were still numerically higher than those in Marshall Creek and Arnold Slough, which are considered reference locations since they are unaffected by asbestos sediments of the Sumas.

Figure 2.2. Total Ni in Sumas River fine bed sediments collected in 1993, 1994, and 2009.

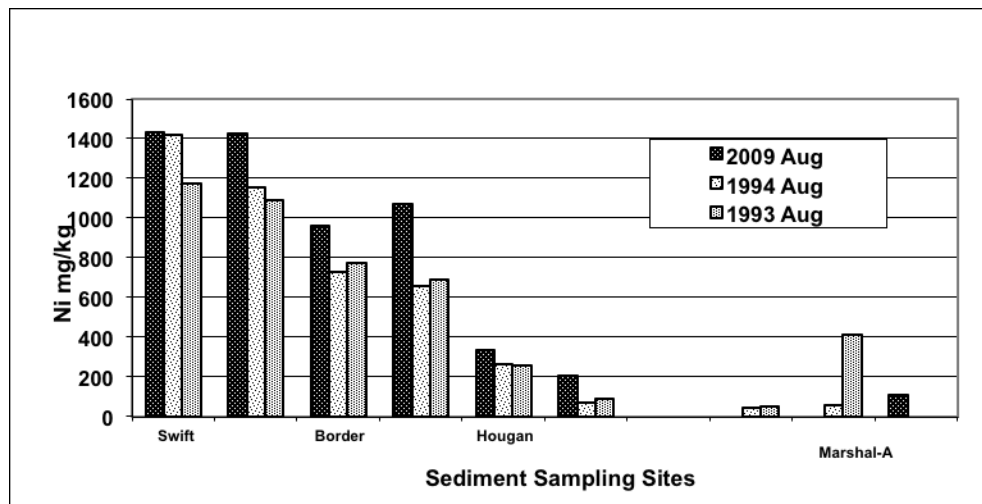
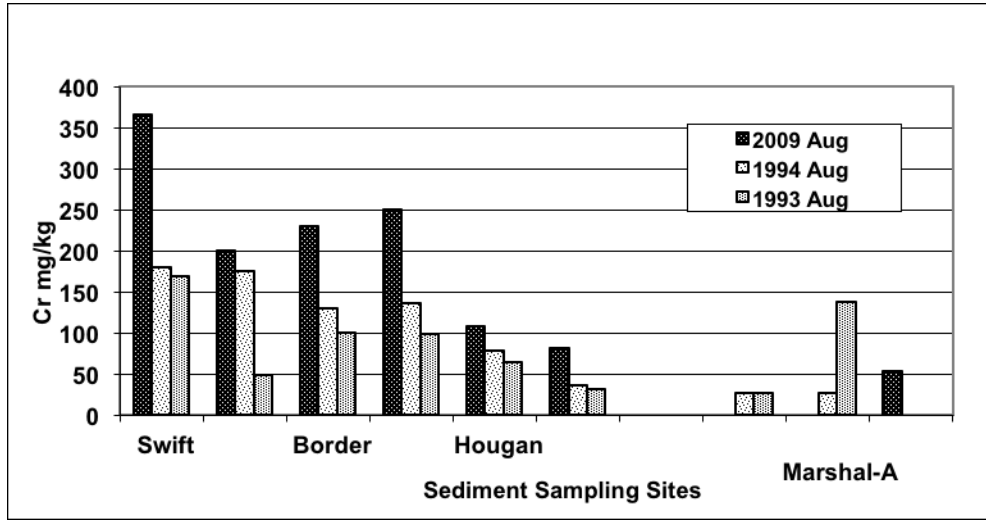


Figure 2.3. Total Cr in Sumas River fine bed sediments collected in 1993, 1994, and 2009.



As the sediment is transported, deposited on the floodplain and subjected to pedogenesis, the chemical environment of the chrysotile changes from alkaline (pH ~ 9) to less alkaline and organic matter increases substantially. Solubility and mobility of the metals released respond to these new dynamic changes. Aqua regia extraction of metals from asbestos enriched sediment from the Swift Creek location, and sediment and soil from the Ap horizon of the border location in April 2009 are presented in Table 2.2. Since aqua regia does not extract framework elements within the crystalline aluminosilicates but dominantly the recoverable, or most chemically reactive, components of the material (Andersen & Kisser 2004), values can represent the most reactive outer coatings or amorphous layers on the minerals.

Table 2.2. Total recoverable metal concentrations in sediments and soils from the Sumas River watershed (aqua regia digestion). (n=2).

Sample	Swift Creek Sediment		Int'l Border Sediment			Int'l Border Soil
Year	2009	2010	2009	2008	1994	2010
Magnesium (mg kg ⁻¹)	176570	101680	138390	152640	127180	n.d.
Nickel (mg kg ⁻¹)	2112	964	1272	1317	1020	1244
Zinc (mg kg ⁻¹)	25	71	66	163	72	93
Chromium (mg kg ⁻¹)	341	230	247	244	198	33
Aluminum (mg kg ⁻¹)	2182	9377	9568	7902	10485	11896
Iron (mg kg ⁻¹)	56950	49750	54020	49730	58210	28650

Data in Table 2.2 provide information pertaining to the biogeomorphic and pedologic history and composition of natural sediments and soil. With the exception of 2008, the measured elemental concentrations of metals in sediments remained relatively constant at the international border site over time. As the sediment moved downstream from Swift Creek to the border station aluminum concentrations increased 4 fold, chromium and magnesium concentrations slightly decreased, iron remained relatively constant, and nickel decreased by half. This is likely due to the dilution of the asbestos rich sediment as the Sumas River moves downstream. The concentration of zinc increased dramatically, 3 fold, likely a result of anthropogenic contamination from the high intensity agriculture in the region (Schreier et al. 1998).

Comparing sediment samples at the border with soil samples at the border provides insight into the effects of pedogenesis because the sediment can be considered the parent material of the floodplain soil. Aluminum concentrations increased slightly in soil over that of the parent sediment. Chromium concentration was ten times lower than that of the original sediment. Iron decreased substantially by 7 fold suggesting pedogenic processes, probably organic matter complexing mobilized some of the readily weatherable iron from the mafic serpentine minerals. When magnesium decreases so does iron, chromium and nickel. This is attributed to the weathering of the brucite layer which results in reduced values of all four of these elements, since iron, chromium, and nickel commonly substitute for magnesium in the brucite layer.

2.4.2 Acid treatment

Effective dissolution of the samples varied numerically among the four weak acids by sample origin (Table 2.3). Oxalic acid extracted the most magnesium, aluminum, and iron from both the sediment and soil samples. Citric acid also extracted high amounts of magnesium and aluminum from both soil and sediment samples. Carbonic acid extracted the most zinc from both the sediment and soil samples, followed by acetic acid. From alluvial sediments, carbonic acid extracted the largest amount of nickel, and oxalic acid and citric acid extracted the most chromium. From the floodplain soil, acetic and oxalic acid extracted the most nickel, and citric acid extracted the most chromium. Overall, acetic acid and carbonic acid were the least effective extractants for the sediment

samples, and carbonic was the least effective extractant for the soil samples. In general the chelating acids, oxalic and citric acid, were the most effective extractants.

Table 2.3. Total metal concentrations extracted from soil and sediment samples taken from the Sumas River watershed after treatment with different organic acid (n=2).

Sample	Swift Creek Sediment				Int'l Border Soil Ap Horizon			
Acid Extraction	Acetic	Carbonic	Citric	Oxalic	Acetic	Carbonic	Citric	Oxalic
Magnesium (mg kg ⁻¹)	47710	71280	82940	89820	3165	1798	3497	8016
Nickel (mg kg ⁻¹)	2235	2758	2415	2682	131	80	92	103
Zinc (mg kg ⁻¹)	140.6	208.5	59.2	67	5.1	6	0	0
Chromium (mg kg ⁻¹)	153	197	211	209	4.5	4.1	13.7	1.5
Aluminum (mg kg ⁻¹)	568	744	831	860	121	93	147	327
Iron (mg kg ⁻¹)	32110	40430	39190	42190	2267	1440	2139	3505

Knowledge of Pk_a and solubility of reaction products is necessary for understanding the effects of natural acids on chrysotile asbestos fibers. Soil organic acids have pK_a values from 1.2-13.0 (Lee 1991). David & Vance (1991) have shown that the major natural organic acids in lakes and streams are those with pK_a values from 4.0-4.6. The pK_a values of the acids selected (carbonic = 6.4, acetic = 4.7, citric = 3.1, and oxalic = 1.2) were similar in magnitude to soil fulvic acids (= 2.6-3.1) (Esteves da Silva & Machado 1997).

Treating sediments and soil samples with organic acids resulted in mineral surfaces being dissolved. Rate of leaching was dependent on the strength (pK_a) and type of acid (chelating or non-chelating). Oxalic acid, the strongest acid used in this study and a chelating acid, extracted the highest concentrations of elements from the fibers, and was especially effective at removing magnesium, iron and nickel. Citric acid, which has a lower pK_a , but is also a chelating acid, removed high concentrations of chromium, aluminum, and magnesium. Acetic acid and carbonic acid, weak non-chelating acids, had generally low extraction capabilities. Chelating acids removed greater amounts of oxidizing elements, such as chromium and nickel, which have a higher potential for negatively affecting mammalian lung tissue.

2.5 Conclusions

Results of this study demonstrate the need to understand the biogeomorphic environment and the processes that alter structure and surfaces of chrysotile asbestos. Time and movement downstream are important factors affecting chrysotile fibers prior to their deposition as a soil parent material and influence properties of the resulting soil. In a similar manner, soil processes, especially those associated with production of acids, have fundamental impacts on chrysotile properties, most notably destruction of the octahedral layer (Cipolli et al. 2004). Age of parent material since deposition, distance traveled from the serpentine source, and influence of the organic fraction are critical factors that influence any asbestos reclamation strategy.

In agreement with Bales & Morgan (1985) and Bales (1984), the natural weathering processes that occur within soil and aquatic environments combine to modify chrysotile structurally and in chemical composition. The potential toxicological effect of

the fiber surfaces is likely decreased as stream movement and pedogenesis degrade chrysotile. Acids react differently depending on whether they are chelating acids or non-chelating acids, however, in natural environments, chelating and non-chelating acids are likely both present and thus effective in biochemically weathering fibers, rendering them less of a potential human health risk.

Chapter 3 : The Effect of Simple Organic Acids on the Bulk and Surface Properties of Chrysotile Asbestos

3.1 Introduction

Understanding the processes and changes in surface composition provides the basis of predicting the reaction processes and change of minerals during weathering. This chapter presents work exploring the effects of bio-geomorphic processes on chrysotile fibers by simulating these processes in the laboratory with acids and examining the effect this has on the bulk and surface chemistry of chrysotile asbestos.

3.2 Materials and Methods

3.2.1 Acid treatment

A bulk sample of natural chrysotile was obtained from Cassiar Mine, British Columbia, Canada. The sample is high-grade fibrous-matted-ore (Grade AY) noted for its high purity (Ilgren 2008). Nine 0.5 g of chrysotile sample were weighed and subjected to one of three acid treatments:

- carbonic acid (prepared by bubbling CO₂ gas slowly into 500 mL of distilled water until a constant pH of 3.6 is reached),
- 0.25 M solution of oxalic acid (pH = 1.9)
- 0.1 M solution of hydrochloric acid (pH = 1)

Each 0.5 g sample was treated with 25 mL of acid and shaken for two hours using a reciprocal shaker at 60 cycles per minute and left to stand overnight. The sample solutions were decanted and filtered through Whatman #42 filter paper. The filtrate was collected in a 100 mL volumetric flask, made to volume with 5% HNO₃ and stored in plastic bottles. The filter papers were scraped and the precipitate was stored in glass containers in preparation for other analysis. A portion of the precipitate was placed in a 50 mL beaker of double deionized water and pH was measured using the Orion model 420A pH meter (Thermo scientific, Waltham, MA). All samples were measured 3 times and averaged for a representative reading.

3.2.2 Bulk mineral analysis

3.2.2.1 XRD

The chrysotile samples and precipitate samples from the acid treatments were ground using an agate mortar and pestle and smear-mounted with anhydrous ethanol on glass plates. XRD data were collected using a Bruker D8 Focus Bragg-Brentano diffractometer with $\text{CoK}\alpha$ radiation and a step size of 0.04° over a range of $3\text{-}80^\circ 2\theta$ at 0.9s/step . Fe monochromator foil, 0.6mm divergence slit, incident and diffracted beam slits, and a Lynx Eye detector were used. A long fine focus Co X-ray tube was operated at 35 kV and 40 mA using a take-off angle of 6° . A rotation speed of 50 rpm was used. Search-match software by Bruker (DIFFRACplus EVA 16) was used for phase identification. Crystal structure data were obtained from the International Centre for Diffraction Database PDF-4+ 2010.

3.2.2.2 ATR FTIR

ATR FTIR spectroscopy was used to analyze the mineral surface composition. Infrared absorbance occurs in the region where the sample contacts a crystal of high refractive index, enhancing the signal of the surface over that of the bulk mineral (Kubicki et al. 1999).

Spectra of the chrysotile samples and pure carbonate samples (hydromagnesite, magnesite, pypingite, and mesquetonite) was done on a Perkin Elmer Spectrum 100 FTIR Spectrophotometer with a universal ATR sampling accessory, and a diamond coated KRS5 thalium plate. Analysis software by Perkin Elmer (Spectrum version 10) was used for peak analysis.

3.2.3 Bulk elemental analysis

The fresh chrysotile and the chrysotile precipitate from the acid treatment was prepared for elemental analysis using aqua regia digestion method for elements outlined in Martin (et al. 1991). A summary of the Aqua regia method is as follows: approximately 0.5 g of the dried sample is combined with 12 mL of aqua regia and heated. The solutions were then filtered through a Whatman #42 filter, brought to volume with 2% HNO_3 , and stored in plastic bottles that were refrigerated. The filtrate from the acid experiment and

the digested acid treated and untreated samples were analyzed for total elements using ICP-MS (Varian 725-ES). Duplicates were analyzed for each sample, and the samples were repeated if the duplicates varied by more than 10 %.

3.2.4 Surface imaging

Characterization of chrysotile fiber surfaces was carried out using the Hitachi S-4700 FESEM in the UBC BioImaging Facility. The instrument was chosen for its high resolution of 2.5 nm. Small segments of each sample were mounted on aluminum stubs and sputter coated with platinum in preparation for SEM analysis. Due to the high degree of variability within the samples, three fields of view containing fibers were analyzed and captured as an image under three magnifications: 3000 times, 5,000 times, and 10,000 times.

3.2.5 Surface charge

Surface charge was measured using a Zeta Meter Model 3.0+ (Zeta Meter Inc. USA) in Mining Engineering at the University of British Columbia. 50mg of each sample was transferred into 15 ml of distilled water and shaken by hand for 30 seconds. All the measurements were carried out within 30 seconds of being shaken. The applied voltage was determined based on the specific conductivity of the solution. The particle movement was observed through a microscope and the time taken for a particle to travel the distance of a micrometer was measured. To minimize error, a minimum of five particles were tracked and their average time was calculated.

3.2.6 ToF-SIMS

ToF-SIMS was conducted in the Advanced Materials and Process Engineering at UBC. In preparation for ToF-SIMS measurement, each sample in its powder form was mounted onto a piece of silicon wafer using a double sided tape. ToF-SIMS measurements were performed with a PHI TRIFT V nanoTOF instrument using Au_1^+ gun operated at 30 keV with an aperture size of 100 μm ; current measured at the primary column was ~ 0.5 nA. Materials with fiber characteristics were looked for and analyzed. Positive spectra were acquired from 1,600 μm^2 surface area ($X = 400$ μm and $Y = 400$ μm) at a depth of 2nm

($Z = 2\text{nm}$) for a duration of ~ 12 min where the total ion dose was less than 10^{12} ions cm^{-2} . Charge compensation was accomplished during spectrum acquisition using 10 eV electrons. Mass resolution ($m/\Delta m$) for the Si^+ peak was around 8000. Spectra were calibrated with the known masses associated with peaks for the species H^+ , Mg^+ , CH_3^+ , CH_3H_5^+ . 3D and 2D images were created to visually represent the data. The 3D images are not to scale, with the depth (2nm) axis blown up 100,000 times to make it visible.

3.3 Results and Discussion

3.3.1 Bulk mineral analysis

3.3.1.1 XRD

XRD patterns identify the samples as being predominantly composed of chrysotile, and lizardite. Due to overlap and fit of pattern, antigorite may also be present. Minor peaks (<50 % intensity of major peaks) of quartz were present in the untreated, hydrochloric acid treated, and oxalic acid treated samples. An oxalic acid trace peak (<10 % intensity of major peaks) was present in the carbonic acid treated samples, and all samples had trace peaks associated with magnetite and talc. A major peak associated with glushinskite, a magnesium oxalate, was found to be present in the oxalic acid treated sample. Glushinskite commonly forms on lichen colonized serpentine rocks (Favero-Longo et al. 2005) as a result of oxalic acid producing lichen. Table 3.1 outlines the peaks associated with each sample. See Appendix A for the complete XRD patterns.

Table 3.1. Summary of XRD peaks for untreated and acid treated chrysotile samples. M=major peak, Mi=minor peak (<50% major peak), and T=trace peak (<10% major peak).

Sample	Serpentine (Chrysotile, Lizardite, Antigorite)	Glushinskite	Quartz	Magnetite	Talc
Untreated	M		Mi	T	T
Hydrochloric acid	M		Mi	T	T
Oxalic acid	M	M	Mi	T	T
Carbonic acid	M		T	T	T

3.3.1.2 ATR FTIR

All chrysotile samples analyzed exhibited typical chrysotile IR spectra. The IR spectrum of chrysotile exhibits three well-defined spectral groups in the 3800-3600 cm^{-1} region, the 1200-800 cm^{-1} region, and less than 800 cm^{-1} region (Anbalagan et al. 2008). Table 3.2 outlines the peaks, and characteristics causing the peaks, for each of the samples. All samples displayed the broad 3680-3690 cm^{-1} peaks associated with in phase outer Mg-OH stretching of chrysotile fibers (Anbalagan et al. 2008), the 940-960 cm^{-1} peaks associated with asymmetric stretching vibrations of Si-O bonds in chrysotile fibers (Suquet 1989; Yariv & Heller-Kallai 1973), and the 603-610 cm^{-1} peaks associated with OH bending vibrations in chrysotile fibers (Anbalagan et al. 2008; Bishop et al. 2002). The majority of samples displayed the 432 – 438 cm^{-1} peaks associated with out of plane bending of the Mg octahedral (Suquet 1989) and 300-400 cm^{-1} peaks associated with lattice vibrations of Mg-O bending, indicating the basic chrysotile structure is intact (Suquet 1989). The oxalic acid treated sample had peaks at 3381 cm^{-1} and 1661.6 cm^{-1} which are associated with bending vibrations of adsorbed water in chrysotile fibers (Anbalagan et al. 2008; Suquet 1989). This indicates the presence of some hydrated, noncrystalline silica in the sample due to weathering of the fibers (Suquet 1989).

Table 3.2. Summary of ATR-FTIR spectra for untreated and acid treated chrysotile fibers.

Sample	In phase outer Mg-OH stretch	Asymmetric stretching vibrations of Si-O	OH bending vibrations	Out of plane bending mode of the Mg octahedra	Lattice vibrations	Peaks associated with weathered chrysotile fibers	
Untreated	3687.8	947.6	609	-	375.97	-	-
Carbonic acid	3690	955.64	608.5	432.97	300.35	-	-
Oxalic acid	3690	963.44	612.4	432.97	304.25	3381.8	1661.6
Hydrochloric acid	3690	951.74	603.5	436.8	300.3	-	-

3.3.2 Bulk elemental analysis

The amount of elements extracted was dependent on the strength (pK_a) and type of acid (chelating or non-chelating). Despite its higher pK_a value (1.0 vs. -6.3) oxalic acid was better than hydrochloric acid at extracting magnesium, chromium, aluminum, and iron (Table 3.3). This is likely because oxalic acid is a chelating acid, and hydrochloric acid is not. Hydrochloric acid was consistently the best extractor of nickel and zinc. Carbonic acid was a relatively poor extractor for all elements.

Treatment with oxalic acid removed ~ 15 % of the total magnesium from the sample, treatment with hydrochloric removed ~ 11 %, and treatment with carbonic acid removed ~ 1 %. I estimated the number of surface brucite layers that might be removed by treatment with the various acids by determining the dimensions of a magnesium octahedral layer, and the number of magnesium octahedra in 1 m^2 . Since each octahedra contains one magnesium ion, I converted this number to moles and then grams of magnesium in 1 m^2 of a surface brucite layer. The surface area in 1 g of high grade milled Cassiar chrysotile (specific surface) varies from $13 - 50 \text{ m}^2$ (Thom & Dipple 2005). Using a midrange value of 30 m^2 , I determined the grams of surface magnesium per gram of chrysotile. Assuming that 15706 mg/kg of magnesium was extracted by hydrochloric acid, we have 0.015 g of magnesium per gram of hydrochloric acid multiplied by 25 g of hydrochloric acid used in the experiment, which equals 0.393 g of magnesium in solution per monolayer of magnesium brucite. The value for carbonic acid is 0.038 g and oxalic acid is 0.522 g. These calculations indicate that approximately 1150 monolayers of brucite are dissolved by hydrochloric acid, 1500 by oxalic acid, and 100 by carbonic acid. It is important to note that the fibers do not weather evenly across surfaces, and that the edges and sides are weathered along with the surfaces. Thus, the calculation of surface layers removed is an estimate. However, since individual fibers are composed of approximately 40 layers (Bales 1984) and hydrochloric and oxalic acid are dissolving over a thousand layers, it appears these acids are dissolving entire fibers.

Table 3.3. Summary of the ICP elemental analysis data for untreated digested chrysotile and the effluent from chrysotile acid treatments. (bdl = below detection limit). (n=2).

Sample	Magnesium (mg kg⁻¹)	Chromium (mg kg⁻¹)	Nickel (mg kg⁻¹)	Aluminum (mg kg⁻¹)	Iron (mg kg⁻¹)	Zinc (mg kg⁻¹)
Untreated digested sample	147220	780	1200	2735	16961	32
Effluent from acid treatments						
Hydrochloric acid	15706	139	274	470	365	14
Oxalic acid	20868	327	69	914	8246	6
Carbonic acid	1498	bdl	4	164	bdl	6

3.3.3 Surface imaging

The scanning electron micrographs of the chrysotile fibers displayed a high degree of variation in the physical appearance of fibers within each sample. In general, the untreated (Figure 3.1), carbonic acid (Figure 3.2) and hydrochloric (Figure 3.3) treated fibers contained fibers that looked quite intact and unweathered. The oxalic acid (Figure 3.4) treated sample contained fibers that looked ragged and weathered. Many intact fibers were present in the acid treated fibers, sometimes adjacent to the weathered and broken fibers, indicating the high degree of variability within a sample. Based on the bulk elemental analysis data, the hydrochloric and oxalic acid treatments removed over a thousand brucite layers and likely dissolved entire fibers, however, intact fibers existed in these samples. Gronow (1987) also found that fibers which had undergone acid dissolution produced little evidence of changes at the surface of the mineral, and that leaching reactions occurred at discrete sites rather than in uniform layers. This variability within one sample, and between adjacent fibers, is important to consider in the use of ToF-SIMS analysis, which looks at a relatively small area ($1600 \mu\text{m}^2$) of a fibers surface.

Figure 3.1. FESEM image depicting a bundle of untreated chrysotile fibers magnified 3000X.

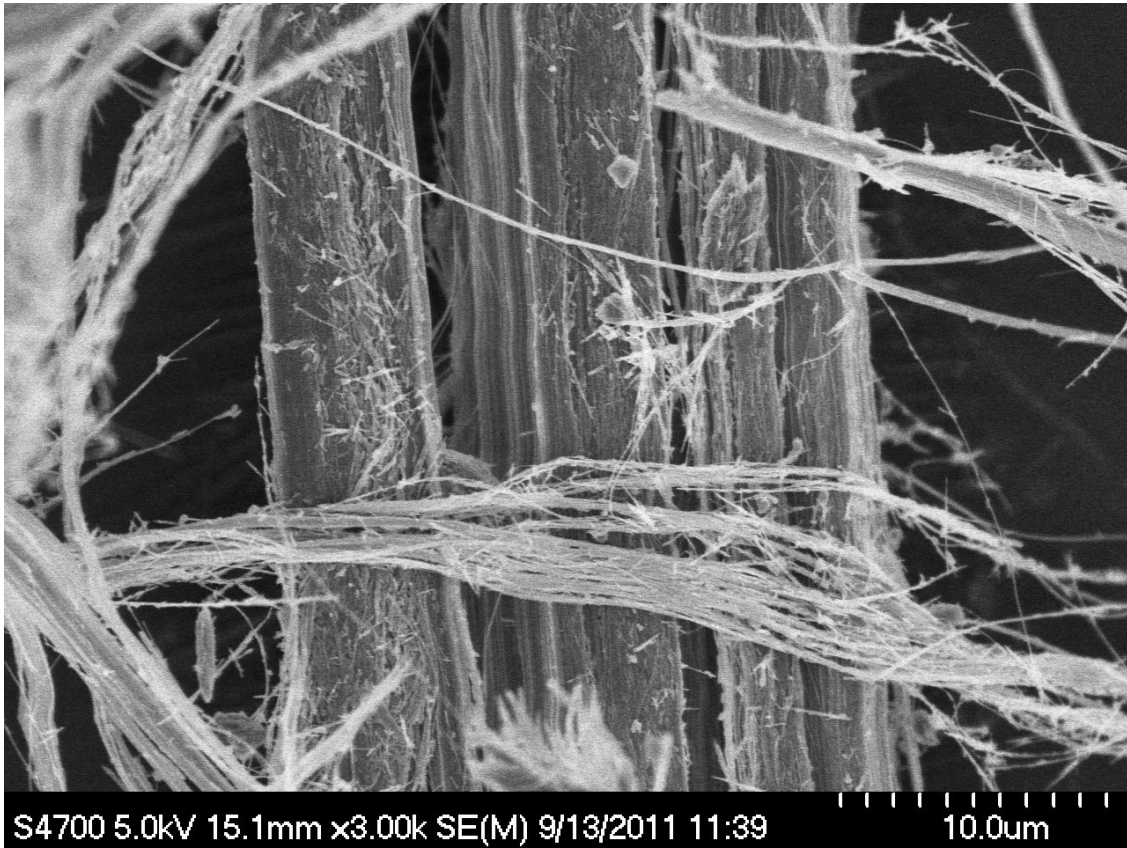


Figure 3.2. FESEM image depicting a bundle of carbonic acid treated chrysotile fibers magnified 3000X.

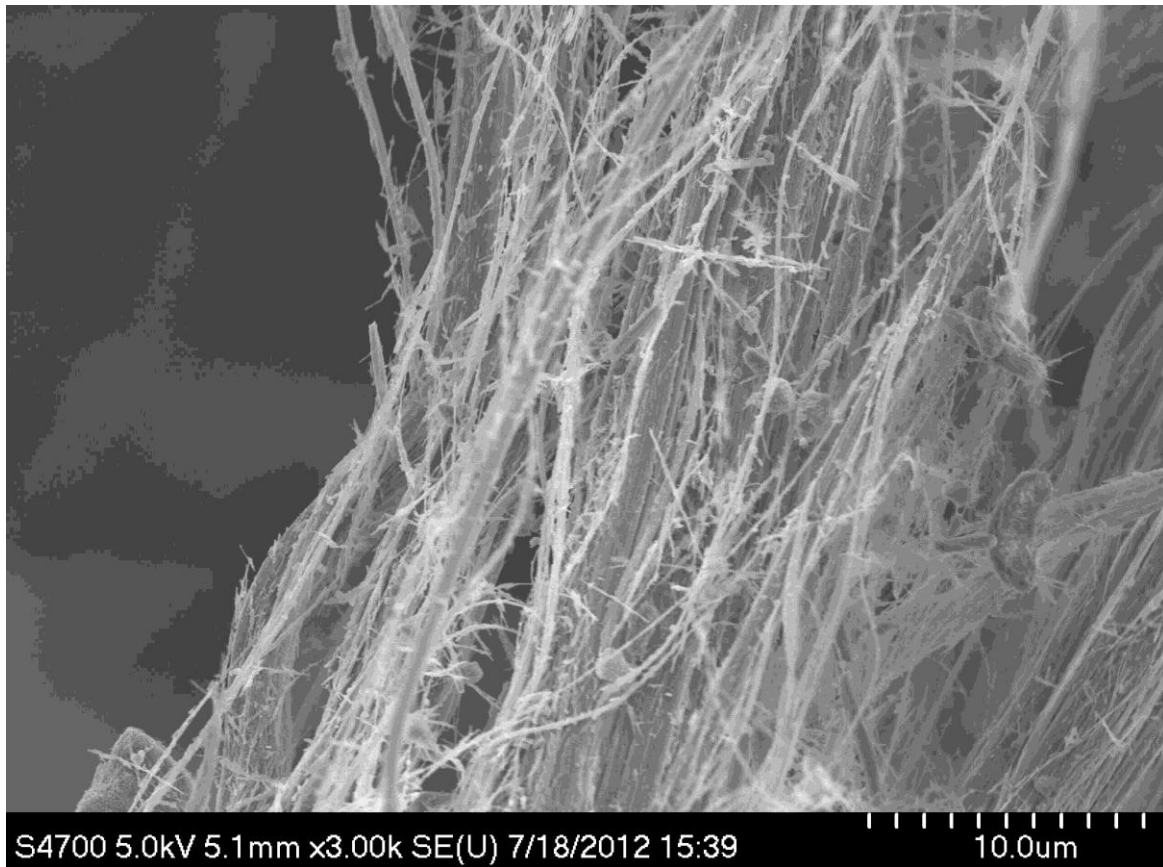


Figure 3.3. FESEM image depicting a bundle of hydrochloric acid treated chrysotile fibers magnified 3000X.

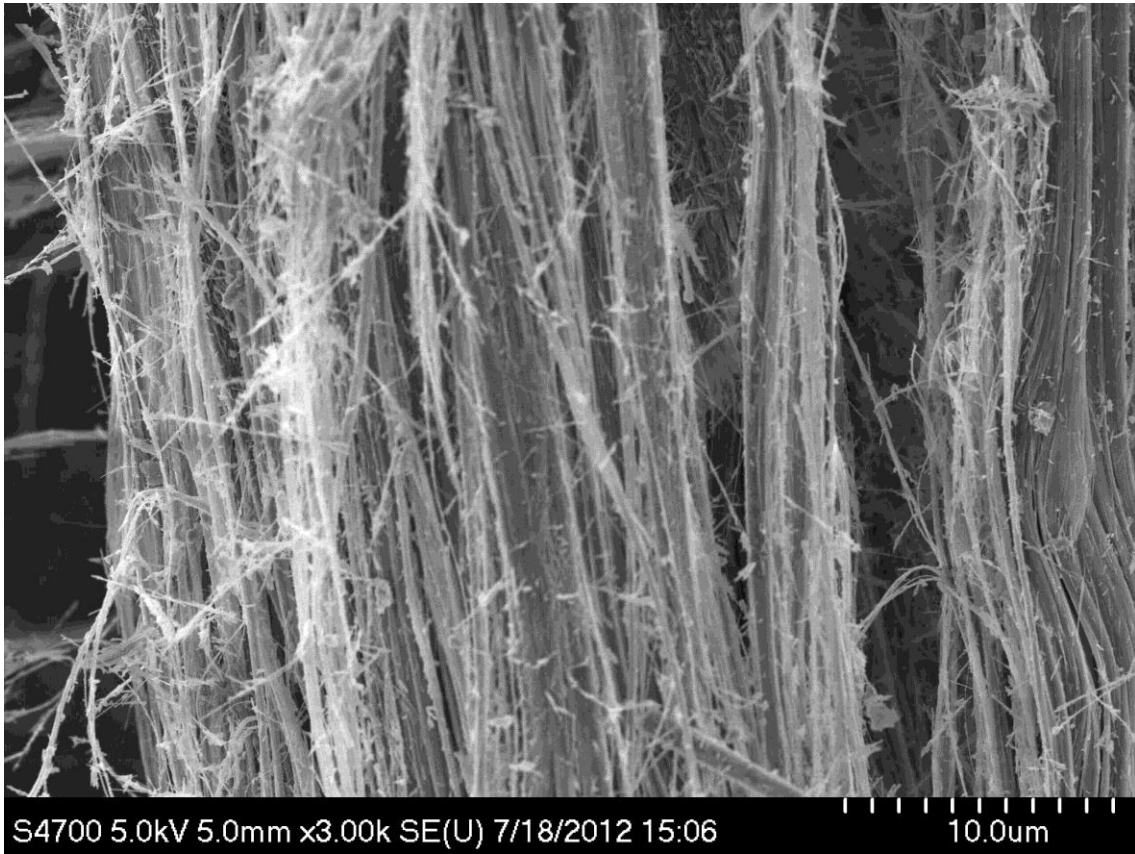


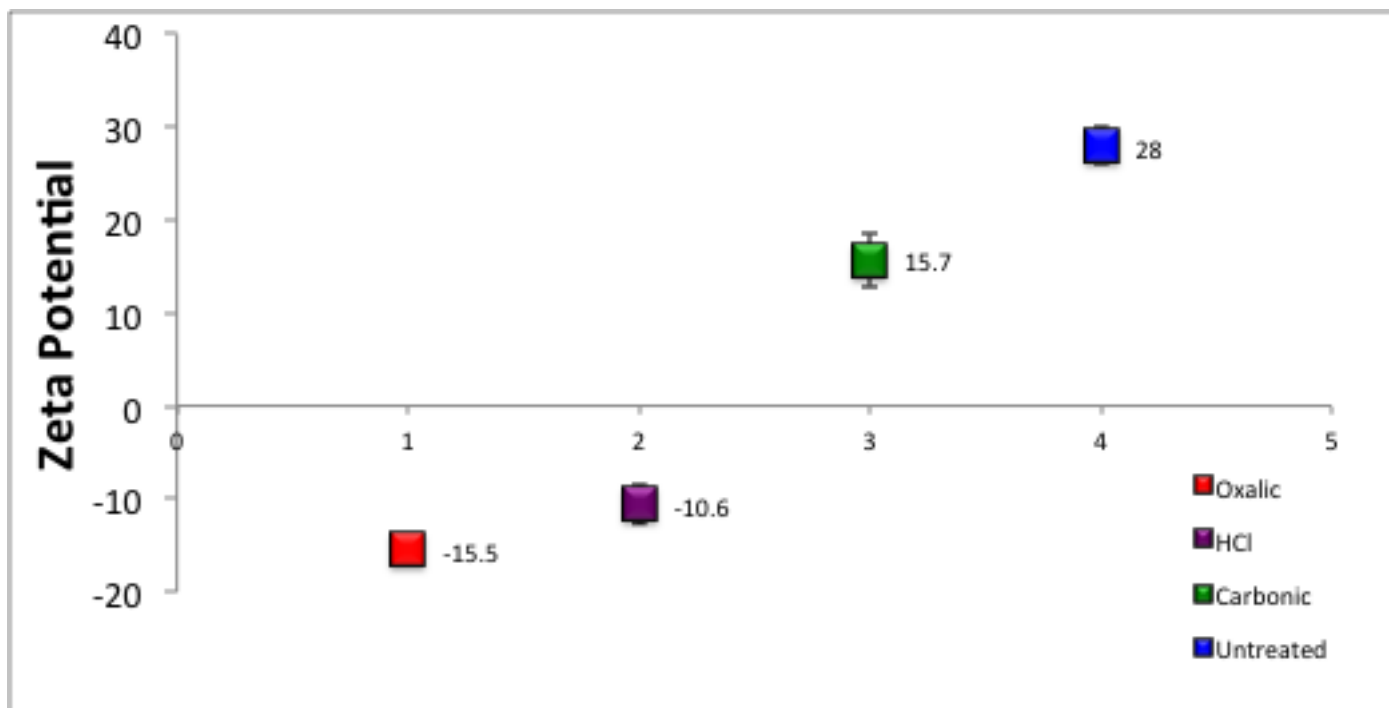
Figure 3.4. FESEM image depicting a bundle of oxalic acid treated chrysotile fibers magnified 3000X.



3.3.4 Surface charge

Treatment with simple acids changed the surface charge from positive to negative. (Figure 3.5). Treatment with oxalic acid resulted in the lowest surface charge (-15.5) and treatment with hydrochloric acid the second lowest (-10.6). Treatment with carbonic acid resulted in a lower surface charge (+15.5) than the untreated fiber (+28). These results are consistent with the elemental analysis showing oxalic and hydrochloric acid removed the most magnesium and heavy metals from the bulk chrysotile samples. The literature states that it is the surface brucite layer that results in a positive charge, and thus the negative surface charge in the oxalic and hydrochloric acid treated samples indicate that these treatments likely altered the surface composition of the fibers, resulting in a silica enriched surface compared to that of an untreated fiber.

Figure 3.5. Zeta Potential values for untreated and acid treated chrysotile samples. Error bars represent standard deviation values. (n=5).



3.3.5 ToF-SIMS

Treatment with simple acids altered the magnesium brucite layer on the surface of the fiber, resulting in a lower magnesium silica surface ratio than the untreated fiber (Figure 3.6). Treatment with oxalic acid resulted in the lowest magnesium silica surface ratio (0.74) and treatment with hydrochloric the second lowest (10.06). Treatment with carbonic acid resulted in an only slightly lower magnesium silica surface ratio (19.77) than the untreated fiber (24.95). Standard deviation of these data are represented by the error bars. No standard deviation values exist for the oxalic acid treated sample due to the lab providing 2 readings for that sample, compared to 5 for all other samples. These results support the results of zeta potential analysis. Treatment with oxalic and hydrochloric acid treatment resulted in a silica-enriched surface, compared to the untreated fibers, which was expected based on their negative surface charge.

Figures 3.7 and 3.8 are three-dimensional ToF-SIMS images of the measured area of an untreated chrysotile sample. Figure 3.7 depicts the top, or the surface area (X and Y), of the chrysotile fiber and Figure 3.8 shows the side, or depth (Z), of the chrysotile fiber. The Z axis in Figure 3.8 is not to scale, and was blown up ~ 10,000 times to make it similar in dimension to the X and Y axis so that the features are visible. Although silica was measured in the fibers, it is not present in the images because of the relative signal strength of magnesium, which dominates the surface on all of the fibers except the oxalic acid treated sample. Due to magnesium masking silica in the samples, it was determined these images are less useful than the two-dimensional images in which silica and magnesium are represented separately. See appendix B for the complete set of 3D ToF-SIMS images.

Figure 3.9 is a two-dimensional representation of the magnesium and silica measured in a 1600 um^2 area and 2 nm depth of untreated and acid treated chrysotile. In the untreated and carbonic acid treated samples, there is more magnesium than silica, indicating an intact surface brucite layer and only moderate weathering. This is expected since treatment with carbonic acid only removed 1 % of the samples magnesium, and the surface charge as measured by zeta potential is high, which indicates that the brucite layer is intact and that very moderate weathering has affected the fiber. The images of the hydrochloric acid treated samples also show there to be much more magnesium than

silica; approximately 10 times more based on the magnesium silica ratio. The images of the oxalic acid treated sample shows a similar amount of magnesium and silica, which is consistent with the 0.74 magnesium to silica ratio. Both acids are strong and removed a high amount of magnesium from the bulk mineral, indicating entire fibers were dissolved. The differences in the surface chemistry can be explained by the fact that oxalic acid is a chelating acid and preferentially removes magnesium and associated heavy metals from the brucite layers of the fiber, resulting in a silica enriched surface compared to the other samples.

Figure 3.6. The Mg:Si of untreated and acid treated chrysotile fibers. Error bars represent the standard deviation. (n=5). No standard deviation data for oxalic acid treated fibers.

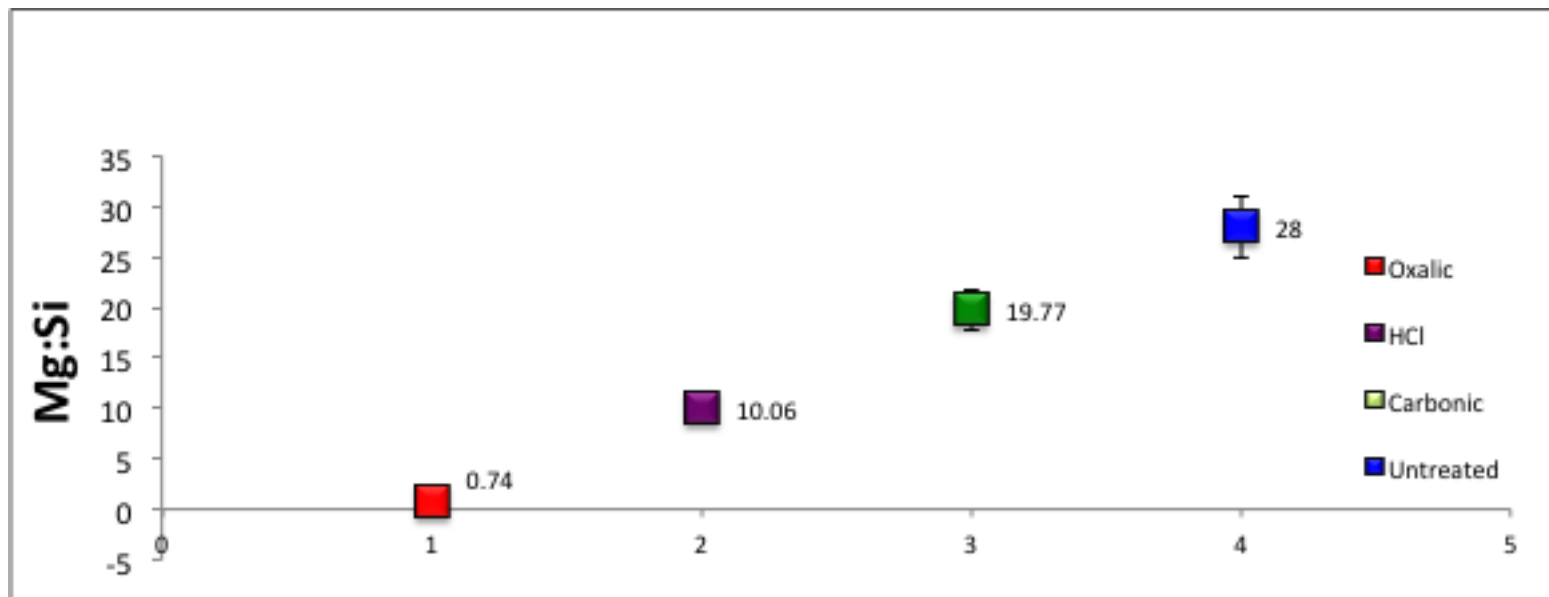


Figure 3.7. ToF-SIMS image of the surface area ($\approx 1600 \mu\text{m}^2$; $X=400 \mu\text{m}$, $Y=400 \mu\text{m}$) of an untreated fiber. Green = Mg, Blue = Si, and Red = Al.

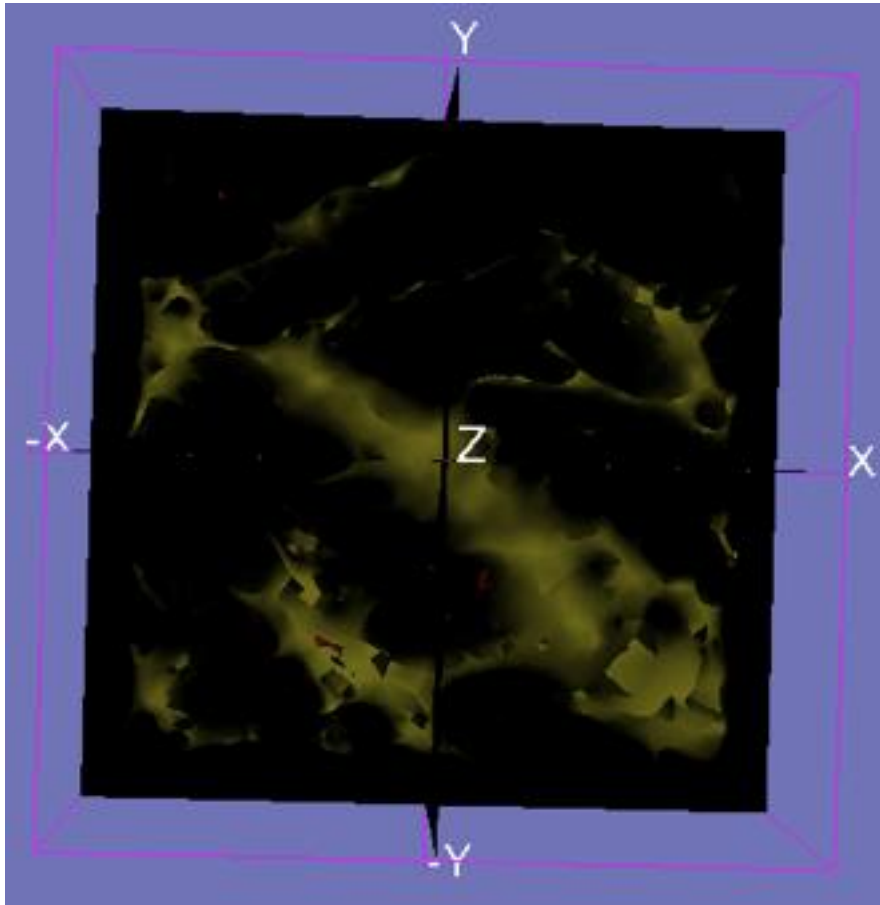


Figure 3.8. ToF-SIMS image of the depth view of an untreated chrysotile fiber.
Surface area = $1600 \mu\text{m}^2$; X=400 μm , Y=400 μm and depth of analysis (Z) is 2 nm.
The Z axis is blown up $\sim 10,000\times$ to make features visible. Green = Mg, Blue = Si,
and Red = Al.

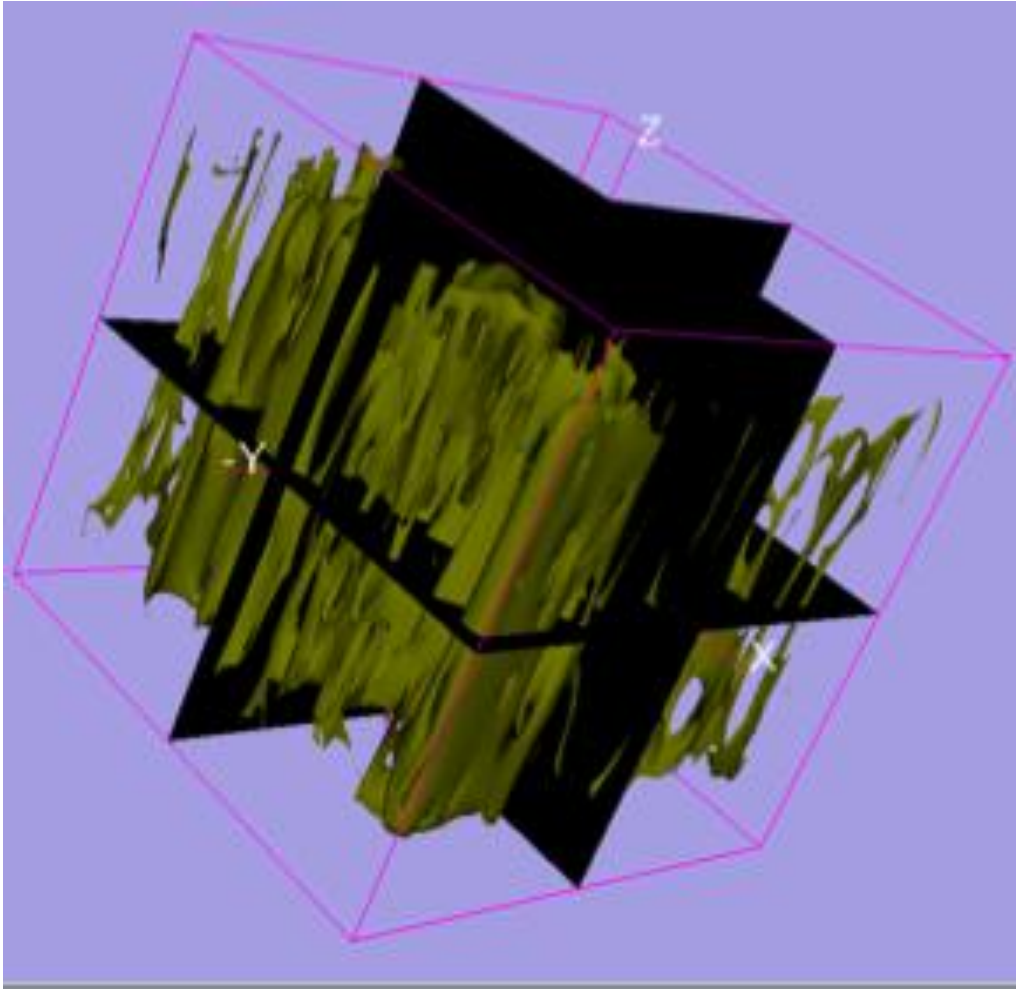
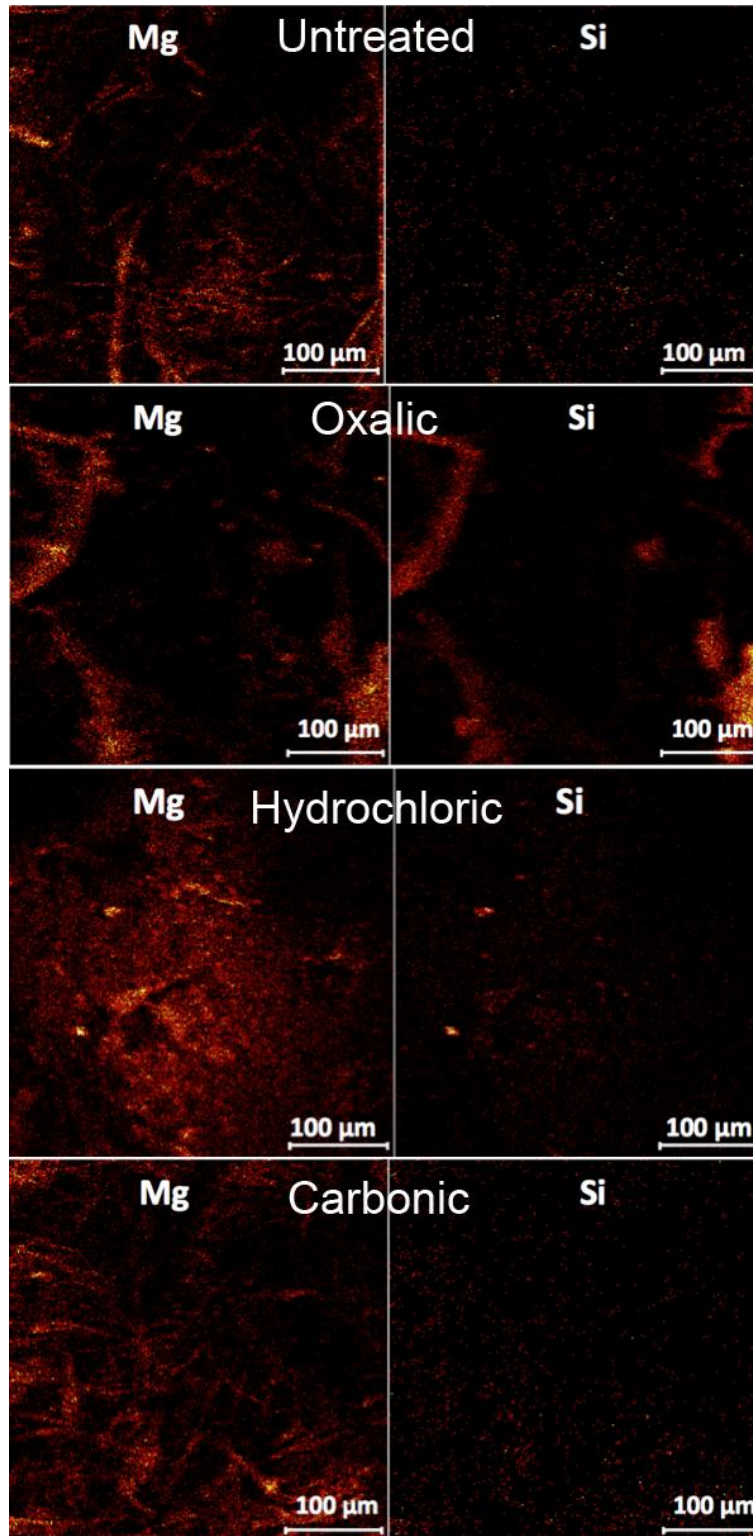


Figure 3.9. ToF-SIMS images of the magnesium and silica ions on the surface of the untreated and acid treated chrysotile fibers. Surface area = 1600 μm^2 ; X=400 μm , Y=400 μm and depth of analysis (Z) is 2 nm.



3.3.6 Comparisons between techniques

Figure 3.11 compares the zeta potential values with the magnesium silica ratio values for each sample. The data shows a positive correlation between surface charge and surface composition, as expected based on previous research (Bales 1984). Samples with low magnesium to silica ratio values demonstrated negative zeta potential values, whereas samples with high magnesium silica ratios had positive zeta potential values.

Figure 3.12 compares the bulk magnesium values of the acid treated samples after the leaching experiment with the surficial magnesium silica ratios. The oxalic acid and hydrochloric acid treated samples have both low magnesium silica ratios (0.74 and 10.06) and ICP-MS total magnesium values (122,200 ppm and 130,328 ppm), and the carbonic acid treated sample and the untreated sample have high magnesium silica ratios (19.77 and 24.95) and ICP-MS total magnesium values ($145,708 \text{ mg kg}^{-1}$ and $147,200 \text{ mg kg}^{-1}$). This correlation between bulk magnesium and surface magnesium indicates that as magnesium is removed from the bulk mineral, it is stripped from the surface layer. The comparison between the bulk magnesium values and zeta potential values (Figure 3.13) shows a similar correlation. The oxalic acid and hydrochloric acid treated samples had lower bulk magnesium values and lower zeta potential values than the carbonic acid treated and untreated samples indicating that as the fibers are weathered, magnesium is leached, lowering the surface charge.

Despite a slightly higher pH than hydrochloric acid (pH=1.44), oxalic acid (pH=1.76) was the best extractant of the majority of the elements as demonstrated by ICP-MS, and resulted in the greatest degree of surface weathering as demonstrated by the FESEM and ToF-SIMS analysis. This is because oxalic acid is a chelating acid, which enables it to preferentially remove magnesium and metal cations. Carbonic acid had a higher pH than the other two acids (pH = 2.96), which may explain why it is a relatively poor extractant. All three treatments had a much lower pH values than the untreated sample (7.70) (Figure 3.14).

Figure 3.10. Mg:Si vs. Zeta Potential for untreated and acid treated chrysotile fibers. Error bars represent standard deviation for Mg:Si and Zeta Potential. (n=5). No Mg:Si standard deviation data for the oxalic acid treatment.

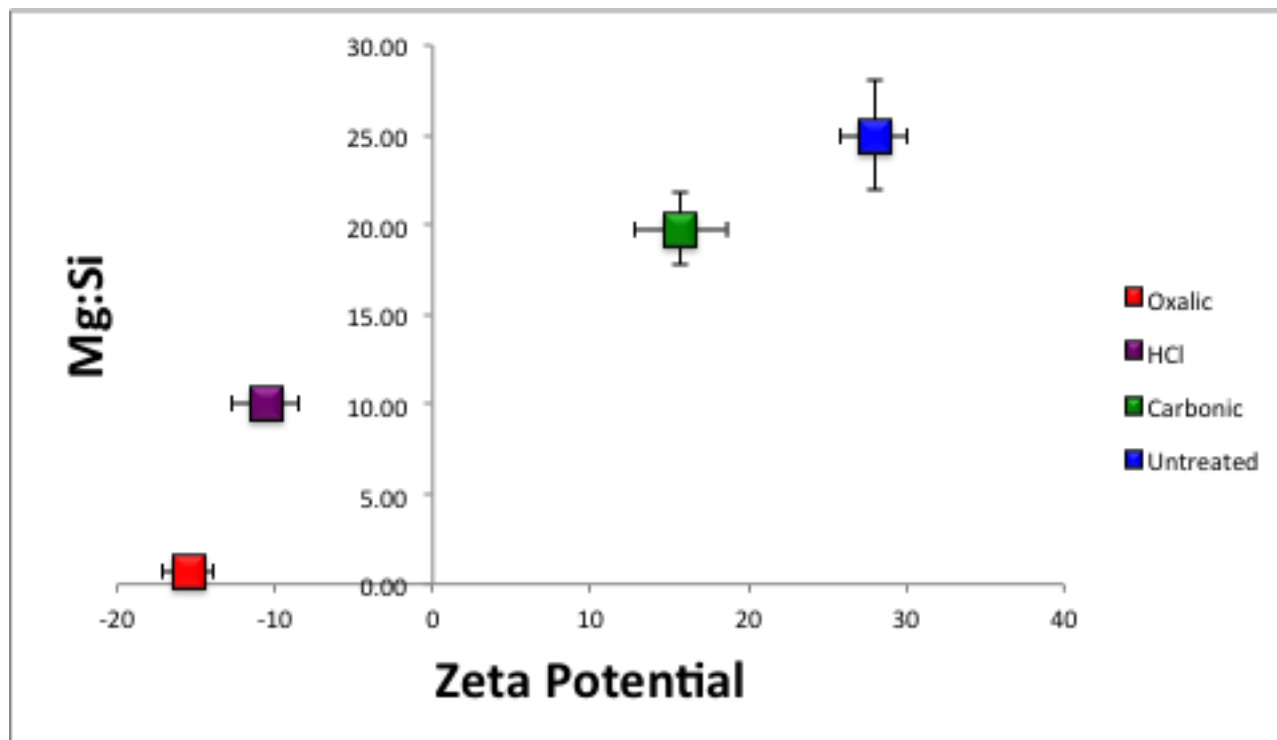


Figure 3.11. Mg (ppm) of the bulk mineral after acid treatment vs. Mg:Si for untreated and acid treated chrysotile fibers. Error bars represent standard deviation of the Mg:Si values. (n=5). No Mg:Si standard deviation data for the oxalic acid treatment.

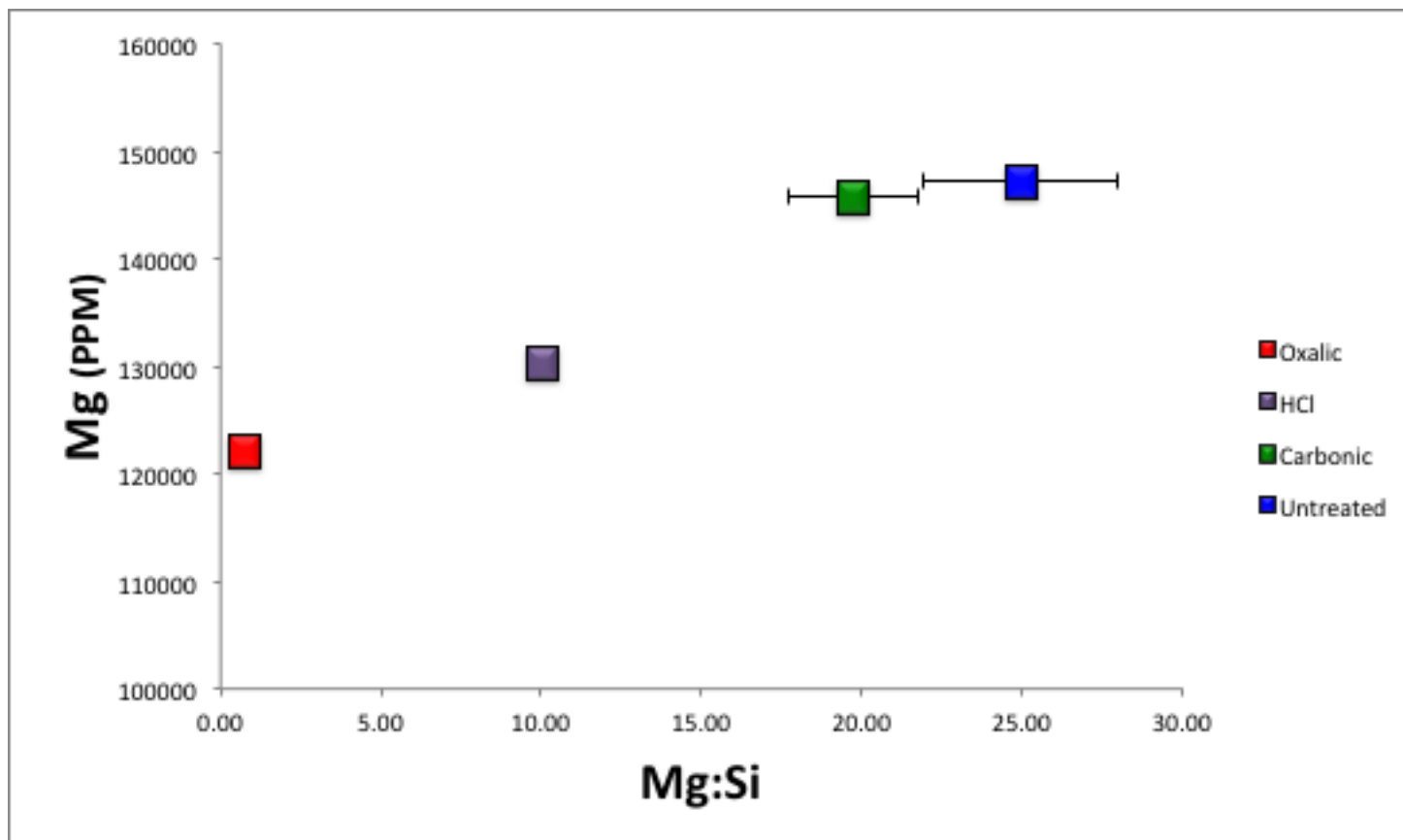


Figure 3.12. Mg (ppm) vs. Zeta Potential for untreated and acid treated chrysotile fibers. Error bars represent standard deviation of the Zeta Potential values. (n=5).

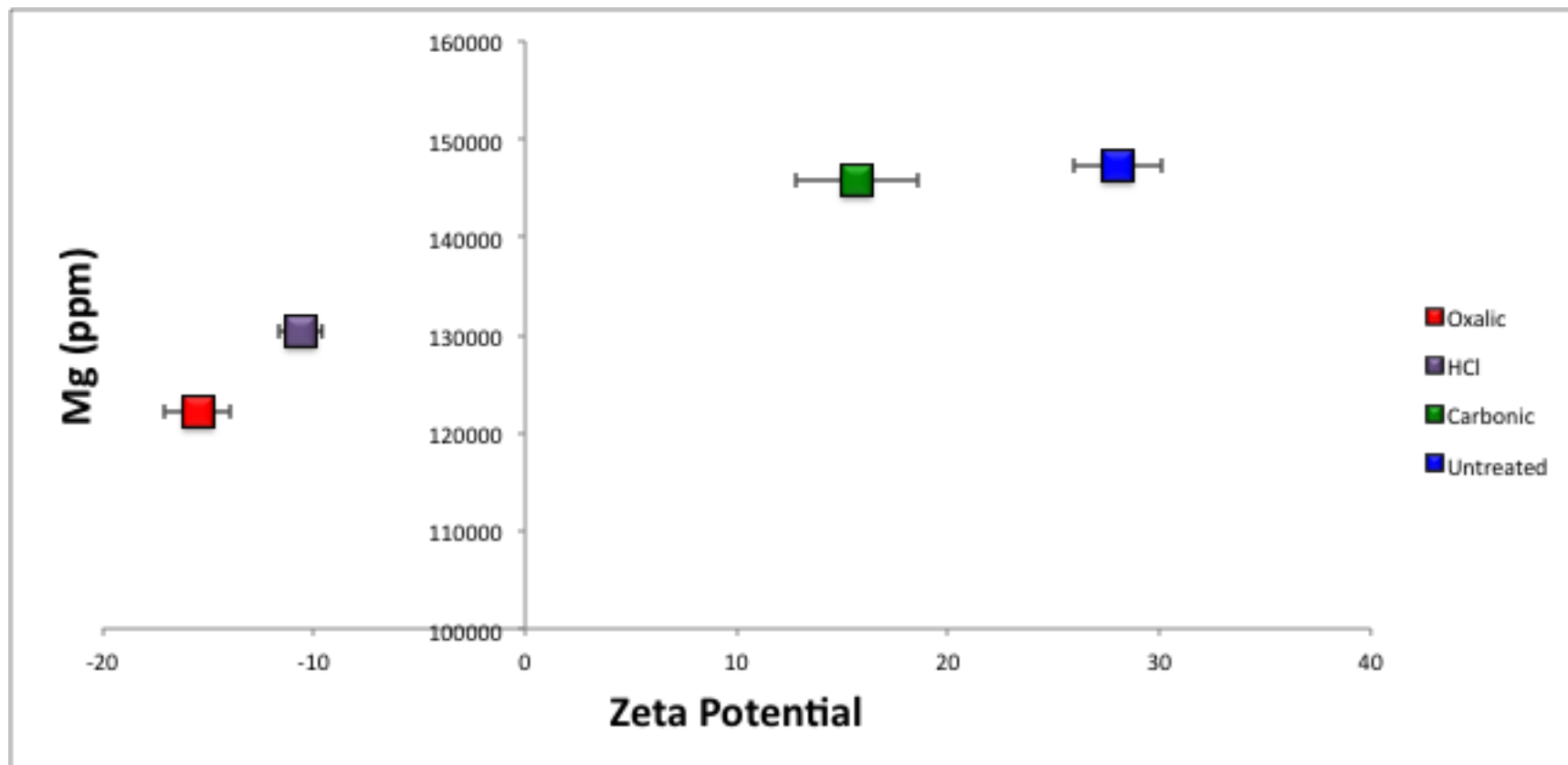
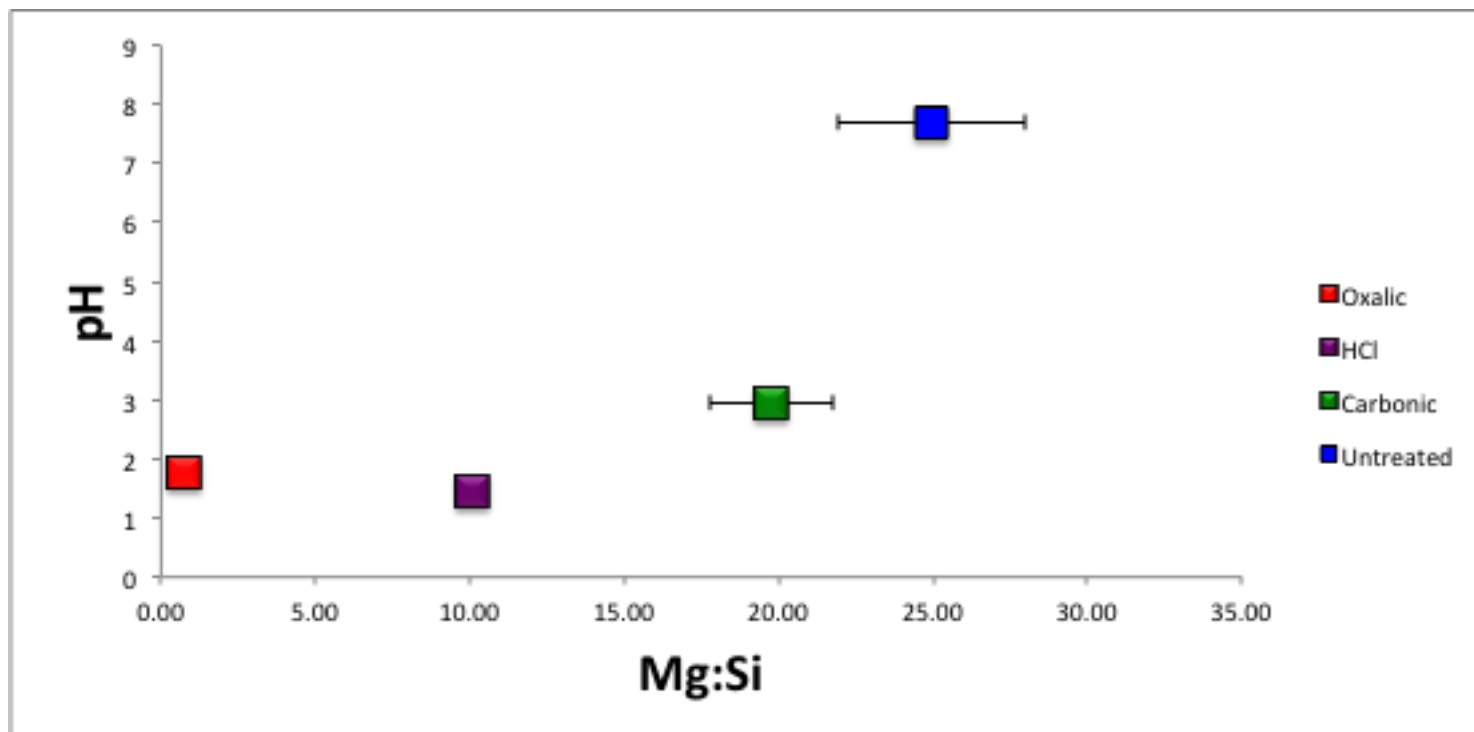


Figure 3.13. pH vs. Mg:Si for untreated and acid treated chrysotile fibers. Error bars represent standard deviation of the Mg:Si values. (n=5). No Mg:Si standard deviation data for the oxalic acid treatment.



3.4 Conclusions

Oxalic acid, a strong chelating acid, was the most effective at extracting the majority of elements present in chrysotile fibers. It also was the most effective at removing magnesium from the bulk sample and reducing the surface charge of the chrysotile fibers. Oxalic acid was the only treatment to produce visible changes at the surface of the fibers, as witnessed by FESEM work, and to show signs of being weathered as imaged by FTIR analysis. The effectiveness of oxalic acid as a weathering agent can be credited to the fact that it is a chelating acid. Hydrochloric acid was the second most effective at extracting elements from the bulk sample, reducing the concentration of surface magnesium, and reducing the surface charge. Based on the previous research findings that negative surface charge and low magnesium silica surface ratios cause fibers to be less toxic, it is likely the fibers treated with oxalic and hydrochloric acid are less hazardous from a human health perspective. The significance of the oxalic acid treatments is that oxalic acid is ubiquitous in the weathering environment and thus is an effective acid for naturally occurring chrysotile asbestos surface modification and amelioration.

Fibers treated with carbonic acid appeared to have the least effect on surface properties and were the most similar to the untreated fibers. The brucite layer was largely intact and the surface charge was positive. The intact brucite layer of the untreated and carbonic acid treated fibers indicates it could be the slow dissolution of magnesium that is the rate limiting step for the mineral carbonation reaction.

The results of zeta potential analysis, a surface specific technique measured on a bulk sample, are supported by ToF-SIMS analysis, a very fine scale surface specific technique measuring a small area of one fiber. Zeta potential analysis is much less expensive and time consuming to carry out than is ToF-SIMS. It also measures the surface characteristics of a larger sample, approximately 0.5 g compared to 1600 μm^2 , which enables it to better account for the variability within a sample.

Chapter 4 : Bulk and Surface Properties of Environmentally Exposed Chrysotile Samples

4.1 Introduction

Chapter four builds on the work presented in chapter three towards understanding the processes and changes in surface composition of chrysotile asbestos in order to predict the reaction processes and change of mineral properties during weathering. This chapter presents work exploring the effects that weathering processes, occurring in the natural environment, have on chrysotile fibers by examining the bulk and surface chemistry of naturally occurring chrysotile samples from the Sumas River watershed and chrysotile mine tailings from Cassiar, B.C. Comparisons are made between the bulk and surface properties of the laboratory treated and naturally occurring samples.

4.2 Materials and Methods

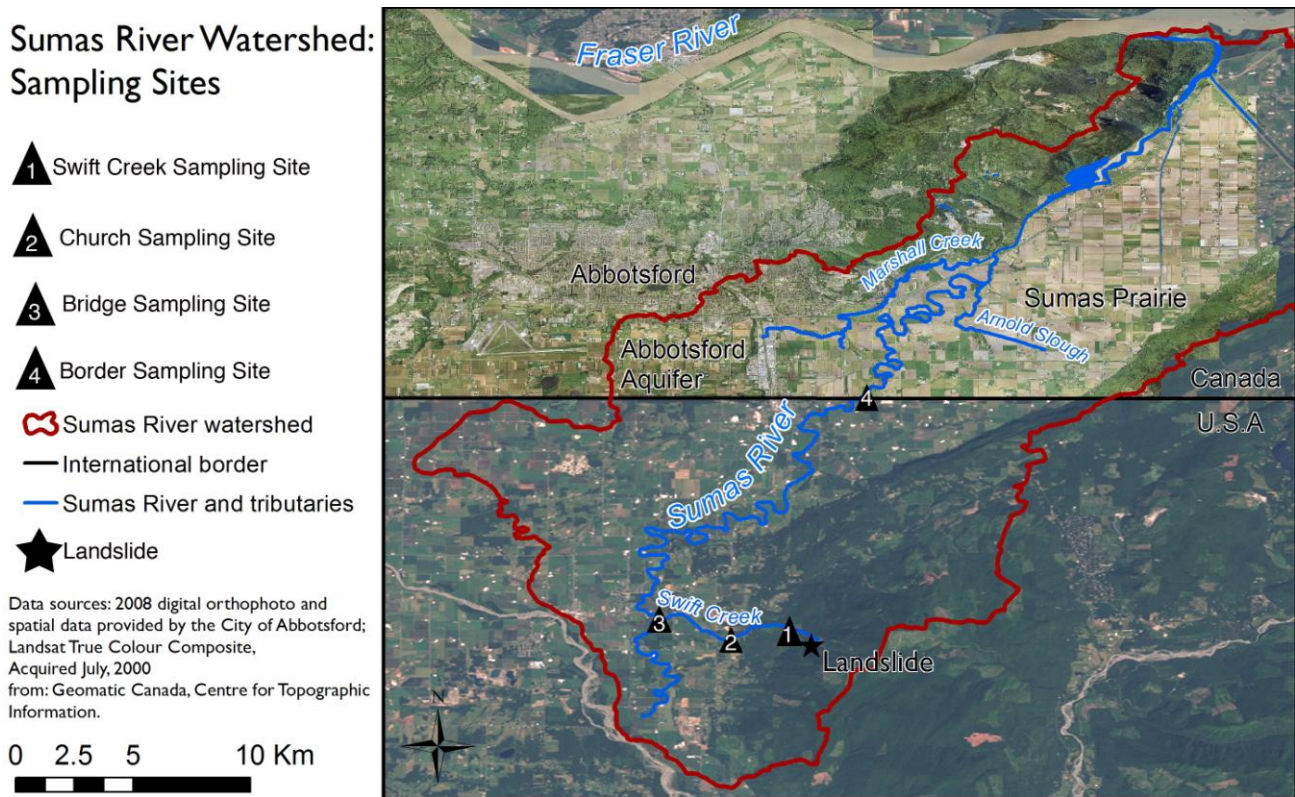
4.2.1 Materials

4.2.1.1 Suspended sediment samples

Suspended sediment samples were collected from four locations along the Sumas River (Figure 4.1) using a time-integrated suspended sediment sampler (Phillips et al. 2000). The samples were collected on November 26th, 2011, after the samplers had been collecting sediment for 12 days. The contents of the samplers were emptied into 4 L acid washed Nalgene bottles and transported to the laboratory on ice in a cooler.

In the laboratory, the sediment samples were wet-sieved through stainless steel sieves in order to obtain the <63 μm fraction, which includes both silt and clay particles. This size range represents the fraction of sediment that is transported in suspension, and contains the greatest concentration of chrysotile asbestos fibers. The sieved sediment was placed in acid-washed beakers, which were oven dried at 70°C overnight. Once fully dried, the beakers were allowed to cool for 30 minutes. An agate mortar and pestle was used to break apart large aggregates of the dried sediment and the samples were stored in sealed labeled plastic containers until analysis.

Figure 4.1. Map of Sumas River Watershed, including sampling sites.



4.2.1.2 Mine tailings

Three mine tailing samples were obtained from Cassiar Mine, British Columbia, Canada in 2003. Two samples were taken from the flanks of the tailing piles at 10 cm (14-1) and 1 m (16-1) depth, and one taken from inside a large storage shed adjacent to the tailing pile (17-1).

4.2.2 Bulk mineral analysis

4.2.2.1 XRD

The samples were ground using an agate mortar and pestle and smear-mounted with anhydrous ethanol on glass plates. XRD data were collected using a Bruker D8 Focus Bragg-Brentano diffractometer with $\text{CoK}\alpha$ radiation and a step size of 0.04° over a range of $3\text{--}80^\circ 2\theta$ at 0.9s/step . Fe monochromator foil, 0.6 mm divergence slit, incident and diffracted beam slits, and a Lynx Eye detector were used. A long fine focus CO X-ray tube was operated at 35 kV and 40 mA using a take-off angle of 6° . A rotation speed

of 50 rpm was used. Search-match software by Bruker (DIFFRACplus EVA 16) was used for phase identification. Crystal structure data were obtained from the International Centre for Diffraction Database PDF-4+ 2010.

4.2.2.2 ATR FTIR

ATR FTIR spectroscopy was used to analyze the mineral surface composition. Infrared absorbance occurs in the region where the sample contacts a crystal of high refractive index, enhancing the signal of the surface over that of the bulk mineral (Kubicki et al. 1999).

FTIR Spectroscopy of the environmental samples and pure carbonate samples (hydromagnesite, magnesite, pypingite, and mesqueonite) was done on a Perkin Elmer Spectrum 100 FTIR Spectrophotometer with a universal ATR sampling accessory, and a diamond coated KRS5 thalium plate. Analysis software by Perkin Elmer (Spectrum version 10) was used for peak analysis.

4.2.3 Bulk elemental analysis

The environmental samples were prepared for elemental analysis using aqua regia digestion method for elements outlined in Martin (et al. 1991). A summary of the Aqua regia method is as follows: approximately 0.5 g of the dried sample is combined with 12 mL of aqua regia and heated. The solutions were then filtered through a Whatman #42 filter, brought to volume with 2 % HNO₃, and stored in plastic bottles that were refrigerated. The filtrate from the acid experiment and the digested acid treated and untreated samples were analyzed for total elements using Inductively Coupled Plasma Atomic Emission Spectroscopy (ICP-MS) Varian 725-ES. Duplicates were analyzed for each sample, and the samples were repeated if the duplicate results varied by more than 25 %.

4.2.4 Surface charge

Surface charge was measured using a Zeta Meter Model 3.0+ (Zeta Meter Inc. USA) in Mining Engineering at the University of British Columbia. Fifty mg of each sample was transferred into 15 ml of distilled water and shaken by hand for 30 seconds. All the measurements were carried out within 30 seconds of being shaken. The applied voltage was determined based on the specific conductivity of the solution. The particle movement was observed through a microscope and the time taken for a particle to travel the distance of a micrometer was measured. To minimize error, a minimum of five particles were tracked and their average time was calculated.

4.2.5 ToF-SIMS

ToF-SIMS was conducted in the Advanced Materials and Process Engineering at UBC. In preparation for ToF-SIMS measurement, each sample in its powder form was mounted onto a piece of silicon wafer using a double sided tape. ToF-SIMS measurements were performed with a PHI TRIFT V nanoTOF instrument using Au_1^+ gun operated at 30 keV with an aperture size of 100 μm ; current measured at the primary column was ~ 0.5 nA. Materials with fiber characteristics were looked for and analyzed. Positive spectra were acquired from 1,600 μm^2 surface area ($X = 400$ μm and $Y = 400$ μm) at a depth of 2 nm ($Z = 2$ nm) for a duration of ~ 12 min where the total ion dose was less than 10^{12} ions cm^{-2} . Charge compensation was accomplished during spectrum acquisition using 10 eV electrons. Mass resolution ($m/\Delta m$) for the $^{28}\text{Si}^+$ peak was around 8000. Spectra were calibrated with the known masses associated with peaks for the species H^+ , Mg^+ , CH_3^+ , CH_3H_5^+ . Three-dimensional and two-dimensional images were created to visually represent the data. The three-dimensional images are not to scale, with the depth (2 nm) axis blown up 100,000 times to make it visible. Samples that had a composition not consistent with chrysotile (ie. high aluminum) were removed from the data set.

4.3 Results and Discussion

4.3.1 Bulk mineral analysis

4.3.1.1 XRD

XRD patterns identify the samples as being predominantly composed of chrysotile, and lizardite. Due to overlap and fit of pattern, antigorite may also be present. Swift Creek, Church, and the Border samples contained minor peaks (<50 % intensity of major peaks) of quartz and trace peaks (<10 % intensity of major peaks) of clinocllore. All of the sediment samples contained sjorgrenite magnetite, albite, biotite, and talc. The mine tailing samples all contained minor sjogrenite and magnetite peaks. Sample 17-1 also contained trace biotite and talc. Table 4.1 outlines the peaks associated with each sample. All of the samples displayed a high degree of heterogeneity, which was kept in mind when analyzing techniques that measure bulk samples, such as ATR-FTIR, elemental analysis, and surface charge. The heterogeneity also made ToF-SIMS analysis more difficult, because it increased the chance of something other than a chrysotile fiber being measured. See Appendix A for a complete XRD patterns.

Table 4.1. Summary of XRD peaks for suspended sediment samples from the Sumas River watershed and mine tailings from Cassiar, BC. M = major peak, Mi = minor peak (<50 % of major peak), and T = trace (<10 % major peak).

Sample	Serpentine (Chrysotile, Lizardite, Antigorite)	Quartz	Clinochlore	Sjorgrenite	Magnetite	Albite	Biotite	Talc
Sediment								
Swift Creek	M	Mi	T	T	T	T	T	T
Church	M	Mi	T	T	T	T	T	T
Bridge	M	T	Mi	T	T	T	T	T
Border	M	Mi	T	T	T	T	T	T
Mine tailings								
14-1	M			Mi	Mi			
16-1	M			Mi	Mi			
17-1	M			Mi	Mi		T	T

4.3.1.2 ATR FTIR

The three mine tailing samples, and the Swift Creek sediment exhibited typical chrysotile IR spectra. The IR spectrum of chrysotile exhibits three well-defined spectral groups in the 3800-3600 cm^{-1} region, the 1200-800 cm^{-1} region, and less than 800 cm^{-1} region (Anbalagan et al. 2008). Table 3.3 outlines the peaks, and characteristics causing the peaks, for each of the samples. All samples displayed the broad 3680-3690 cm^{-1} peaks associated with in phase outer Mg-OH stretching of chrysotile fibers (Anbalagan et al. 2008), the 940-960 cm^{-1} peaks associated with asymmetric stretching vibrations of Si-O bonds in chrysotile fibers (Suquet 1989; Yariv & Heller-Kallai 1973), and the 603-610 cm^{-1} peaks associated with OH bending vibrations in chrysotile fibers (Anbalagan et al. 2008; Bishop et al. 2002). The sediment sample has a 543 cm^{-1} peak indicating out-of-plane bending of the Si-O (Suquet 1989). Two of the mine tailing samples displayed the 432 – 438 cm^{-1} peaks associated with out of plane bending of the Mg octahedral (Suquet 1989) and the sediment sample and the other mine tailing sample display 300-400 cm^{-1} peaks associated with lattice vibrations of Mg-O bending. These peaks indicate the basic chrysotile structure is intact (Suquet 1989). Peaks at 3381 cm^{-1} and 1661.6 cm^{-1} indicate the presence of some hydrated, noncrystalline silica in the sample due to weathering of the fibers (Suquet 1989). None of the sediment or mine tailing samples displayed these peaks.

Pure samples of hydromagnesite, pypingite, nesquetonite, and magnesite displayed peaks in the 875 cm^{-1} and 1420 cm^{-1} range, which is consistent with other FTIR carbonate studies (Rehman & Bonfield 1997; Suquet 1989). None of the environmental chrysotile samples displayed peaks in this range.

Table 4.2. Summary of ATR-FTIR spectra for Swift Creek suspended sediment from the Sumas River watershed and mine tailings from Cassiar, BC.

Sample	In phase outer Mg-OH stretch	Asymmetric stretching vibrations of Si-O	OH bending vibrations	Out of plane bending of the Si-O	Out of plane bending mode of the Mg octahedra	Lattice vibrations
Swift Creek Sediment	3688.3	940.3	608.4	543.29	543.29	366.3
Mine tailing 14-1	3690.00	951.74	612.40	-	-	386.16
Mine tailing 16-1	3682.10	947.84	616.30	-	436.87	-
Mine tailing 17-1	3693.80	963.40	608.50	-	436.87	-

4.3.2 Bulk elemental analysis

In the sediment samples, magnesium, nickel, and iron decrease downstream, due to the dilution of the asbestos containing sediment. This trend is supported by the data in chapter 2. Aluminum, chromium, and zinc remain relatively constant. In the mine tailing samples, 14-1 has the highest values for all the elements except zinc, and 17-1 has the lowest values. See Table 4.3 for a summary of the elemental analysis data. As expected, the environmental samples had a much higher degree of variability than the acid treated samples in chapter 3. The original goal of having duplicates within ten percent of one another was changed to twenty-five percent, which is consistent with other environmental studies (BC Ministry of Environment 2005)

Table 4.3. Summary of the ICP elemental analysis data for suspended sediment samples from the Sumas River watershed and mine tailings from Cassiar, BC.

Sample	Magnesium (mg kg⁻¹)	Chromium (mg kg⁻¹)	Nickel (mg kg⁻¹)	Aluminum (mg kg⁻¹)	Iron (mg kg⁻¹)	Zinc (mg kg⁻¹)
Sediment						
Swift Creek	167662	235	1593	5032	44538	47
Church	157262	188	1791	4718	49367	63
Bridge	153812	161	1406	3375	33717	43
Border	146187	205	1395	5182	36774	53
Mine Tailings						
14-1	222411	278	323	618	8133	30
16-1	202408	207	266	487	7128	53
17-1	139118	44	158	598	2440	40

4.3.3 Surface charge

The surface charge of the suspended sediment samples decreases downstream from +17.6 at Swift Creek, to ~+12.5 at the following three sampling stations. There is considerable variability in the surface charge of the mine tailing samples, ranging from +1.7 in sample 14-1, the most weathered of the samples, +6.34 in the sample stored in the shed and subjected to moderate weathering, and +30.96 in the sample taken from a 1 m depth in the tailings, and likely highly protected from weathering environments (Table 4.4). These results are consistent with Bales (1984) in that fibers that had spent more time in weathering environments had a less positive surface charge. The environmental samples all contained minerals other than chrysotile and were subject to factors that can affect the zeta potential, such as adsorption of NOM, different pH environments, and differing concentrations of complexing cations (Bales 1984; Martinez & Zucker 1960). None of the environmental samples had negative surface charge values, as we saw with the oxalic acid and hydrochloric acid treated samples, indicating the environmental samples experience much less weathering than that simulated by the laboratory treatments.

Table 4.4. Comparison of the Zeta Potential and Mg:Si values of the suspended sediment, mine tailing, and acid treated chrysotile samples. Standard deviation values are provided. (n=5). (nd = no data).

Sample	Zeta Potential	Mg:Si
Suspended Sediment		
Swift Creek	17.6 ± 1.5	16.2 ± 0.8
Church	12.3 ± 2.1	20.0 ± 1.4
Bridge	12 ± 1.2	19.0 ± 1.7
Border	13 ± 1.0	nd
Mine Tailings		
Cassiar 14-1	1.7 ± 0.2	24.0 ± 4.4
Cassiar 16-1	31.0 ± 0.8	25.9 ± 1.9
Cassiar 17-1	6.3 ± 0.4	6.8 ± 1.1
Acid Treatments		
Oxalic	-15.1 ± 1.6	0.74
HCl	-10.6 ± 2.1	10.1 ± 0.4
Carbonic	15.7 ± 2.9	19.77 ± 2.0
Untreated	28 ± 2.1	24.95 ± 3.1

4.3.4 ToF-SIMS

The magnesium to silica ratios were similar among the suspended sediment samples (16.21, 19.96, and 19.00), and consistent with the carbonic acid treated sample, indicating limited weathering (Table 4.4). No data exists for the Border station because the sediment sample was too heterogeneous for ToF-SIMS analysis. 14-1 and 16-1 had magnesium to silica ratios in the mid-twenty range (23.94 and 25.89), which is in the range of the untreated sample from the acid experiment (24.95). 17-1 had a much lower value (6.78) than is expected for a sample that has undergone only moderate weathering, however this low value is consistent with the low surface charge. Figure 4.2 and 4.3 are two-dimensional representations of the magnesium and silica measured in a 1600 μm^2 area and 2 nm depth on the Sumas River watershed suspended sediment and mine tailing chrysotile samples respectively. All of the environmental samples had surfaces dominated by magnesium. These results indicate that except for 17-1, the environmental samples experience very moderate weathering compared to the acid treated samples.

Because of the small size of the area of measurement, the heterogeneity of the environmental samples, and the high cost and time required per sample, there is always the possibility of non-representative measurements, and potential measuring error. Leaching reactions occur at discrete sites rather than in uniform layers (Gronow 1987) meaning there could be a high degree of variability in the magnesium to silica surface ratios of chrysotile fiber. Therefore, slight differences, such as that between Swift Creek suspended sediment (16.21), and Bridge suspended sediment (19.00) may not mean there are significant differences between the chrysotile fibers at these two sites. The mine tailing sample taken from the storage shed, 17-1 (Figure 4.7) displays more aluminum than would be expected in a chrysotile fiber, and had a very low magnesium silica ratio. Because this sample seemed questionable, it was re-run. The second run was very similar to the first. Due to the high cost of ToF-SIMS analysis, the samples were not run a third time. These results are important as they illustrate the challenge of using ToF-SIMS, a very scale fine technique, on heterogeneous environmental samples.

Figure 4.2. ToF-SIMS images of the magnesium and silica ions on the surface of the chrysotile fibers found in suspended sediment from the Sumas River watershed. Surface area = $1600 \mu\text{m}^2$; X=400 μm , Y=400 μm and depth of analysis (Z) is 2 nm.

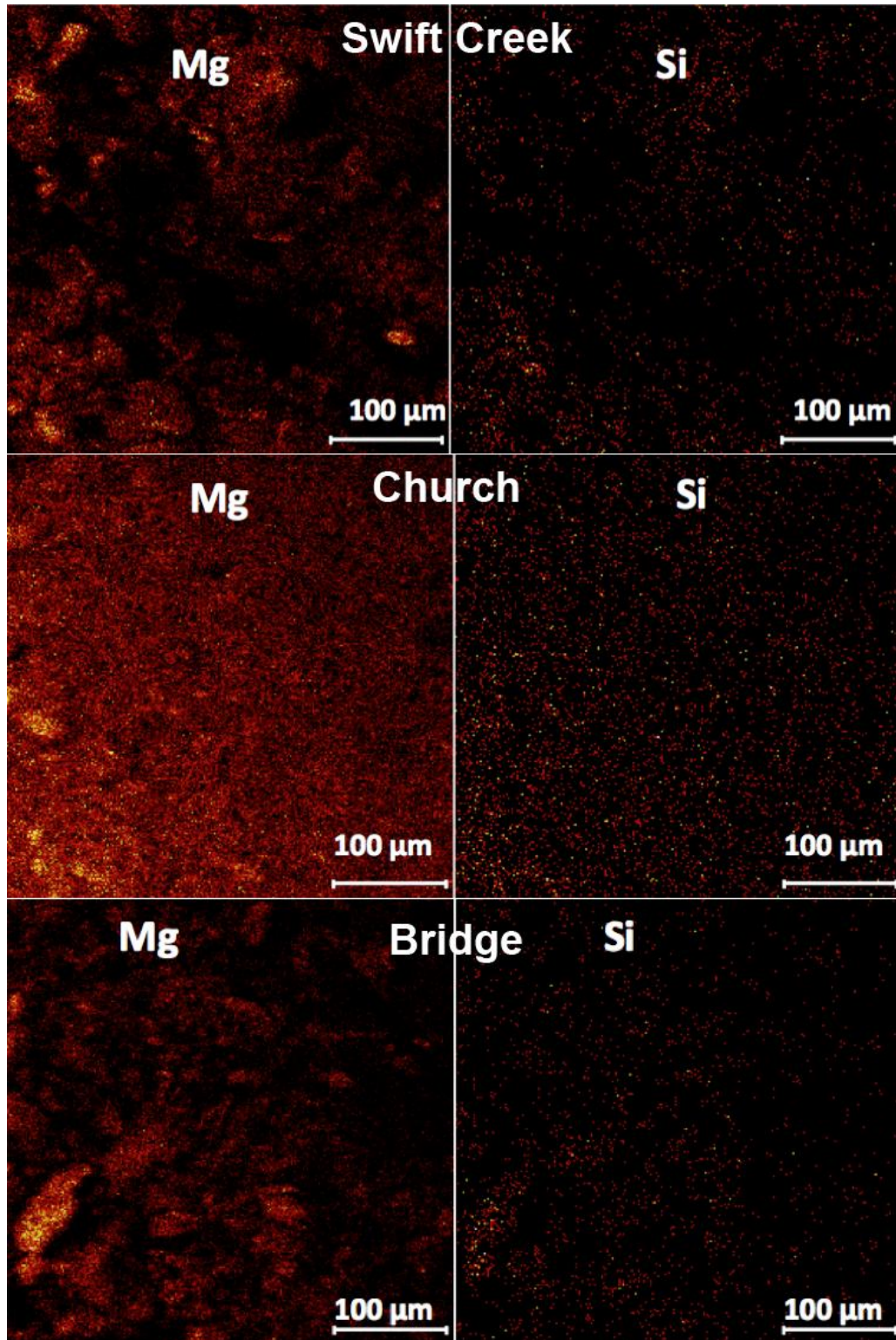
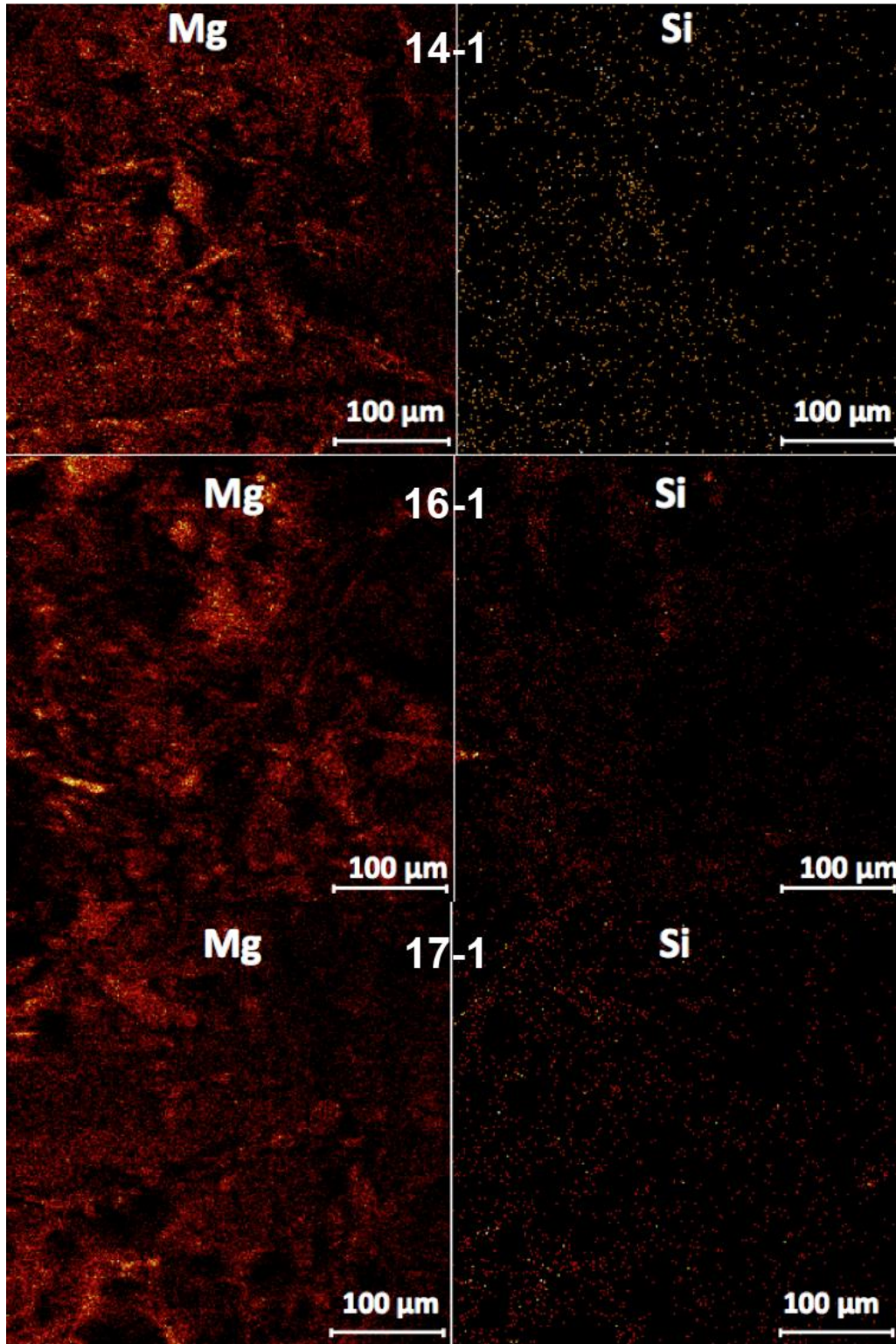


Figure 4.3. ToF-SIMS images of the magnesium and silica ions on the surface of chrysotile fibers from Cassiar mine tailings. Surface area = $1600 \mu\text{m}^2$; X=400 μm , Y=400 μm and depth of analysis (Z) is 2 nm.



4.3.5 Comparisons between techniques

Figure 4.12 compares the zeta potential values with the surficial magnesium silica ratios for each sample. The data shows that the Sumas River suspended sediment samples all congregate and have a very narrow magnesium to silica surface ratio between 16 and 20, and zeta potential values between 12-18. There is a much higher degree of variability in the magnesium to silica ratios and zeta potential values in the mine tailing samples. The suspended sediment samples are affected by similar processes and have the same geological origin, which is not the case for the mine tailing samples, and helps explain the high degree of variability in the results. Low zeta potential values are correlated with low magnesium to silica surface ratios, except for sample 14-1 which shows the opposite trend. The positive correlation between the zeta potential and magnesium to silica ratios values is consistent with the findings from chapter 3.

Figure 4.13 compares the bulk magnesium values of the digested samples with the surficial magnesium silica ratios. In general, lower bulk magnesium values correspond to a lower magnesium to silica ratio. Lower bulk magnesium values appear to be correlated with less positive zeta potential values, except for the 14-1 sample (Figure 4.14).

The pH values of the environmental samples were all within a very similar range between 7 and 8 (Figure 4.15). However, the surficial magnesium silica ratios displayed a highly variable range between 6.78 and 25.89. This is likely due to the small size of the measurement area of each sample, the heterogeneity of the environmental samples, and the variability of leaching reactions which occur at discrete sites rather than in uniform layers (Gronow 1987).

Figure 4.4. Mg:Si vs. Zeta Potential for suspended sediment samples from the Sumas River watershed and mine tailing samples from Cassiar, BC. Error bars represent standard deviation for Mg:Si and Zeta Potential values. (n=5).

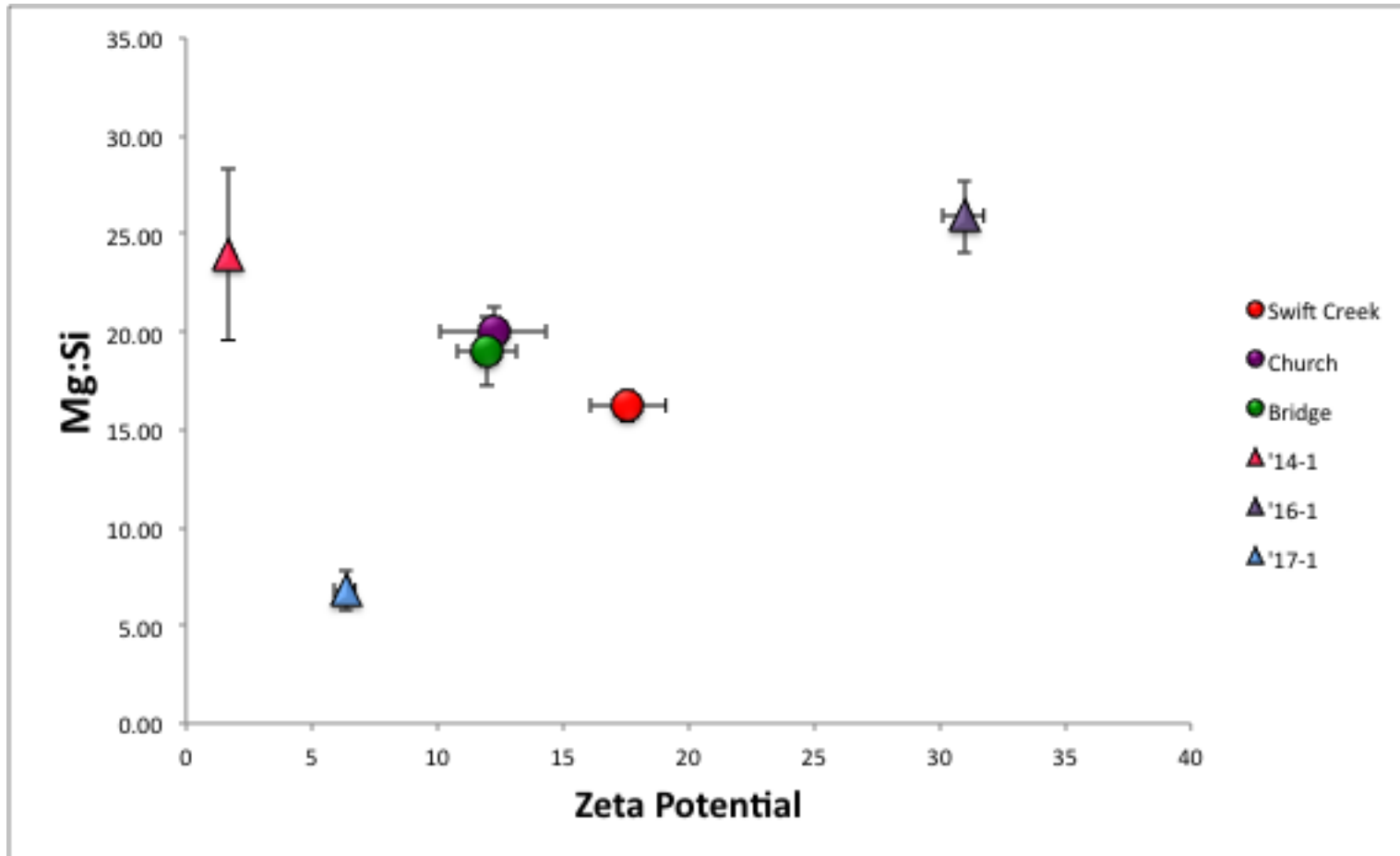


Figure 4.5. Mg (ppm) vs. Mg:Si for suspended sediment samples from the Sumas River watershed and mine tailing samples from Cassiar mine, BC. Error bars represent standard deviation for Mg:Si values. (n=5).

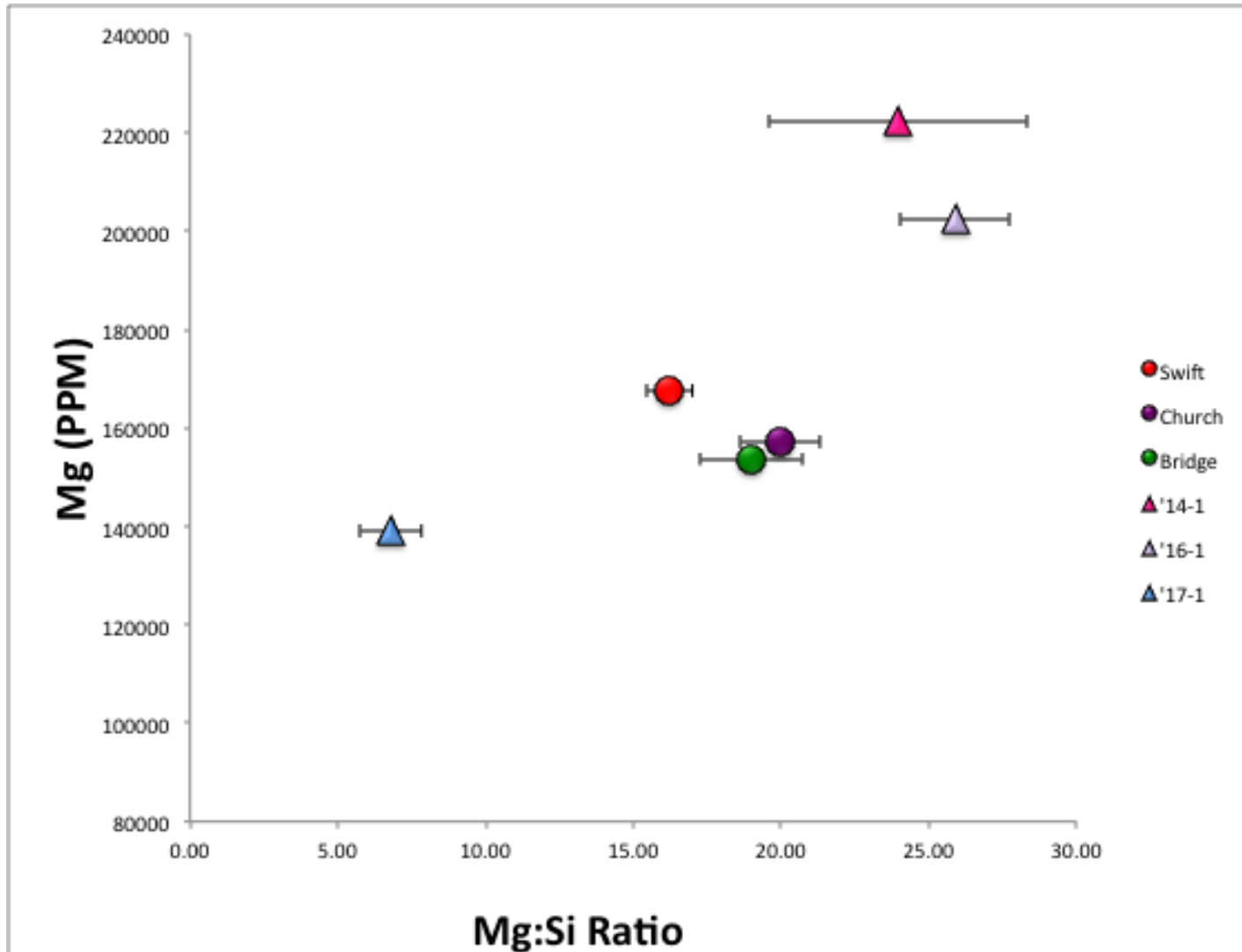


Figure 4.6. Mg (ppm) vs. Zeta Potential for suspended sediment samples from the Sumas River watershed and mine tailing samples from Cassiar mine, BC. Error bars represent standard deviation for Zeta Potential values. (n=5).

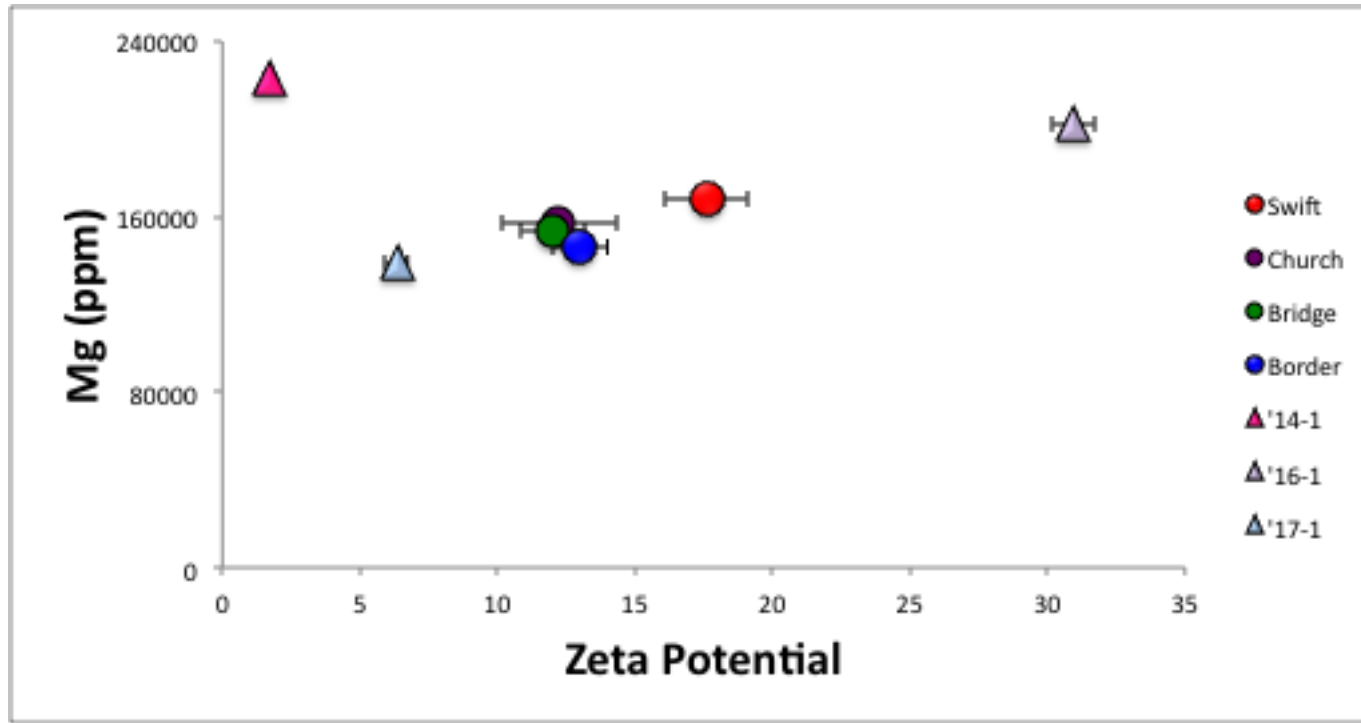
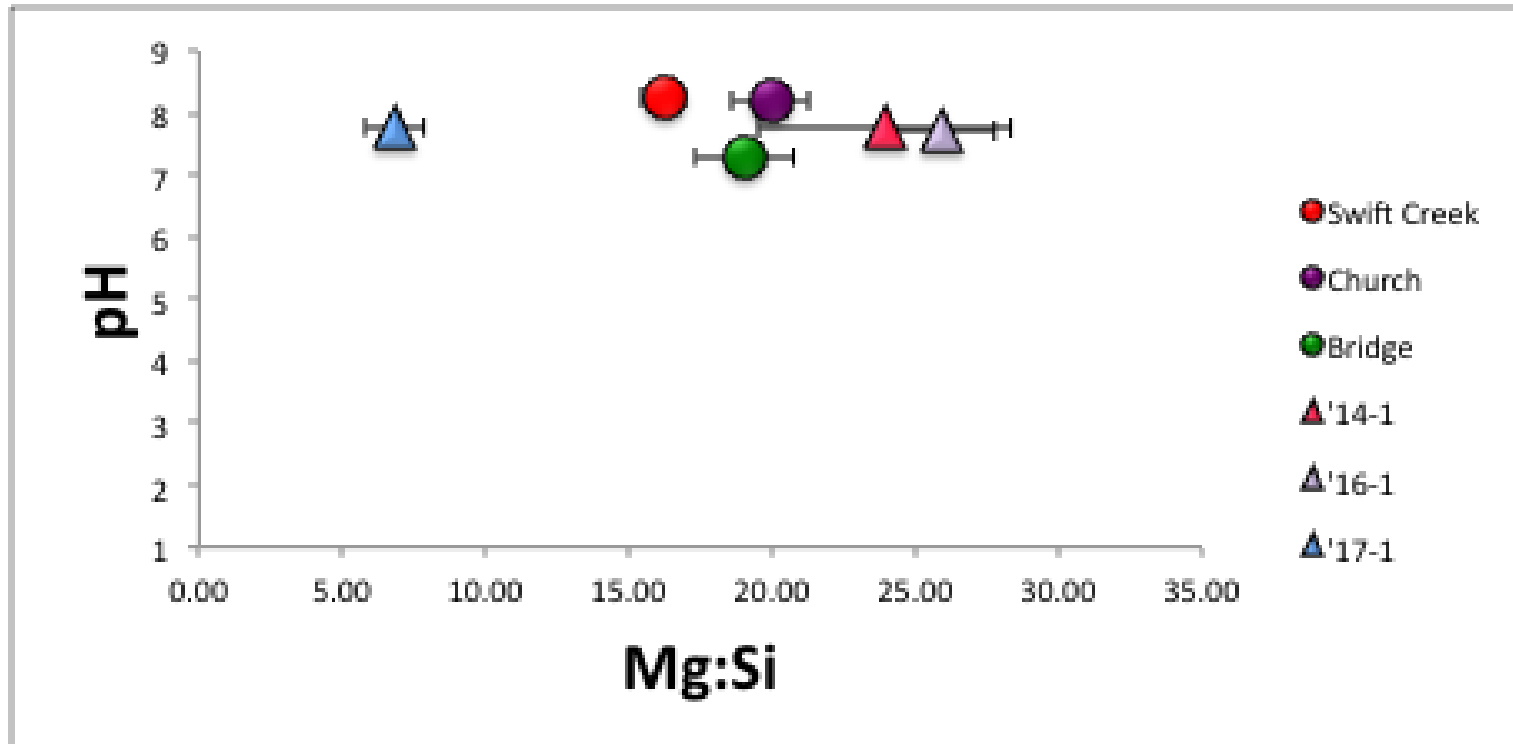


Figure 4.7. pH vs. Mg:Si for suspended sediment samples from the Sumas River watershed and mine tailing samples from Cassiar, BC. Error bars represent standard deviation for Mg:Si values. (n=5).



4.4 Conclusions

Analysis indicates that chrysotile fibers in stream and mine tailing environments experience very mild weathering. In contrast to the acid treatments under controlled conditions in chapter 3, the naturally occurring samples displayed more variability in surface and bulk properties due to greater heterogeneity in both composition and weathering history of the samples. Therefore, although still present, the relationships between the surface properties are not as strongly expressed. This illustrates the importance of knowing a) the geological history and mineralogy of the sample, b) the conditions of the weathering environment be it aqueous or deposition, and c) any impacts after deposition, for example mineral processing or additions of agricultural land use impacts. Techniques such as elemental composition and zeta potential are useful in the sense that they give broad characteristics of the samples, but they are very difficult to relate to very specific small scale analysis like ToF-SIMS because of the size of sample being analyzed, and the extremely large and heterogeneous population the samples comes from. For future studies, it is recommended that sample history and composition be documented prior to detailed analysis. For instance, measuring the water quality data at the various sediment sampling locations, and understanding what additions or processes have been affecting the tailing samples both prior and after deposition.

Chapter 5 : Conclusions and Recommendations

An understanding of the processes affecting the surface properties of chrysotile asbestos provides the basis for predicting the reaction processes and changes affecting the surface properties during weathering. This information is important for a range of considerations, including chrysotile amelioration in the natural environment and CO₂ sequestration in serpentine mine tailings. Naturally occurring acids, such as oxalic acid and hydrochloric acid, are effective at removing the magnesium brucite layer and associated trace metals, and reducing the surface charge of chrysotile asbestos. The fibers treated with these acids are likely less hazardous from a human health perspective due to these surface modifications. Oxalic acid is ubiquitous in the weathering environment, especially in soils with high microorganism activity, and thus may weather and reduce the negative health effects of naturally occurring chrysotile asbestos. Carbonic acid, a much weaker acid, is much less effective at altering the surface properties of chrysotile. Natural weathering in stream and mine tailing environments did alter the surface properties of chrysotile asbestos, but the extent, in terms of human health effects, remains unknown.

Recommendations for reclamation focus treatment on the floodplain sediment immediately following deposition. Non-polluting organic material, such as peat, compost, and sawdust could be applied to the asbestos contaminated sediment to increase the production of acids, which will alter the surface chemistry of the fibers over time. The organic matter will also act as a barrier, preventing asbestos fibers from entering the air where they will pose an inhalation hazard to local residents.

Samples weathered in mine tailing piles experienced only moderate weathering and had intact magnesium rich surface brucite layers, indicating it could be the slow dissolution of magnesium that is the rate limiting step for the mineral carbonation reaction. To increase the release of magnesium ions, acids could be added to the tailing piles. However, in order for carbonates to form and mineral sequestration to occur, bases would need to be added to bring the pH back up to a basic level. This suggestion requires further study.

Laboratory protocols are useful for understanding processes but recognition of sample heterogeneity of natural materials must be kept in mind. Laboratory examinations provide information on processes but in order to generalize to field conditions, statistically large

numbers of samples need to be considered. In addition, it is imperative that the site history, geologic, hydrologic and anthropogenic be documented. It must also be kept in mind that different laboratory protocols have unique mechanisms, some more reflective of the entire sample, such as XRD and aqua regia digestion, whereas others are more limited in the amount of the sample that is examined, for example, FESEM and ToF-SIMS.

The results of zeta potential analysis, a surface specific technique measured on a bulk sample, are supported by ToF-SIMS analysis, a very fine scale surface specific technique measuring a small area of one fiber. Zeta potential analysis is much less expensive and time consuming to carry out than is ToF-SIMS. It also measures the surface characteristics of a larger sample, approximately 0.5 g compared to 1600 μm^2 , which enables it to better account for the variability within a sample.

References

- ATSDR. (2003). *Report on the Expert Panel on Health Effects of Asbestos and Synthetic Vitreous Fibers: The Influence of Fiber Length. Assessment* (p. 69). Atlanta, GA.
- Anbalagan, G., SakthiMurugesan, K., Balakrishnan, M., & Gunasekaran, S. (2008). Structural analysis, optical absorption and EPR spectroscopic studies on chrysotile. *Applied Clay Science*, 42(1-2), 175–179.
- Andersen, K., & Kissler, M. (2004). *Digestion of Solid Matrices Desk Study* (p. 59). Eurofins A/X, Denmark.
- BC Ministry of Environment. (2005). *Environmental Quality: Water Quality Assessment and Objectives. Technical Report*. (p. 42). Surrey, B.C.
- Bales, R. C. (1984). *Surface chemical and physical behaviour of chrysotile asbestos in natural waters and water treatment. Environmental Engineering Science*. California Institute of Technology.
- Bales, R., & Morgan, J. (1985). Dissolution kinetics of chrysotile at pH 7 to 10. *Geochimica et Cosmochimica Acta*, 49, 2281–2288.
- Bayer, T. M., & Linneman, S. (2011). The nature and transport of the fine-grained component of Swift Creek Landslide, Northwest Washington. *Earth Surface Processes and Landforms*, 36(5), 624–640.
- Bearat, H., Mckelvy, M. J., Chizmeshya, A. V. G., Sharma, R., & Carpenter, R. W. (2002). Magnesium Hydroxide Dehydroxylation / Carbonation Reaction Processes: Implications for Carbon Dioxide Mineral Sequestration. *Journal of the American Ceramic Society*, 48, 742–748.
- Bernstein, D. M., & Hoskins, J. A. (2006). The health effects of chrysotile: current perspective based upon recent data. *Regulatory toxicology and pharmacology*: RTP, 45(3), 252–64.
- Bishop, J., Murad, E., & Dyar, M. D. (2002). The influence of octahedral and tetrahedral cation substitution on the structure of smectites and serpentines as observed through infrared spectroscopy. *Clay Minerals*, 37(4), 617–628.
- Blber, M. V., & Stumm, W. (1994). An in-situ ATR-FTIR Study: The Surface Coordination of Salicylic Acid on Aluminum and Iron (III) Oxides. *Environmental science & technology*, 28(5), 763–768.

- Braterman, P. S., Xu, Z. P., & Yarberry, F. (2004). Layered Double Hydroxides. In S. M. Auerbach, K. A. Carrado, & P. K. Dutta (Eds.), *Handbook of Layered Materials* (p. 647). New York, NY: Marcel Dekker.
- Brooks, R. R. (1987). *Serpentine and its vegetation*. (p. 454). Portland, Oregon: Dioscorides Press Inc.
- Cheshire, M., & Guven, N. (2005). Conversion of Chrysotile to a Magnesian Smectite. *Clay and Clay Minerals*, 53(2), 155–161.
- Choi, I., & Smith, R. W. (1972). Kinetic Study of Dissolution of Asbestos Fibers in Water. *Journal of Colloid and Interface Science*, 40(2), 253 – 262.
- Cipolli, F., Gambardella, B., Marini, L., Ottonello, G., & Vetuschi Zuccolini, M. (2004). Geochemistry of high-pH waters from serpentinites of the Gruppo di Voltri (Genova, Italy) and reaction path modeling of CO₂ sequestration in serpentinite aquifers. *Applied Geochemistry*, 19(5), 787–802.
- Crummet, C. (2005). *Examination of the thermal decomposition of chrysotile*. The University of Maryland.
- Cyphert, J., Nyska, A., Mahoney, R., Schladweiler, M., Kodavanti, U., & Gavett, S. (2012). Sumas Mountain chrysotile induces greater lung fibrosis in Fischer 344 rats than Libby amphibole, El Dorado tremolite, and Ontario ferroactinolite. *Toxicological sciences*, 37(5).
- David, M. B., & Vance, G. F. (1991). Chemical character and origin of organic acids in streams and seepage lakes of central Maine. *Biogeochemistry*, 12(2), 17–41.
- Dixon, J. R., Lowe, D. B., Richards, D. E., Cralley, L. J., & Stokinger, H. E. (1970). The role of trace metals in chemical carcinogenesis: asbestos cancers. *Cancer Research*, 30, 1068–1074.
- EPA. (2009). *Soil, sediment and surface water sampling: Sumas Mountain naturally-occurring asbestos site. Whatcom County, Washington*. (p. 40). Seattle, WA.
- Esteves da Silva, J., & Machado, A. (1997). Procedure for the classification of fulvic acids and similar substances based on the variation with pH of their synchronous fluorescence spectra. *Analyst*, 122, 1299–1305.
- Fauth, D. J., Soong, Y., & White, C. M. (2002). Carbon sequestration utilizing industrial solid residues. *Fuel Chemistry Division Preprints*, 47(1), 37–38.
- Favero-Longo, S. E., Turci, F., Tomatis, M., Compagnoni, R., Piervittori, R., & Fubini, B. (2009). The effect of weathering on ecopersistence, reactivity, and potential toxicity of

naturally occurring asbestos and asbestiform minerals. *Journal of toxicology and environmental health. Part A*, 72(5), 305–14.

Favero-Longo, S., Turci, F., Tomatis, M., Castelli, D., Bonfante, P., Hochella, M., Piervittori, R., et al. (2005). Chrysotile asbestos is progressively converted into a non-fibrous amorphous material by the chelating action of lichen metabolites. *Journal of environmental monitoring*, 7(8), 764–6.

Foresti, E., Fornero, E., Lesci, I. G., Rinaudo, C., Zuccheri, T., & Roveri, N. (2009). Asbestos health hazard: a spectroscopic study of synthetic geoinspired Fe-doped chrysotile. *Journal of hazardous materials*, 167(1-3), 1070–9.

Fubini, B. (1997). Surface Reactivity in the Pathogenic Response to Particulates. *Environmental Health*, 105(5), 1013–1020.

Gerdemann, S. J., O'Connor, W. K., Dahlin, D. C., Penner, L. R., & Rush, H. (2007). Ex situ aqueous mineral carbonation. *Environmental science & technology*, 41(7), 2587–93.

Gilberti, R. M., Joshi, G. N., & Knecht, D. (2008). The phagocytosis of crystalline silica particles by macrophages. *American journal of respiratory cell and molecular biology*, 39(5), 619–27.

Gloag, D. (1981). Asbestos fibres and the environment. *British Medical Journal*, 282, 623–626.

Goldberg, P., Chen, Z., Connor, W. O., Walters, R., & Ziock, H. (2001). CO₂ mineral sequestration studies in US. *Fifth International Conference on Greenhouse Gas Control Technologies* (pp. 1–10).

Gronow, J. R. (1987). The dissolution of asbestos fibres in water. *Clay Minerals*, 22, 21–35.

Hansen, J., Sato, M., Kharecha, P., Beerling, D., Masson-delmotte, V., Pagani, M., Raymo, M., et al. (2008). Target Atmospheric CO₂: Where Should Humanity Aim? *Open Atmospheric Science Journal*, 2, 217 – 231.

Harrick, N. J. (1967). *Internal Reflection Spectroscopy*. New York, NY: John Wiley & sons.

Holmes, E. P., Wilson, J., Schreier, H., & Lavkulich, L. M. (2012). Processes affecting surface and chemical properties of chrysotile: Implications for reclamation of asbestos in the natural environment. *Canadian Journal of Soil Science*, (92), 229–242.

Huijgen, W. J. J., Comans, R. N. J., & Witkamp, G.-J. (2007). Cost evaluation of CO₂ sequestration by aqueous mineral carbonation. *Energy Conversion and Management*, 48(7), 1923–1935.

- Hume, L. A., & Rimstidt, J. D. (1992). The biodurability of chrysotile asbestos. *American Mineralogist*, 77(1979), 1125–1128.
- Hänchen, M., Prigiobbe, V., Baciocchi, R., & Mazzotti, M. (2008). Precipitation in the Mg-carbonate system—effects of temperature and CO₂ pressure. *Chemical Engineering Science*, 63(4), 1012–1028.
- Ilgren, E. (2008). Review: Coalinga Chrysotile: Dissolution, Concentration, Regulation and General Relevance. *Indoor and Built Environment*, 17(1), 42–57.
- Klein, C., & Hurlbut, C. (1977). *Manual of Mineralogy* (19th ed.). New York: J. Wiley and Sons.
- Krevor, S. C. M., & Lackner, K. S. (2011). Enhancing serpentine dissolution kinetics for mineral carbon dioxide sequestration. *International Journal of Greenhouse Gas Control*, 5(4), 1–8.
- Kubicki, J. D., Schroeter, L. M., Itoh, M. J., Nguyen, B. N., & Apitz, S. E. (1999). Attenuated total reflectance Fourier-transform infrared spectroscopy of carboxylic acids adsorbed onto mineral surfaces. *Geochimica et Cosmochimica Acta*, 63(18), 2709–2725.
- LaDou, J., Castleman, B., Frank, A., Gochfeld, M., Greenberg, M., Huff, J., Joshi, T. K., et al. (2010). The case for a global ban on asbestos. *Environmental health perspectives*, 118(7), 897–901.
- Langer, A. M., & Nolan, R. P. (1994). Chrysotile: its occurrence and properties as variables controlling biological effects. *The Annals of occupational hygiene*, 38(4), 427–51.
- Langer, A. M., & Nolan, R. P. (1997). The amphibole hypothesis: Neither gone nor forgotten. *American Journal of Public Health*, 87(4), 688 – 689.
- Lee, R. J., Strohmeier, B. R., Bunker, K. L., & Van Orden, D. R. (2008). Naturally occurring asbestos: a recurring public policy challenge. *Journal of hazardous materials*, 153(1-2), 1–21.
- Lee, Y. H. (1991). Natural organic acids in acidic surface water: Acid base properties, complex formation with aluminum and their contribution to acidification. In B. Allard, H. Boren, & A. Grimwall (Eds.), *Humic Substances in Aquatic and Terrestrial Environments* (pp. 315–327). Berlin: Springer-Verlag.
- Lim, C., & Jackson, M. (1982). Dissolution for total analysis. *Methods of Soil Analysis Part 2* (pp. 1–12). Madison Wisconsin: Soil Science Society of America.
- Loughan, F. C. (1969). *Chemical Weathering of the Silicate Minerals*. New York: American Elsevier Publishing Company.

- Martin, T., Creed, J., & Long, S. (1991). Method 200.2: Sample preparation procedure for spectrochemical determination of total recoverable elements. *Methods for the Determination of Metals in Environmental Samples* (pp. 13–21). Cincinnati, OH: United States Environmental Protection Agency.
- Martinez, E. and Zucker, G. (1960). Asbestos ore body minerals studied by zeta potential measurements. *Journal of physical chemistry*, 64(7), 924–926.
- Mizukami, T., Kagi, H., Wallis, S. R., & Fukura, S. (2007). Pressure-induced change in the compressional behavior of the O-H bond in chrysotile: A Raman high-pressure study up to 4.5 GPa. *American Mineralogist*, 92(8-9), 1456–1463.
- Monchaux, G., Bignon, J., Jaurand, M. C., Lafuma, J., Sebastien, P., Masse, R., Hirsch, A., et al. (1981). Mesotheliomas in rats following inoculation with acid-leached chrysotile asbestos and other mineral fibres. *Carcinogenesis*, 2(3), 229–36.
- Morgan, A. (1997). Acid leaching studies of chrysotile asbestos from mines in the Coalinga region of California and from Quebec and British Columbia. *The Annals of occupational hygiene*, 41(3), 249–68.
- Mossman, B T. (1983). In vitro approaches for determining mechanisms of toxicity and carcinogenicity by asbestos in the gastrointestinal and respiratory tracts. *Environmental health perspectives*, 53, 155–61.
- Mossman, B. T., & Gee, J. B. L. (1990). The Hypothesis Is Still Supported by Scientists and Scientific Data. *American Journal of Public Health*, 4, 689–690.
- Oberdörster, G., Stone, V., & Donaldson, K. (2007). Toxicology of nanoparticles: A historical perspective. *Nanotoxicology*, 1(1), 2–25.
- Oelkers, E. H., & Schott, J. (2009). Thermodynamics and Kinetics of Water-Rock Interaction. *Reviews in Mineralogy and Geochemistry*, 70.
- Pan, X., Day, H., Wang, W., Beckett, L., & Schenker, M. (2005). Residential proximity to naturally occurring asbestos and mesothelioma risk in California. *American journal of respiratory and critical care medicine*, 172(8), 1019–25.
- Phillips, J. M., Russell, M. A., & Walling, D. E. (2000). Time-integrated sampling of fluvial suspended sediment: a simple methodology for small catchments. *Hydrological Processes*, 12, 2589–2602.
- Pooley, F D. (1976). An examination of the fibrous mineral content of asbestos lung tissue from the Canadian chrysotile mining industry. *Environmental research*, 12(3), 281–98.
- Pooley, F.D. (1976). Pooley1976.pdf. *Environmental Research*, 12, 281 – 298.

- Prousek, J. (2007). Fenton chemistry in biology and medicine. *Pure and Applied Chemistry*, 79(12), 2325–2338.
- Putnis, A. (2009). Mineral Replacement Reactions. *Review in Mineralogy and Geochemistry*, 70, 87–124.
- Rehman, I., & Bonfield, W. (1997). Characterization of hydroxyapatite and carbonated apatite by photo acoustic FTIR spectroscopy. *Journal of Materials Science: Materials in Medicine*, 8, 1–4.
- Roberts, B., & Proctor, J. (1991). *The ecology of areas with serpentized rocks: a world view*. (p. 427). Dordrecht, The Netherlands: Kluwer Academic Publishers.
- Ross, M. (1981). The geologic occurrences and health hazards of amphibole and serpentine asbestos. *Reviews in Mineralogy and Geochemistry*, 9(1), 6466–6466.
- Ross, M., Langer, A. M., Nord, G. L., Nolan, R. P., Lee, R. J., Van Orden, D., & Addison, J. (2008). The mineral nature of asbestos. *Regulatory toxicology and pharmacology*, 52, S26–30.
- Rowlands, N., Gibbs, G. W., & McDonald, A. D. (1982). Asbestos fibres in the lungs of chrysotile miners and millers: a preliminary report. *The Annals of occupational hygiene*, 26(1-4), 411–5.
- Schreier, H. (1989). *Asbestos in the natural environment. Studies in Environmental Science. Science* (p. 159). Amsterdam: Elsevier.
- Schreier, H., Hall, K., Brown, S., Wenick, B., Berka, C., Belzer, W., & Pettie, K. (1998). Agriculture: An important non-point source of pollution. In C. Gray & T. Tuominen (Eds.), *Health of the Fraser River aquatic ecosystem Volume II: A synthesis of research conducted under the Fraser River Action Plan* (pp. 83–89). Ottawa, ON: Environment Canada.
- Smith, A. H., & Wright, C. C. (1996). Chrysotile asbestos is the main cause of pleural mesothelioma. *American journal of industrial medicine*, 30(3), 252–66.
- Smith, I. M., Hall, K. J., Lavkulich, L. M., & Schreier, H. (2007). Trace metal concentrations in an intensive agricultural watershed in British Columbia, Canada. *Journal of the American Water Resources Association*, 43(6), 1455–1467.
- Soil and Plant Analysis Council Inc. (1999). *Soil Analysis: Handbook of Reference Methods* (p. 251). Washington, D.C.: CRC Press.
- Stayner, L. T., Dankovic, D., & Lemen, R. (1996). Occupational exposure to chrysotile asbestos and cancer risk: a review of the amphibole hypothesis. *American journal of public health*, 86(2), 179–86.

- Suquet, H. (1989). Effects of dry grinding and leaching on the crystal structure of chrysotile. *Clays and Clay Minerals*, 37(5), 439–445.
- Titulaer, M. K., Cess van Miltenburg, J., Jansen, B. H., & Geus, J. W. (1993). Characterization of tubular chrysotile by thermoporometry, nitrogen sorption, drifts, and TEM. *Clay and Clay Minerals*, 41(4), 496–513.
- Turci, F., Favero-Longo, S. E., Tomatis, M., Martra, G., Castelli, D., Piervittori, R., & Fubini, B. (2007). A biomimetic approach to the chemical inactivation of chrysotile fibres by lichen metabolites. *Chemistry*, 13(14), 4081–93.
- Virta, R. (2006). *Worldwide asbestos supply and consumption trends from 1900 through 2003*. Director (p. 80). Reston, Virginia.
- White, A. F., & Brantley, S. L. (1995). Chemical weathering rates of silicate minerals; an overview. *Reviews in Mineralogy and Geochemistry*, 31(1), 1–22.
- Wilson, S. (2005). *Carbon sequestration in chrysotile mine tailings*. The University of British Columbia.
- World Health Organization. (2003). *Asbestos in drinking-water: Background document for development of WHO guidelines for drinking-water quality* (Vol. 2). Geneva.
- Wroble, J. (2010). *Environmental monitoring for asbestos: Sumas Mountain asbestos site selected residential properties bulk sampling and analysis activity based sampling surface water sampling* (p. 133). Seattle, WA.
- Yang, L. (2010). *An Experimental Study on the Synthesis of Chrysotile Nanotube by High-temperature Hydrothermal Method*. Xi'an University of Architecture and Technology.
- Yariv, S., & Heller-Kallai, L. (1973). I.R. evidence for migration of protons in H- and organo-montmorillonites. *Clays and Clay Minerals*, 21, 199–200.
- Yost, E., Tejedor-Tejedor, M., & Anderson, M. (1990). In situ CIR-FTIR characterization of salicylate complexes at the goethite/aqueous solution interface. *Environmental science & technology*, 24(6), 822–828.

Appendix A

XRD Patterns

Acid Treatment

- Untreated – T21 raw
- Oxalic treatment – T22 raw
- HCl treatment – T1 raw
- Carbonic treatment – T23 raw

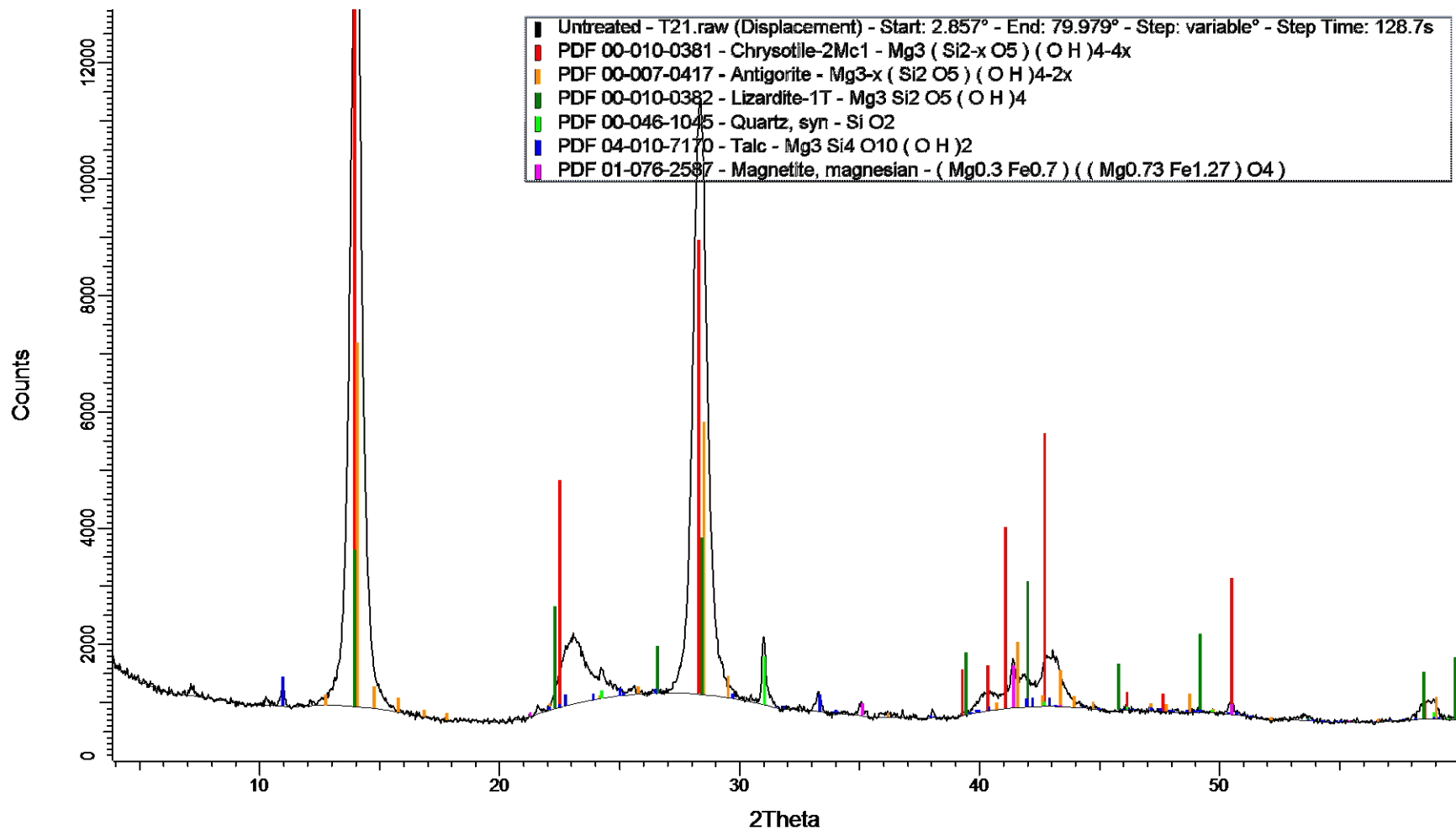
Environmental Samples

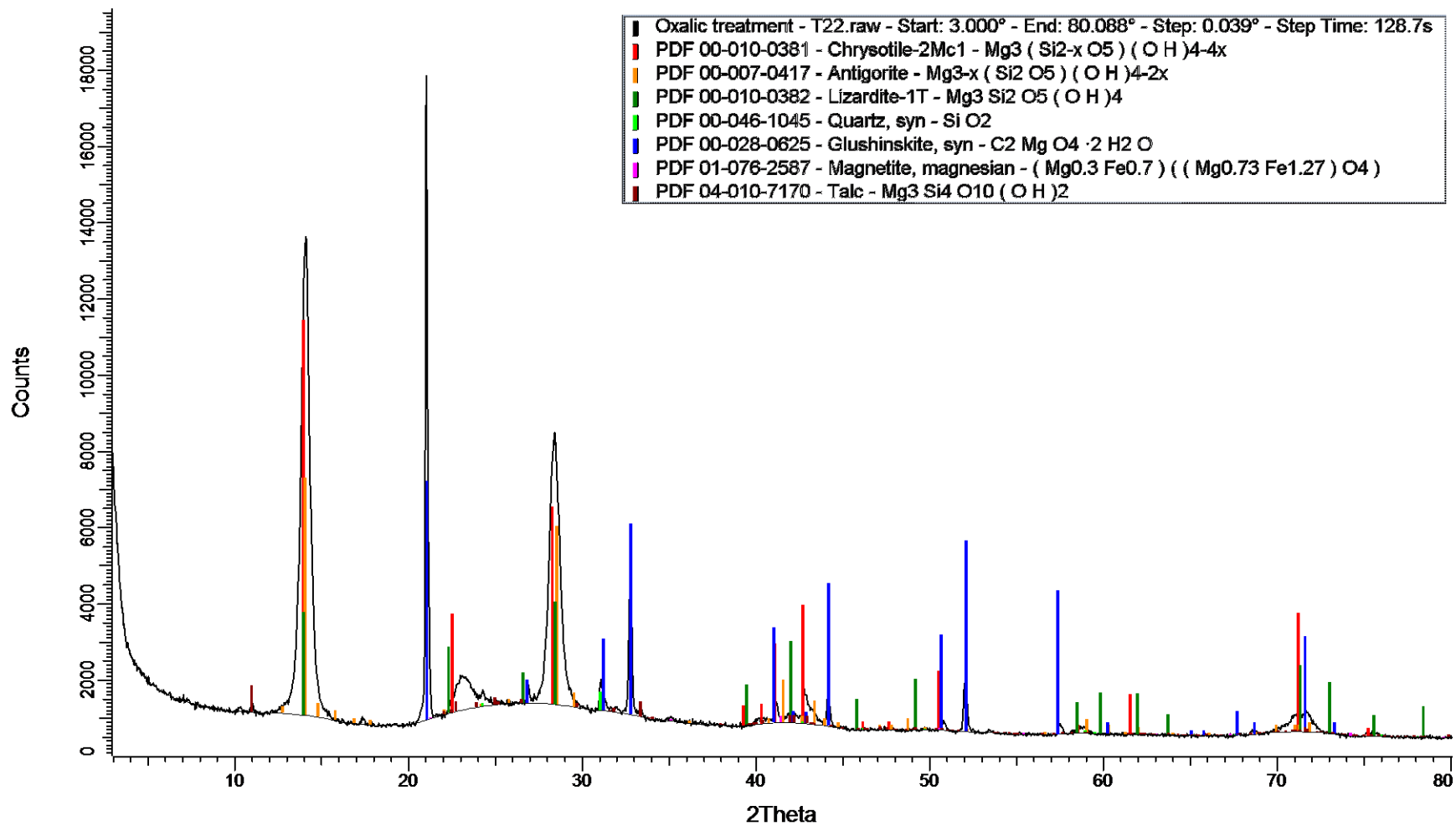
Mine Tailings

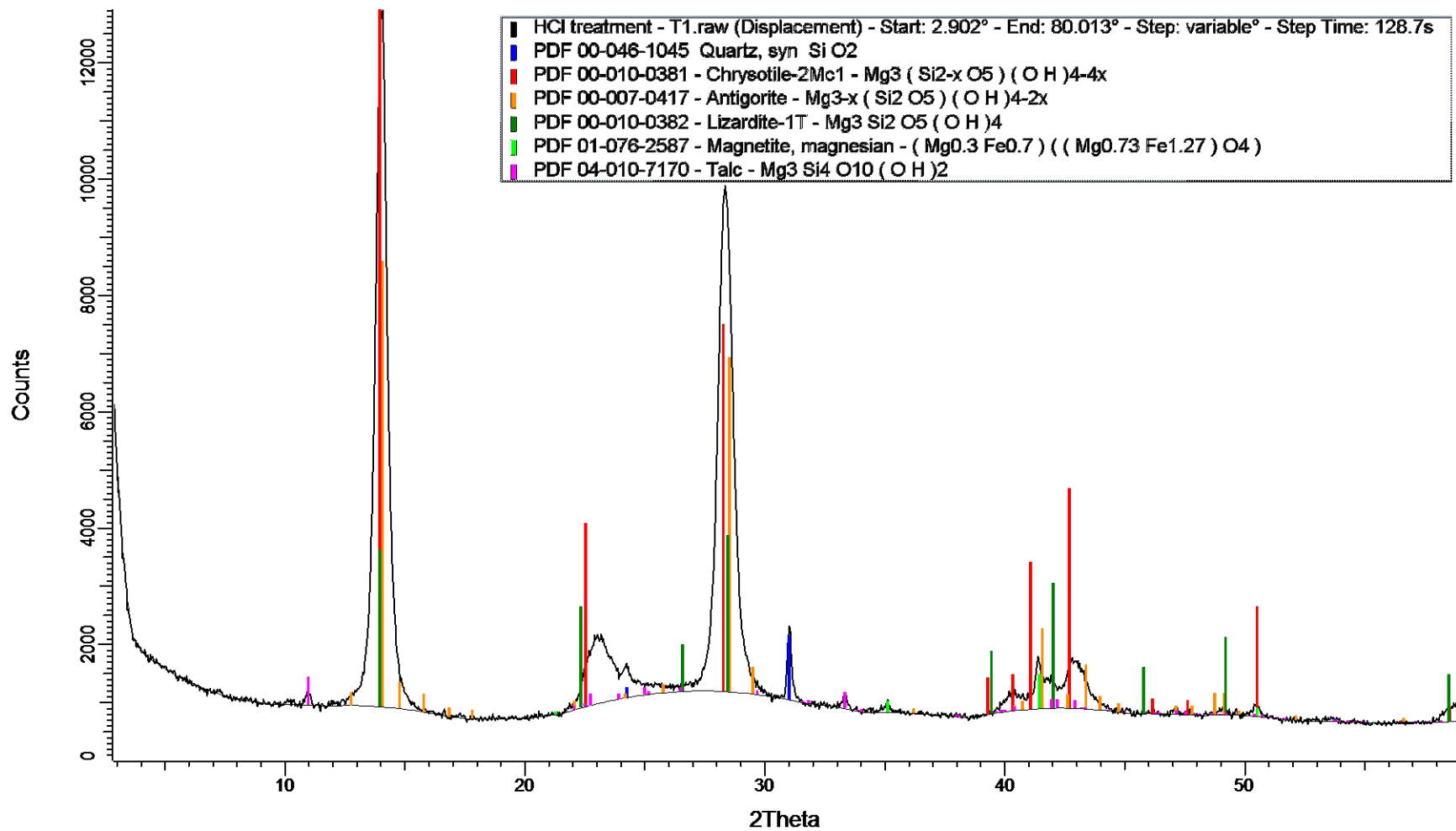
- 14-1 – T18 raw
- 16-1 – T19 raw
- 17-1 – T20 raw

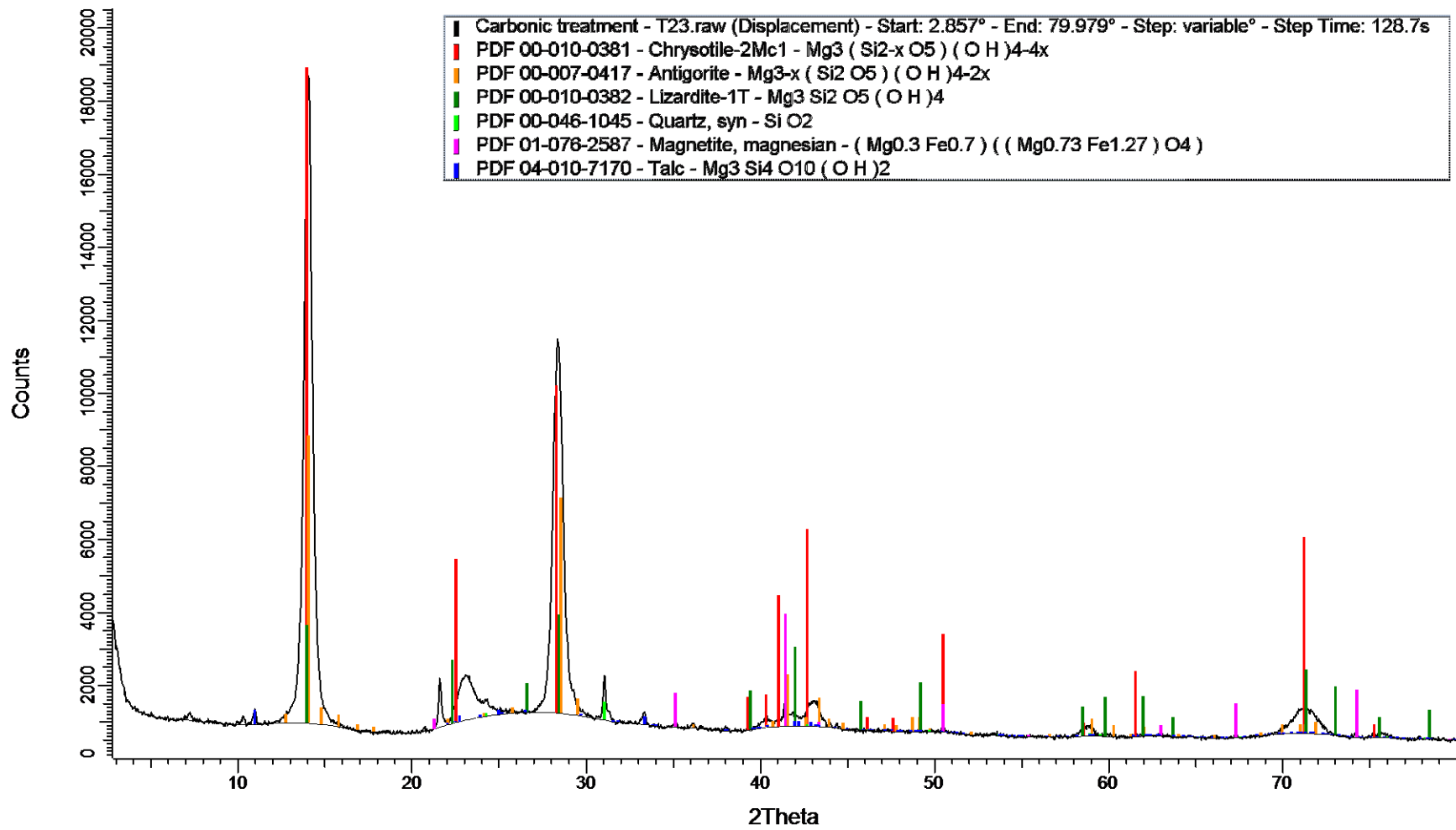
Suspended Sediment

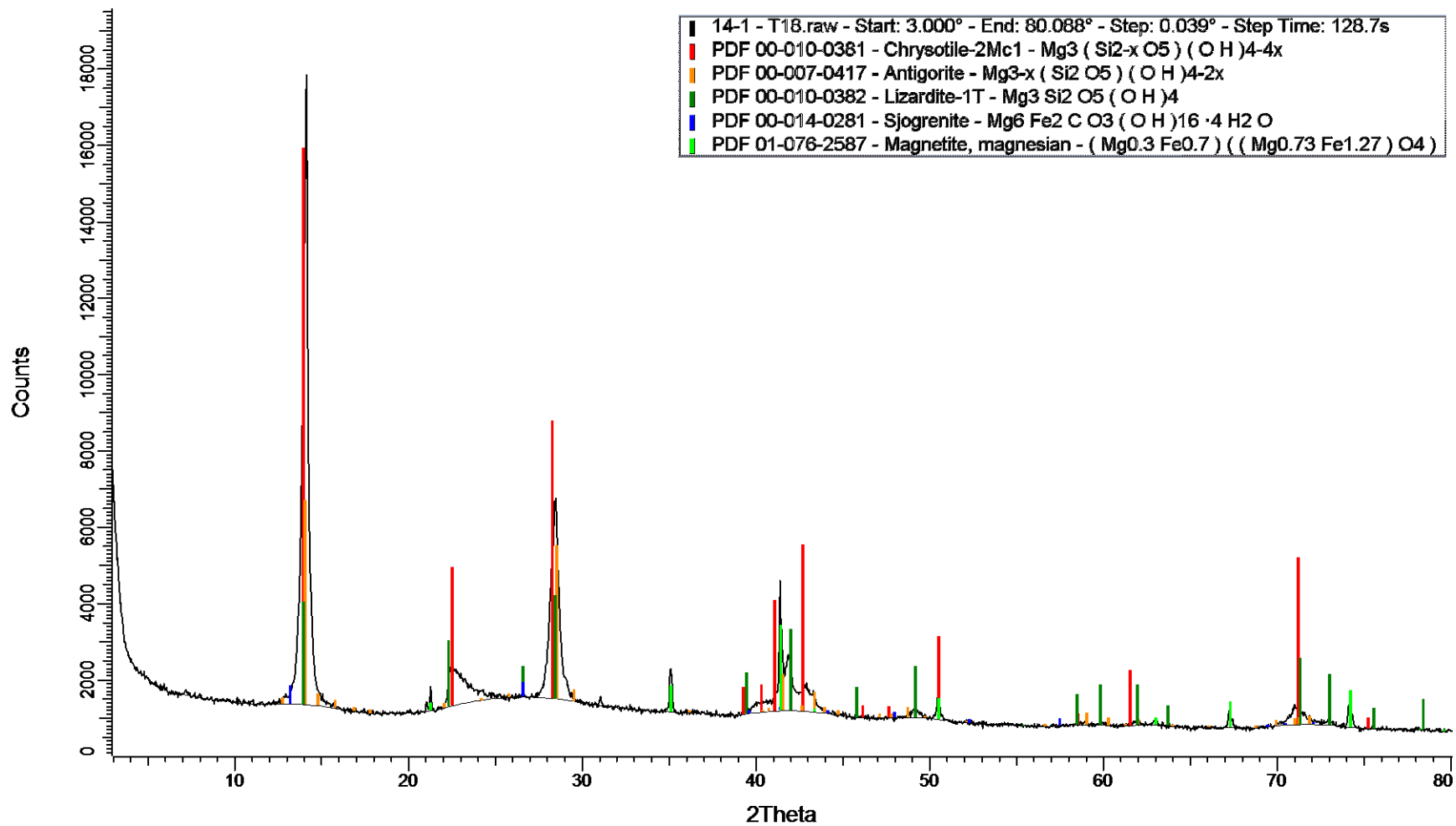
- Swift Creek – T4 raw
- Church – T7 raw
- Bridge – T10 raw
- Border – T13 raw

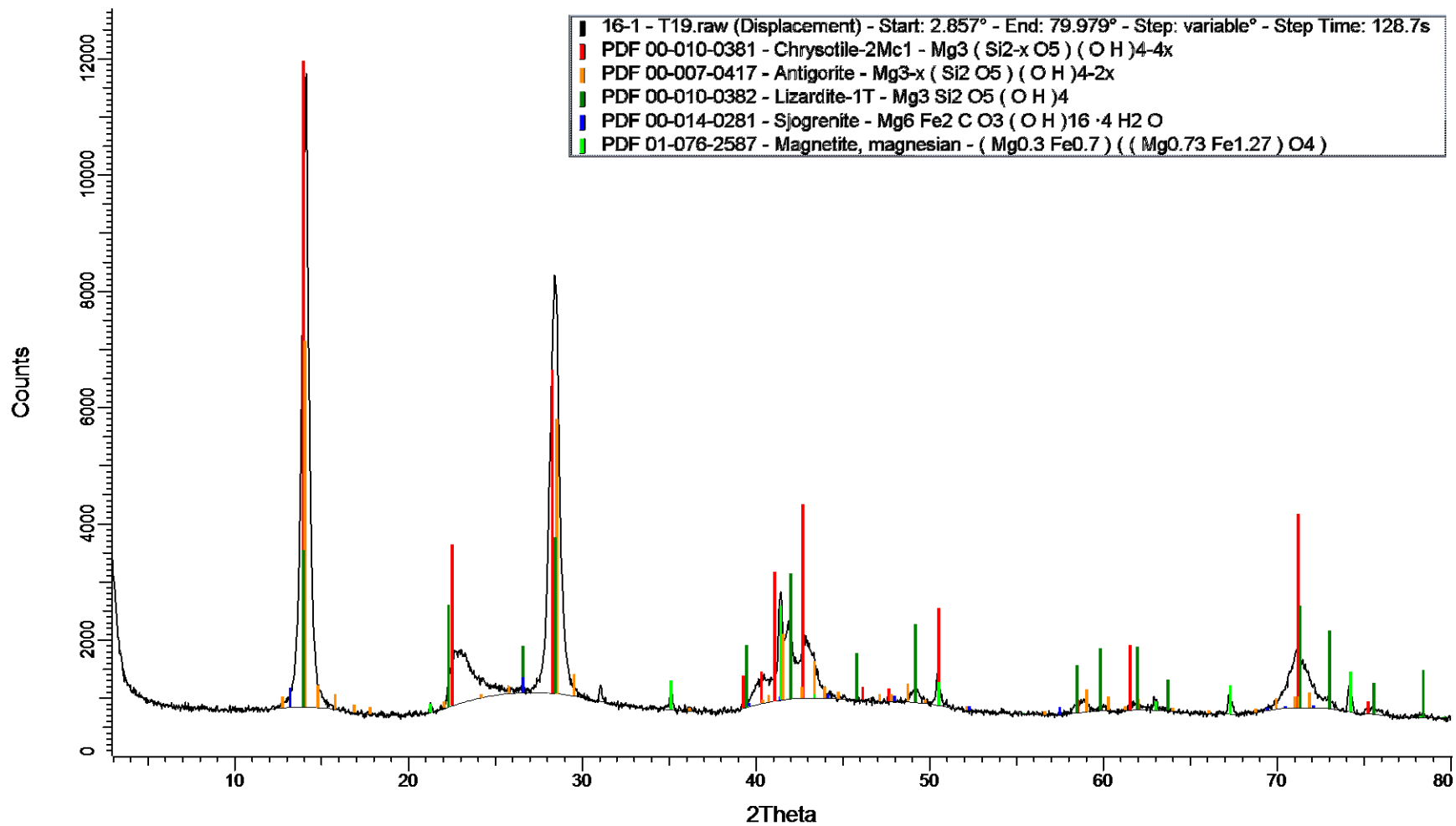


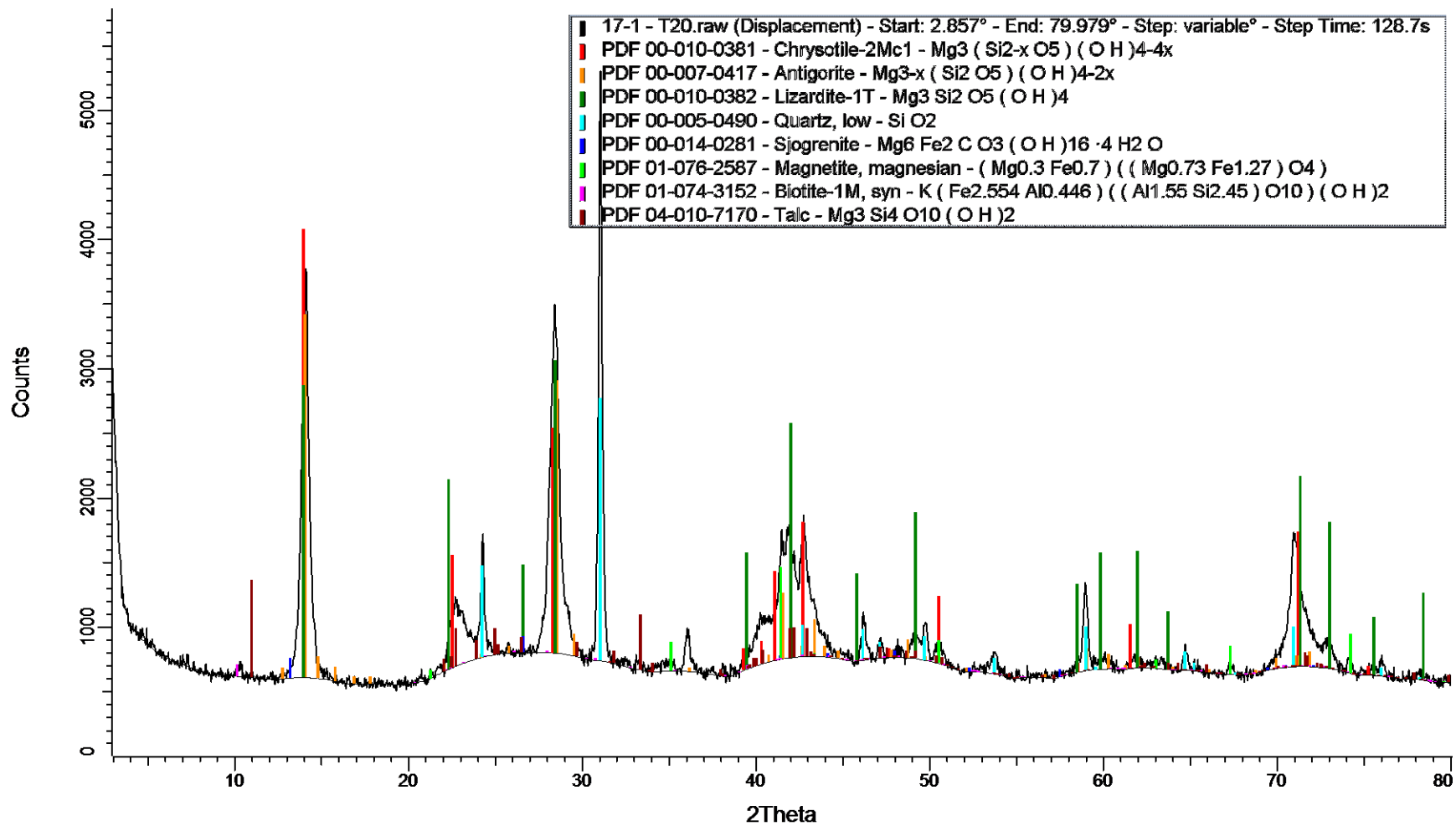


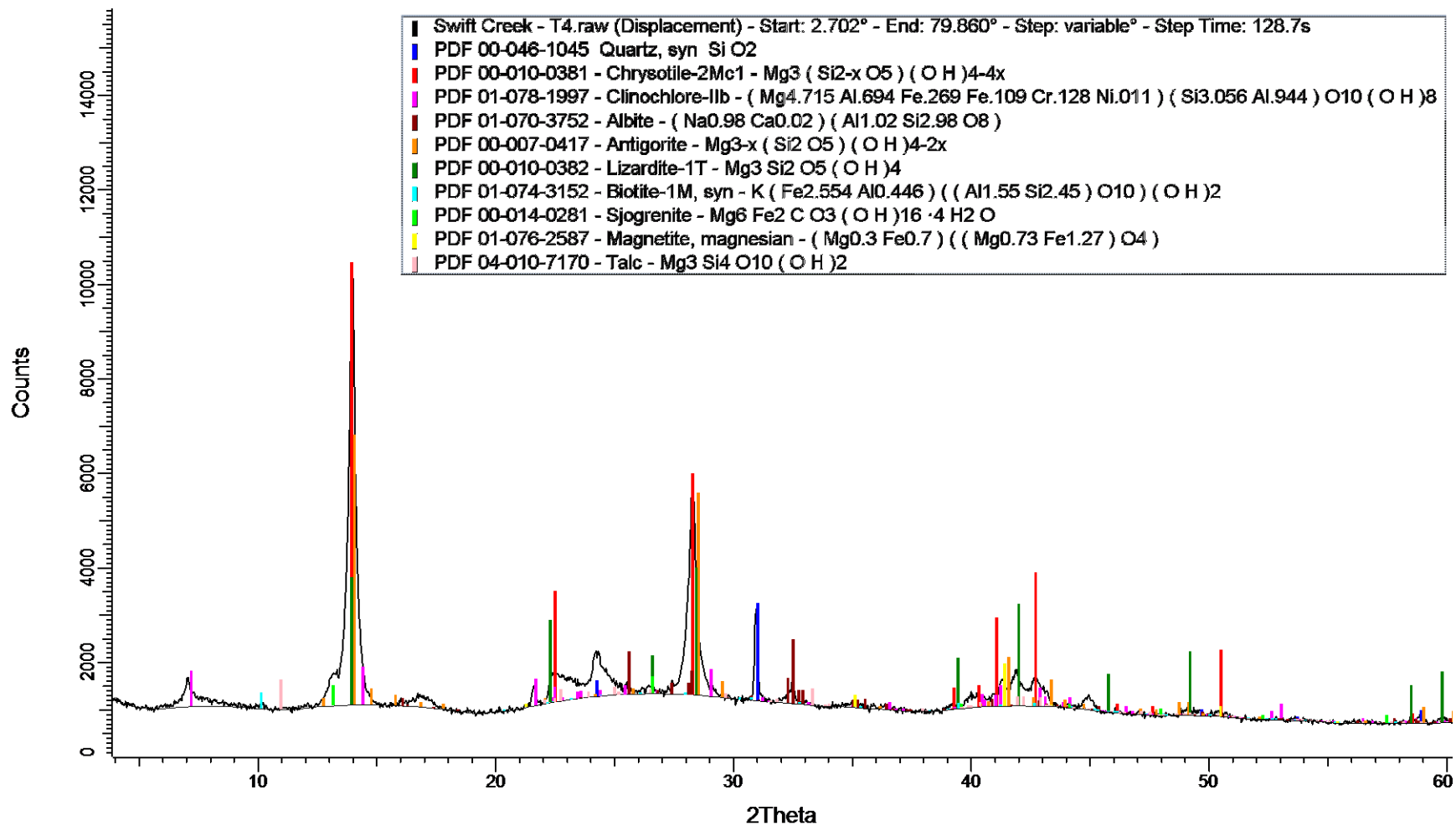


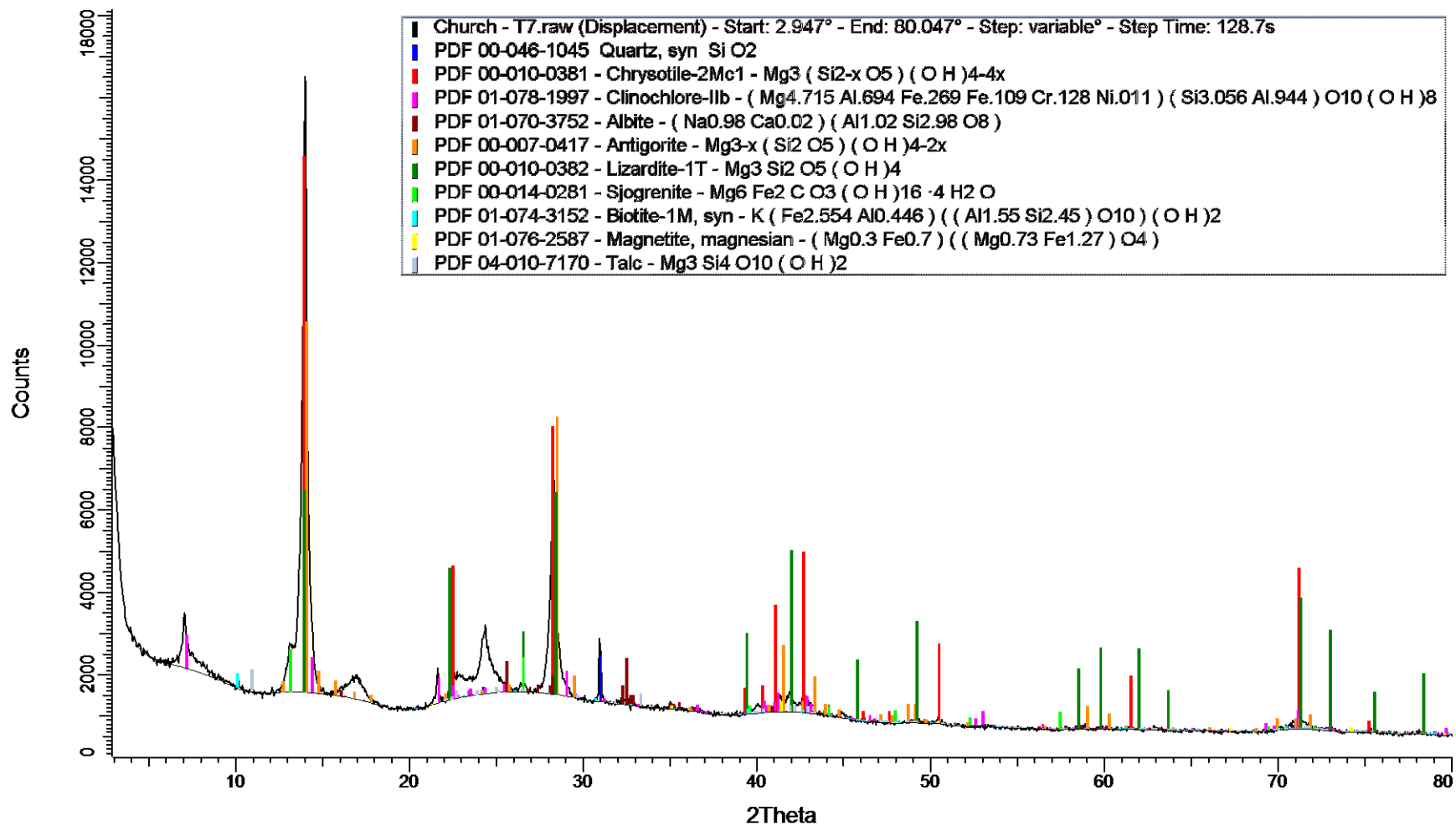


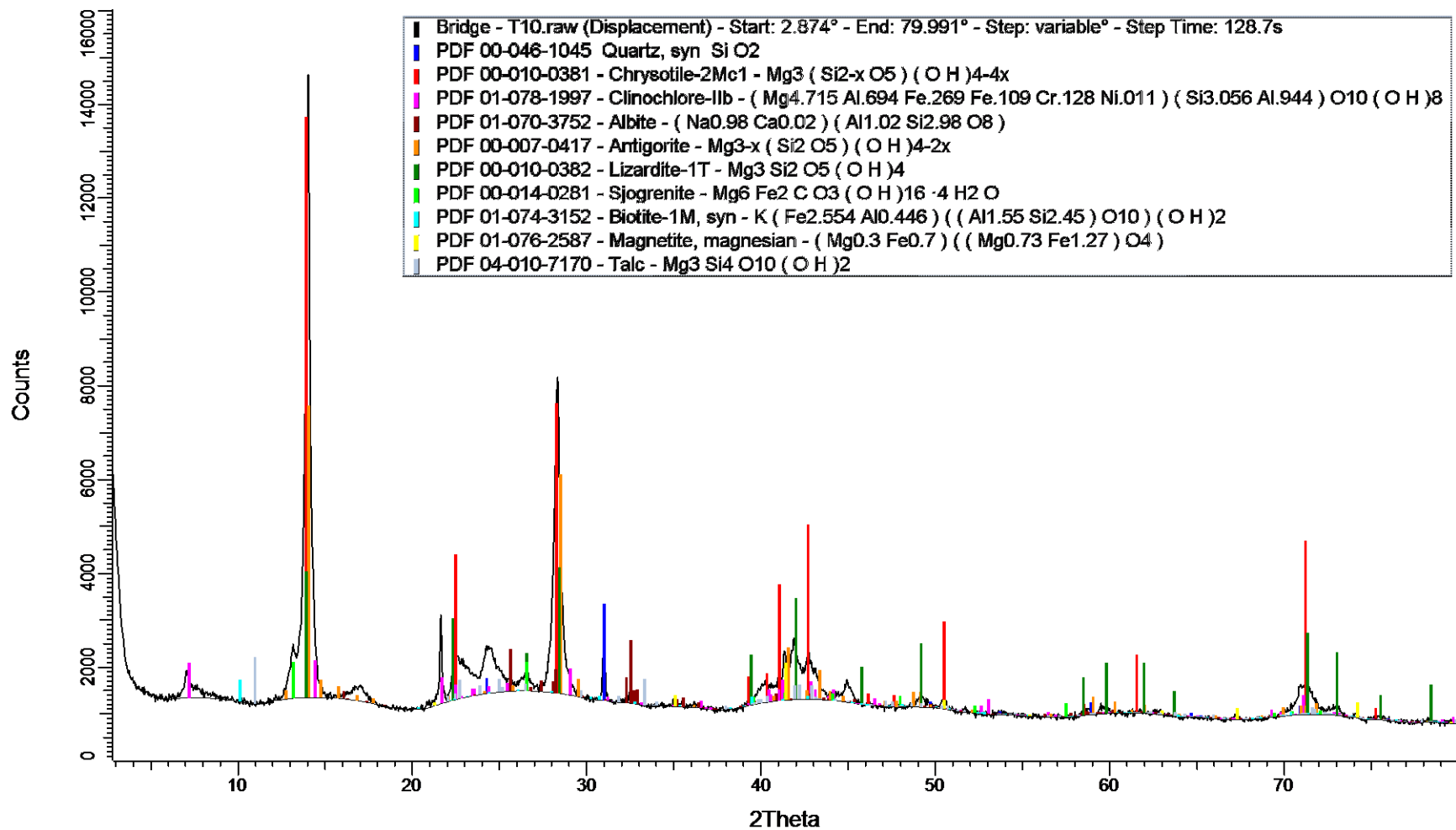


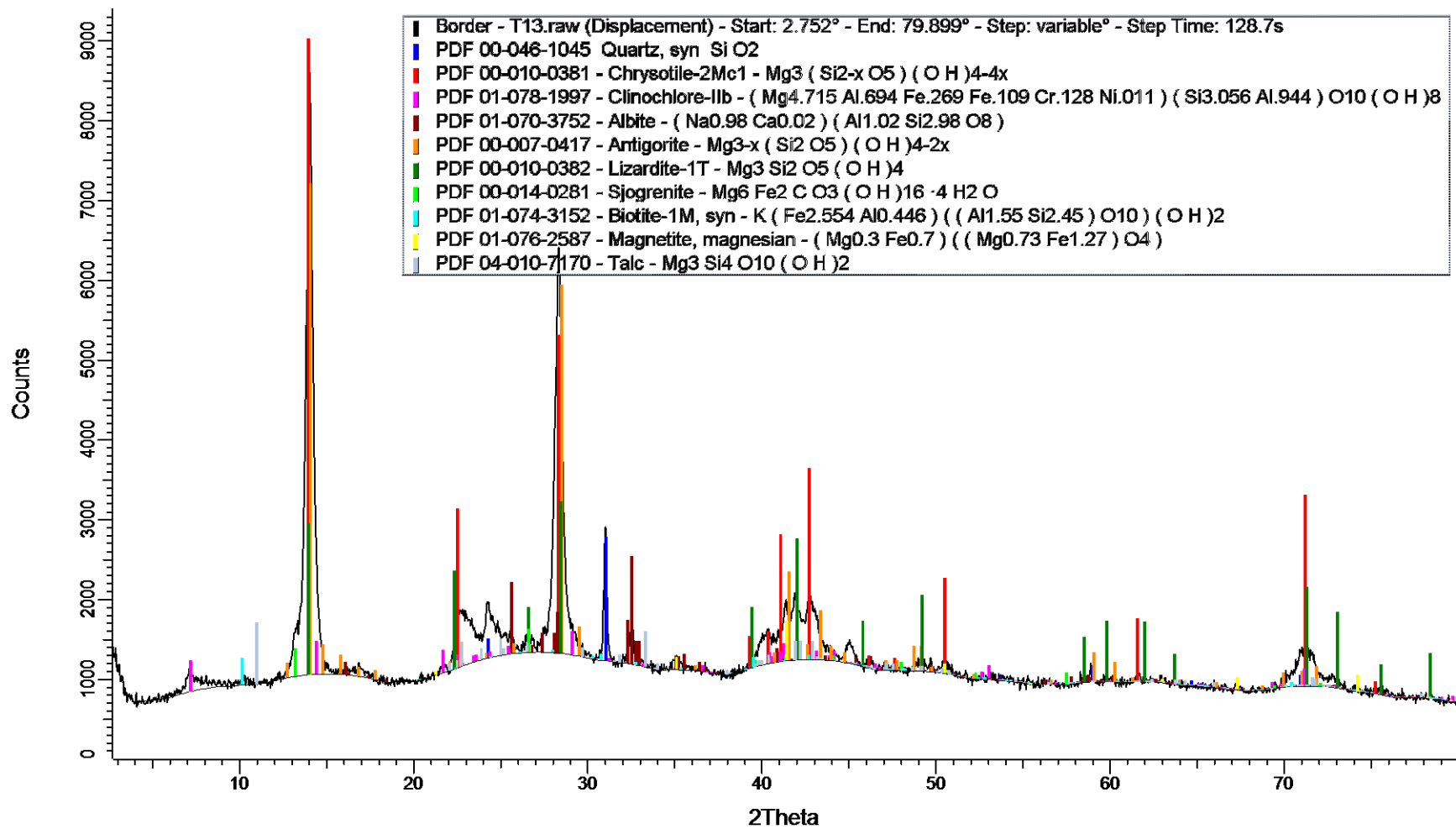






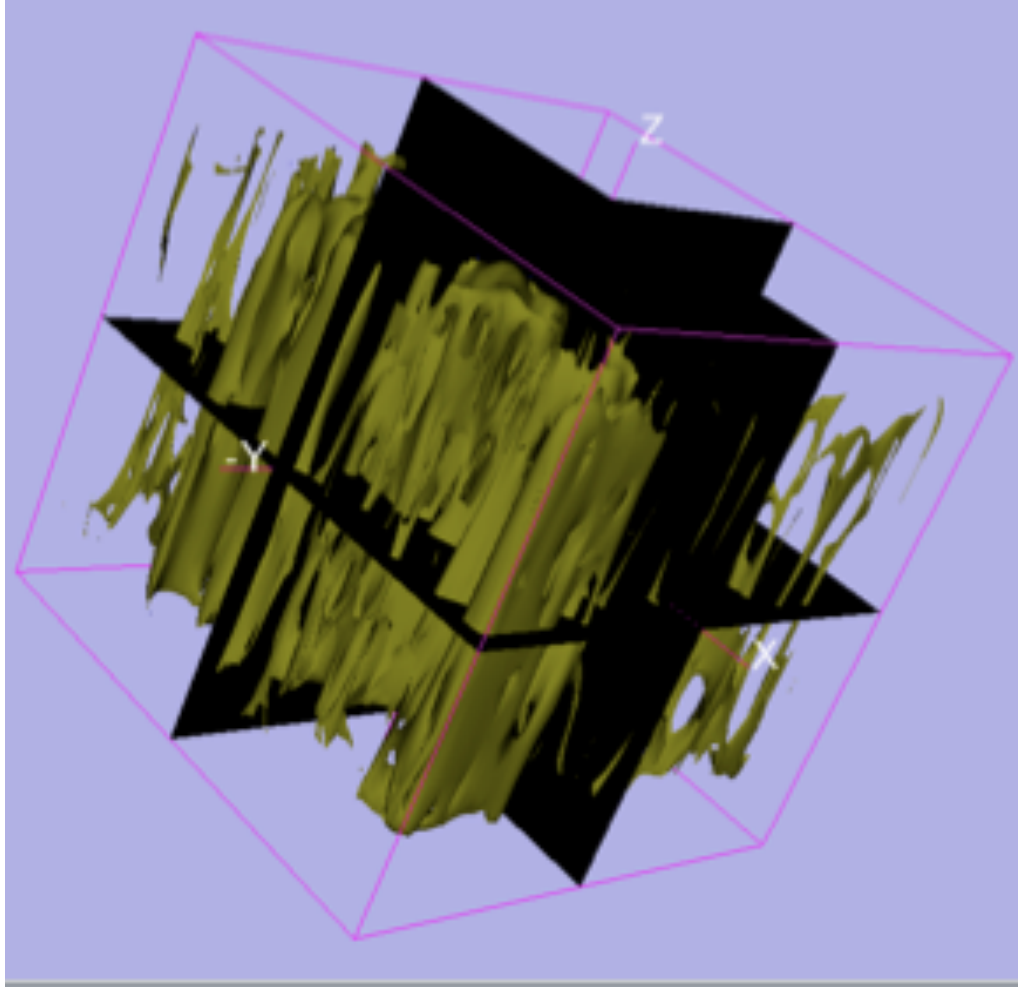




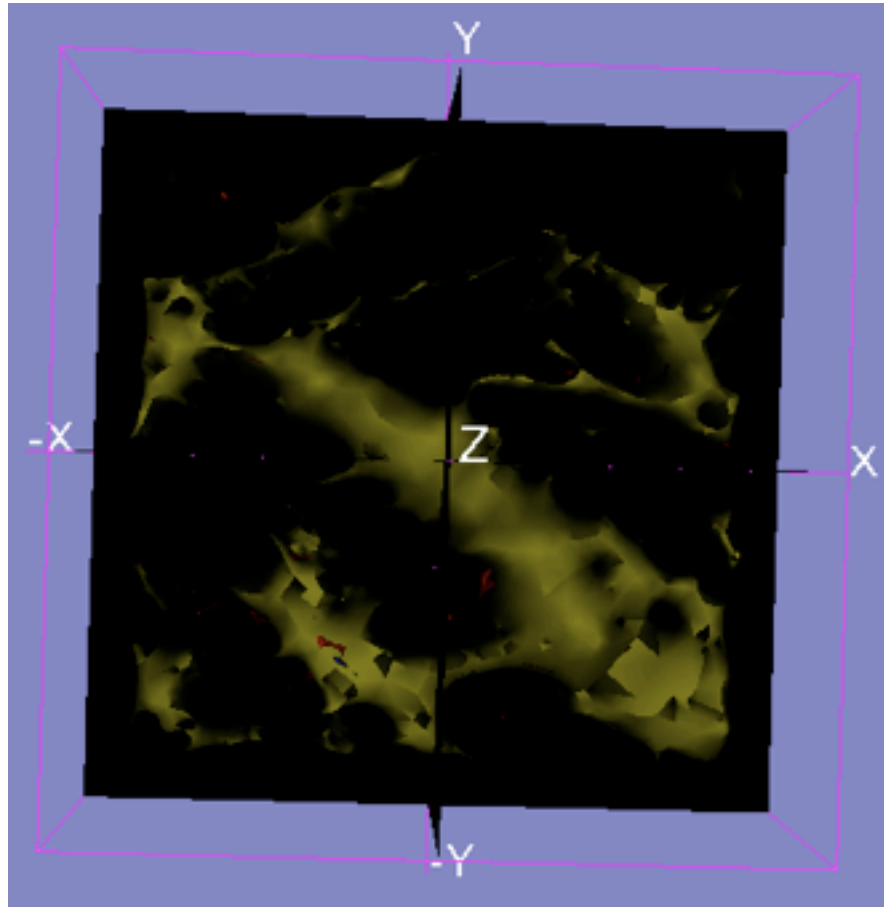


Appendix B

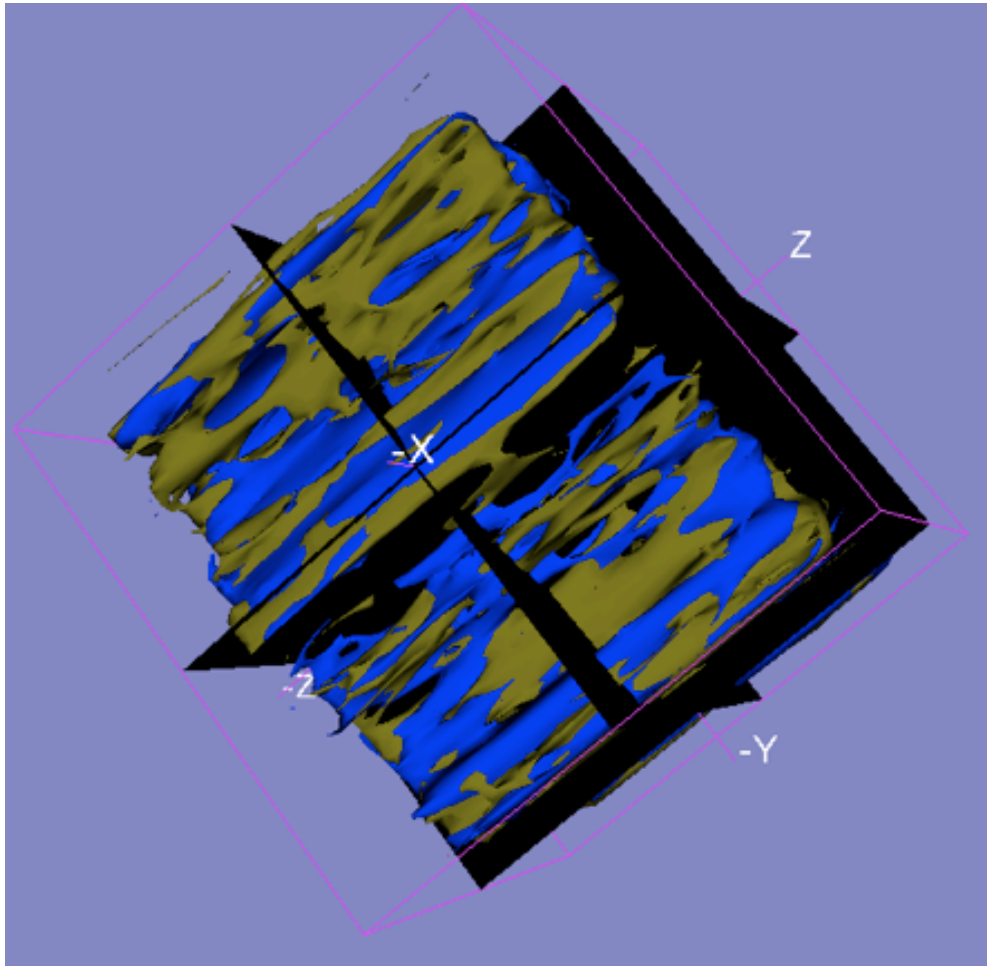
Tof-SIMS image of the depth view of an untreated chrysotile fiber. Surface area = $1600\mu\text{m}^2$ ($X=400\mu\text{m}$, $Y=400\mu\text{m}$) and depth of analysis, Z , is 2nm. The Z axis is blown up $\sim 10,000X$ to make features visible. Green = Mg, Blue = Si, and Red = Al.



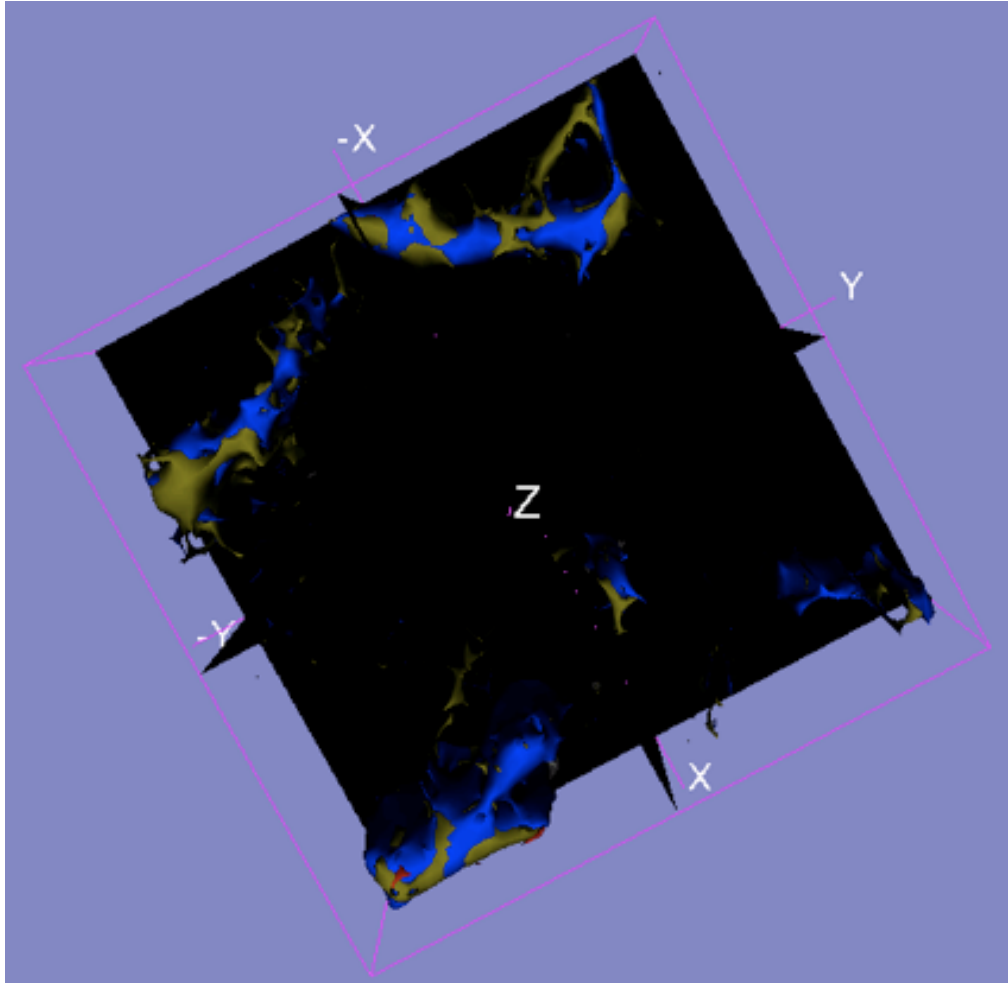
ToF-SIMS image of the surface area ($1600\mu\text{m}^2$; $X=400\mu\text{m}$, $Y=400\mu\text{m}$) of an untreated fiber. Green = Mg, Blue = Si, and Red = Al.



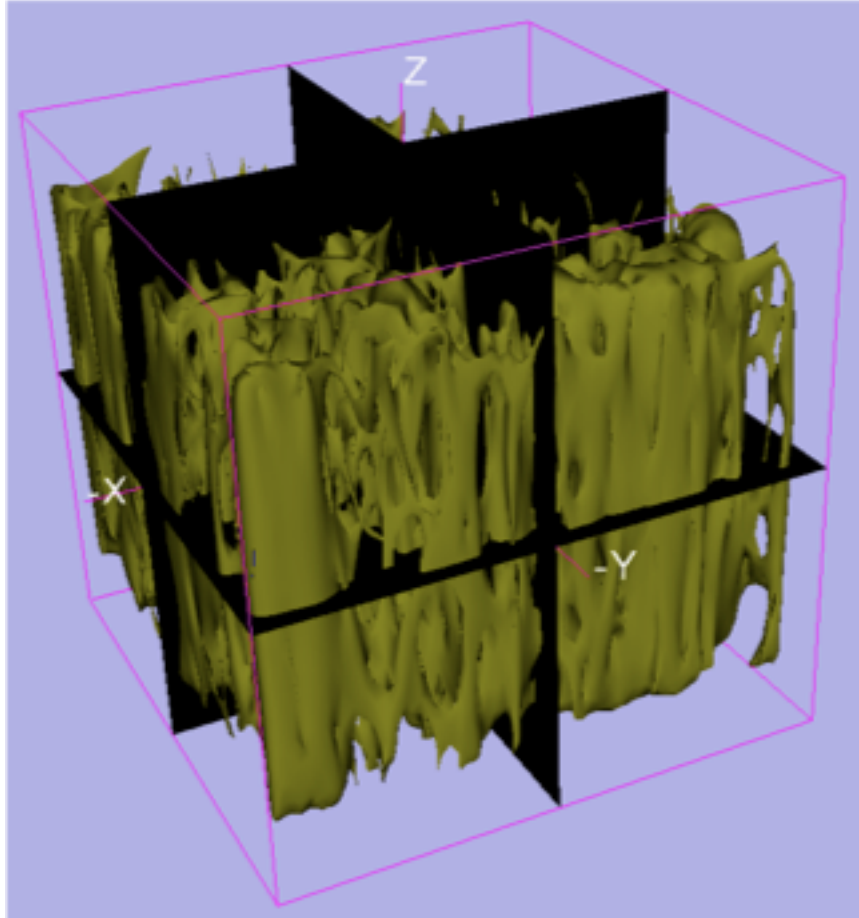
Tof-SIMS image of the depth view of an oxalic acid treated chrysotile fiber. Surface area = $1600\mu\text{m}^2$ ($X=400\mu\text{m}$, $Y=400\mu\text{m}$) and depth of analysis, Z , is 2nm. The Z axis is blown up $\sim 10,000X$ to make features visible. Green = Mg, Blue = Si, and Red = Al.



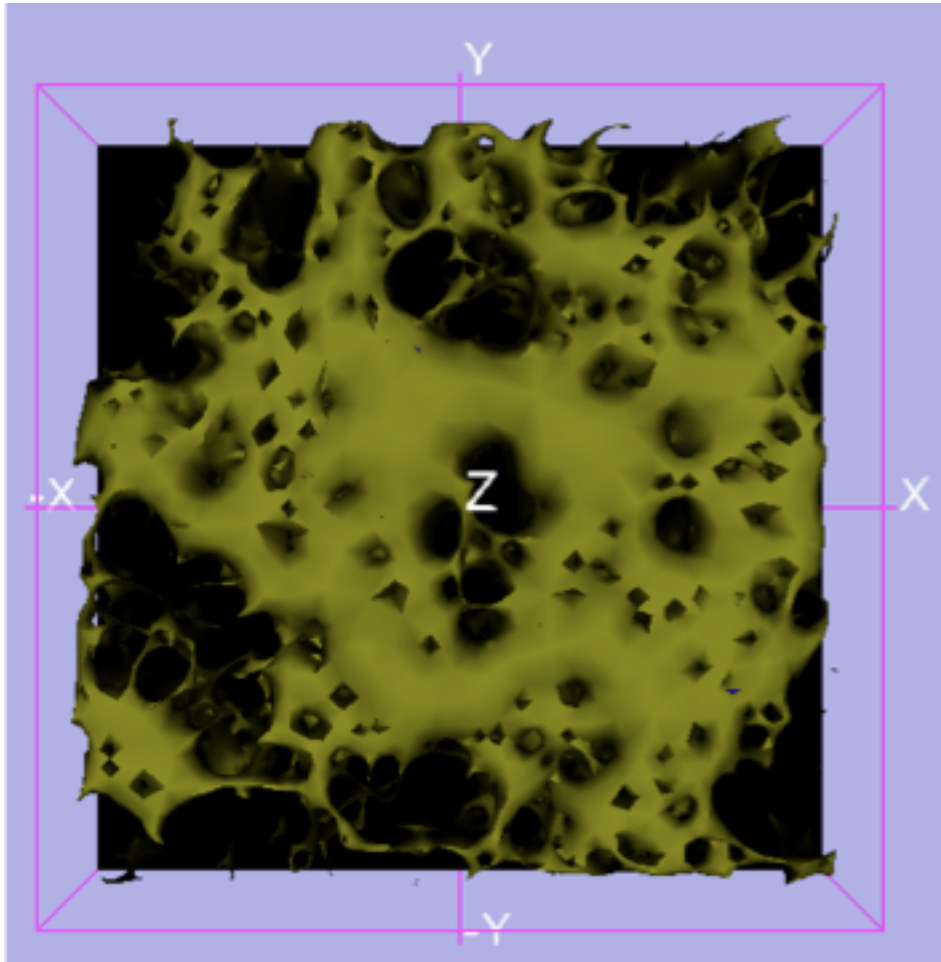
ToF-SIMS image of the surface area ($1600\mu\text{m}^2$; $X=400\mu\text{m}$, $Y=400\mu\text{m}$) of an oxalic acid treated fiber. Green = Mg, Blue = Si, and Red = Al.



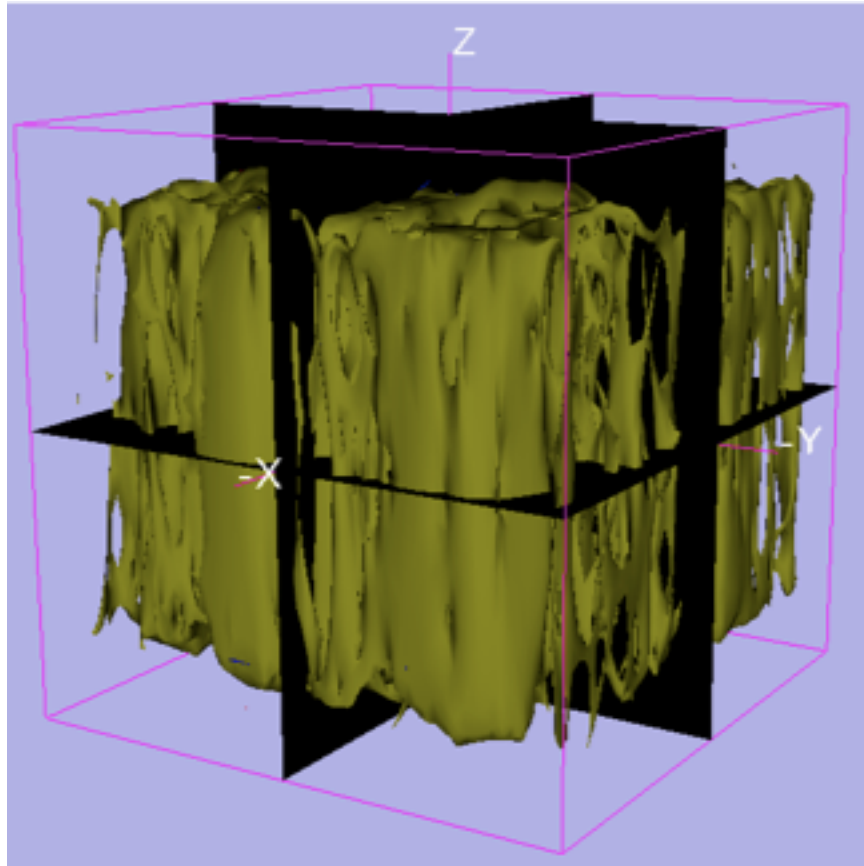
Tof-SIMS image of the depth view of a hydrochloric acid treated chrysotile fiber.
Surface area = $1600\mu\text{m}^2$ ($X=400\mu\text{m}$, $Y=400\mu\text{m}$) and depth of analysis, Z , is 2nm . The Z axis is blown up $\sim 10,000X$ to make features visible. Green = Mg, Blue = Si, and Red = Al.



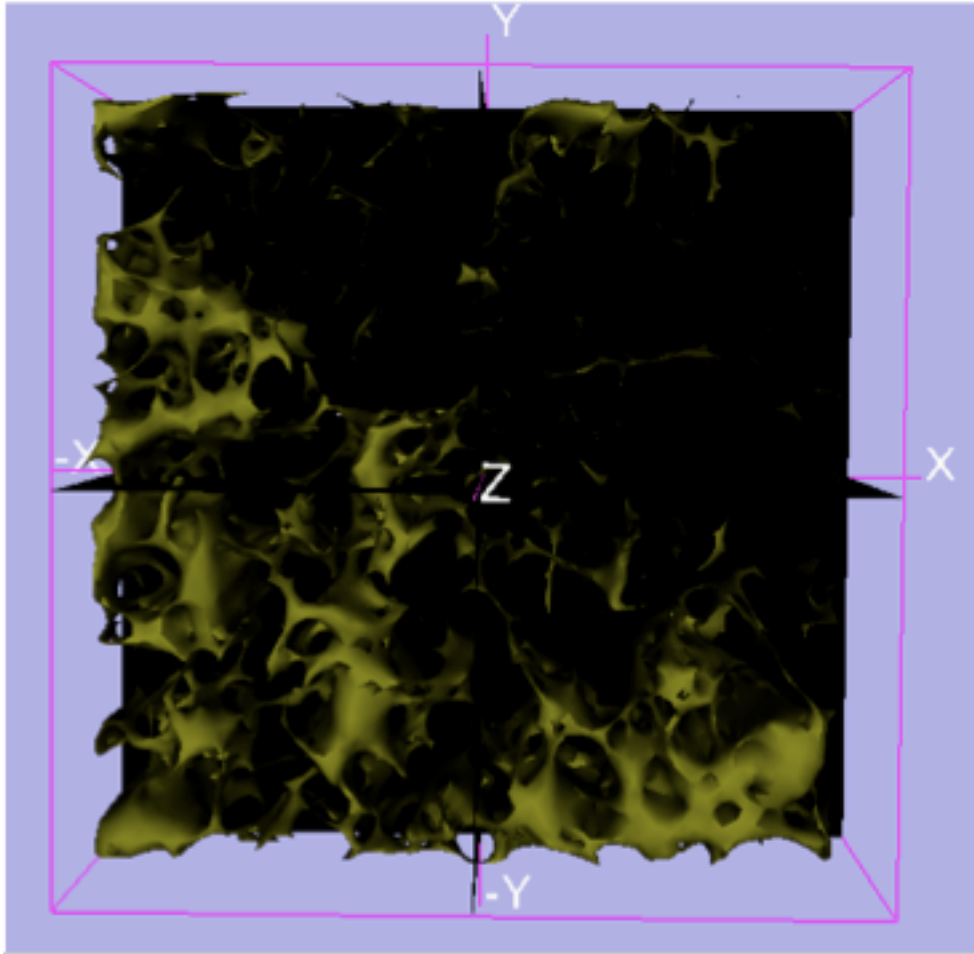
ToF-SIMS image of the surface area ($1600\mu\text{m}^2$; $X=400\mu\text{m}$, $Y=400\mu\text{m}$) of an hydrochloric acid treated fiber. Green = Mg, Blue =Si, and Red = Al.



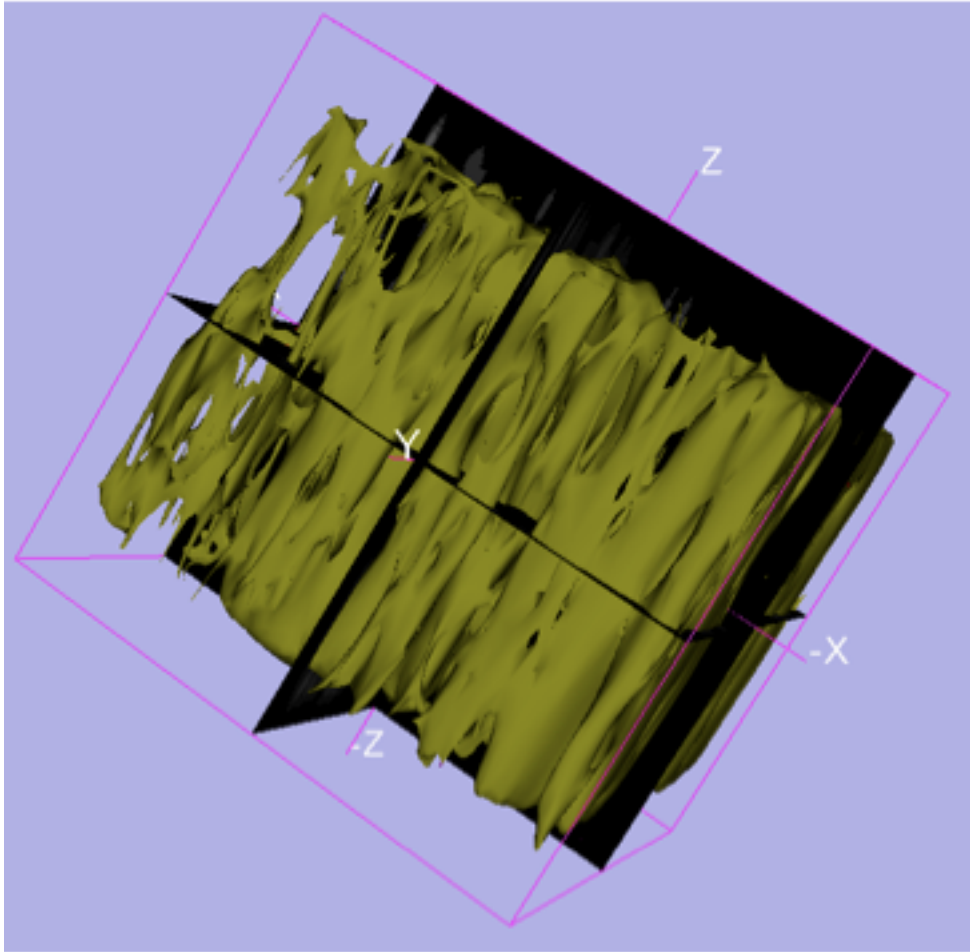
Tof-SIMS image of the depth view of a carbonic acid treated chrysotile fiber. Surface area = $1600\mu\text{m}^2$ ($X=400\mu\text{m}$, $Y=400\mu\text{m}$) and depth of analysis, Z , is 2nm. The Z axis is blown up $\sim 10,000X$ to make features visible. Green = Mg, Blue = Si, and Red = Al.



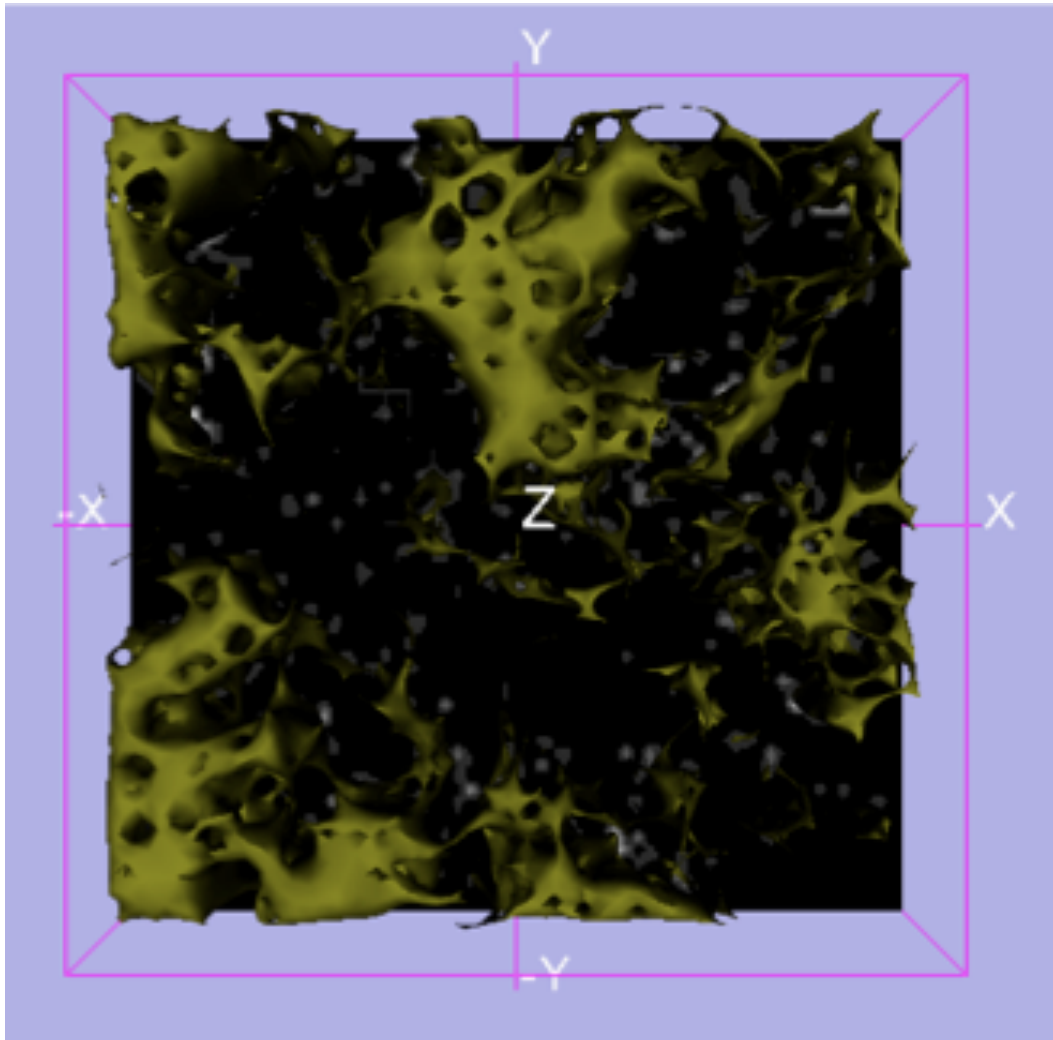
ToF-SIMS image of the surface area ($1600\mu\text{m}^2$; $X=400\mu\text{m}$, $Y=400\mu\text{m}$) of a carbonic acid treated fiber. Green = Mg, Blue = Si, and Red = Al.



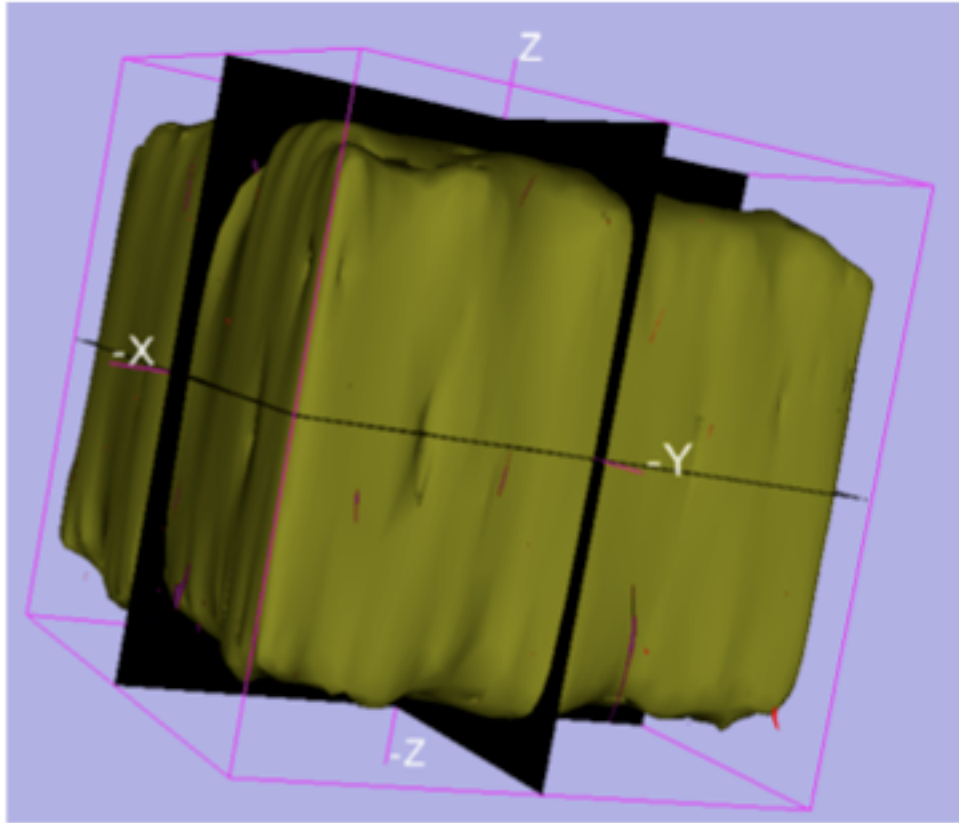
ToF-SIMS image of the depth view of a chrysotile fiber found in a suspended sediment sample taken from the Swift Creek sampling location in the Sumas River watershed. Surface area = $1600\mu\text{m}^2$ ($X=400\mu\text{m}$, $Y=400\mu\text{m}$) and depth of analysis, Z , is 2nm. Green = Mg, Blue = Si, Red = Al.



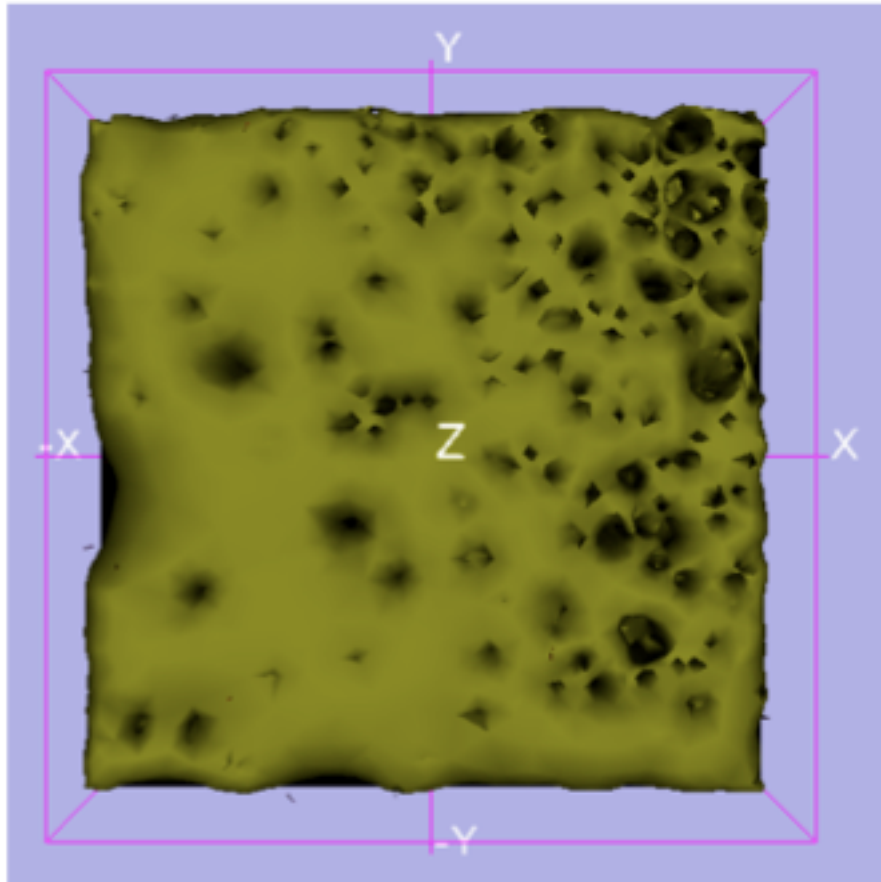
ToF-SIMS image of the surface area ($1600\mu\text{m}^2$; $X=400\mu\text{m}$, $Y=400\mu\text{m}$) of a chrysotile fiber found in a suspended sediment sample taken from the Swift Creek sampling location in the Sumas River watershed. Green = Mg, Blue = Si, and Red = Al.



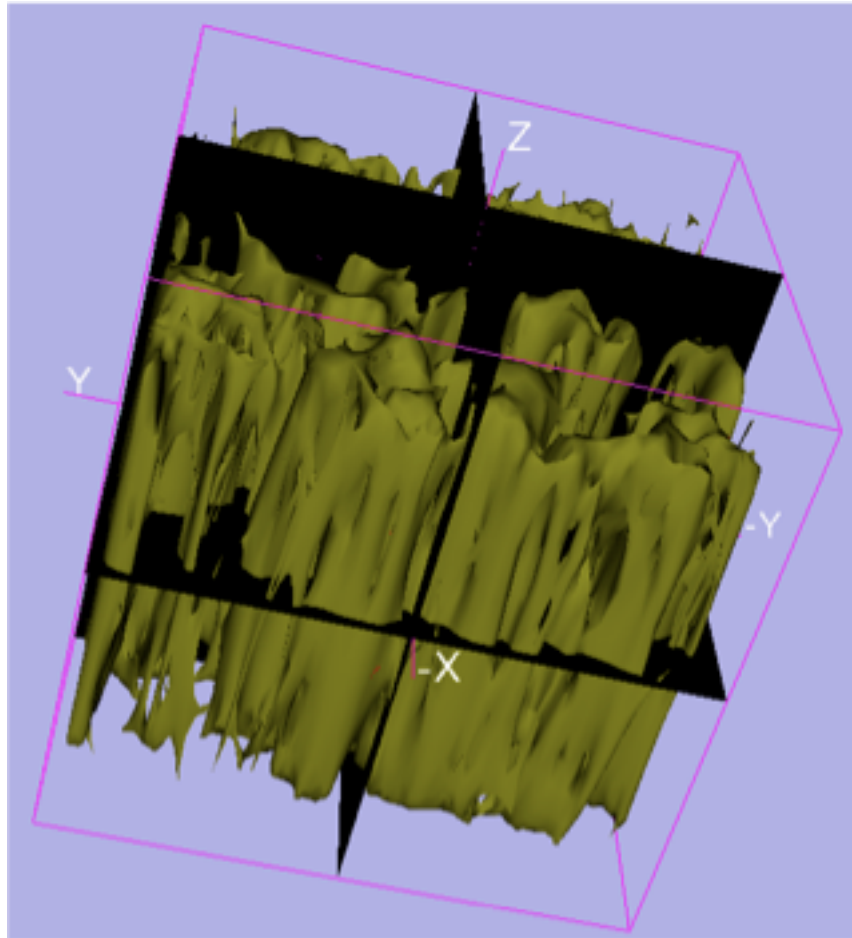
ToF-SIMS image of the depth view of a chrysotile fiber found in a suspended sediment sample collected at the Church sampling location in the Sumas River watershed. Surface area = $1600\mu\text{m}^2$ ($X=400\mu\text{m}$, $Y=400\mu\text{m}$) and depth of analysis, Z , is 2nm. Green = Mg, Blue = Si, Red = Al.



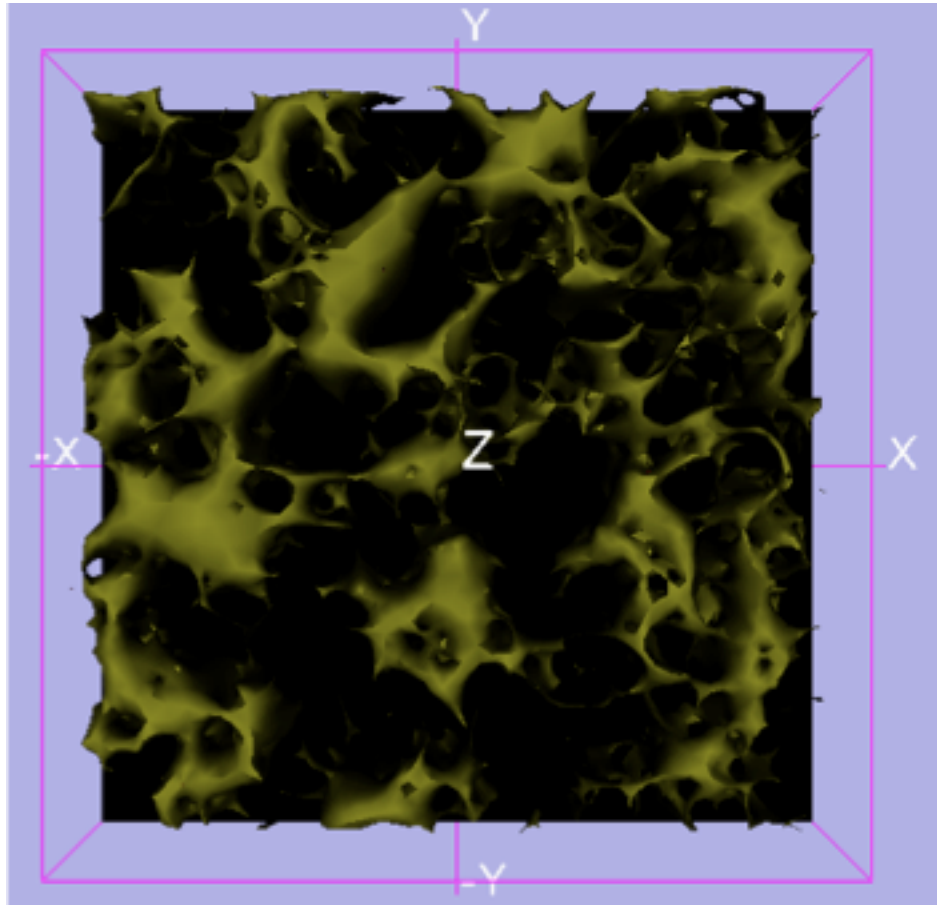
ToF-SIMS image of the surface area ($1600\mu\text{m}^2$; $X=400\mu\text{m}$, $Y=400\mu\text{m}$) of a chrysotile fiber found in a suspended sediment sample taken from the Church sampling location in the Sumas River watershed. Green = Mg, Blue = Si, and Red = Al.



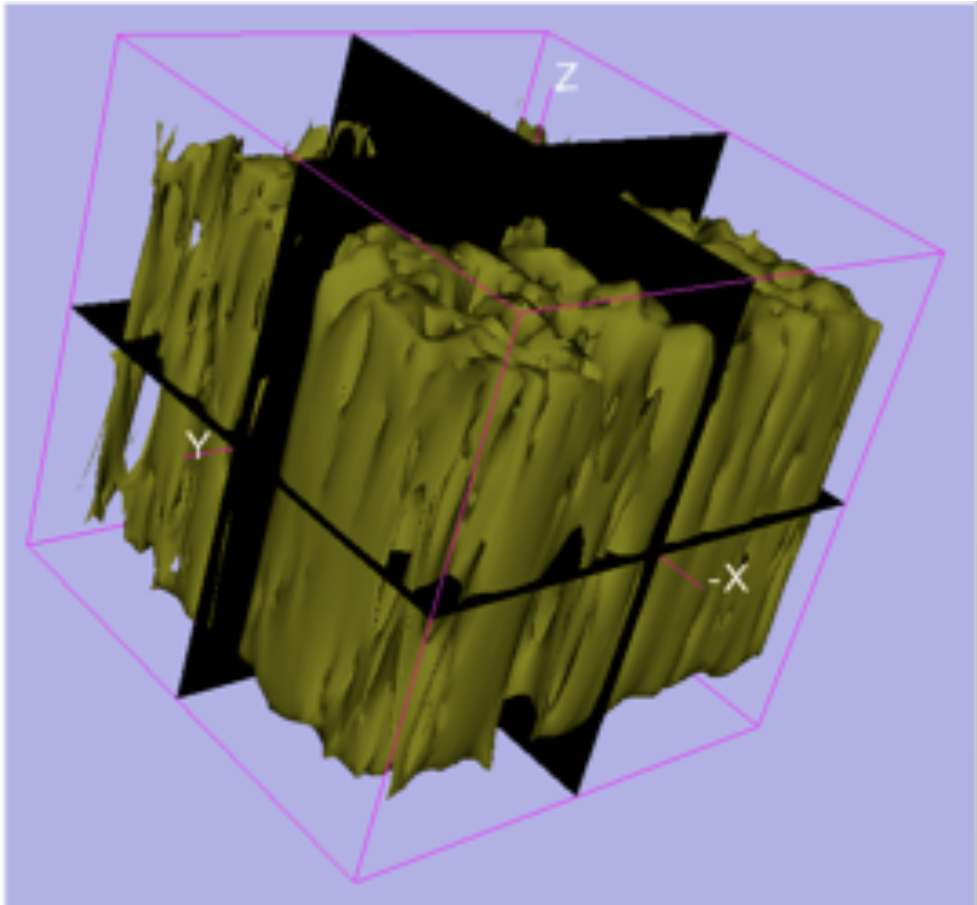
ToF-SIMS image of the depth view a chrysotile fiber found in a suspended sediment sample collected at the Bridge sampling location in the Sumas River watershed. Surface area = $1600\mu\text{m}^2$ ($X=400\mu\text{m}$, $Y=400\mu\text{m}$) and depth of analysis, Z , is 2nm . Green = Mg, Blue = Si, Red = Al.



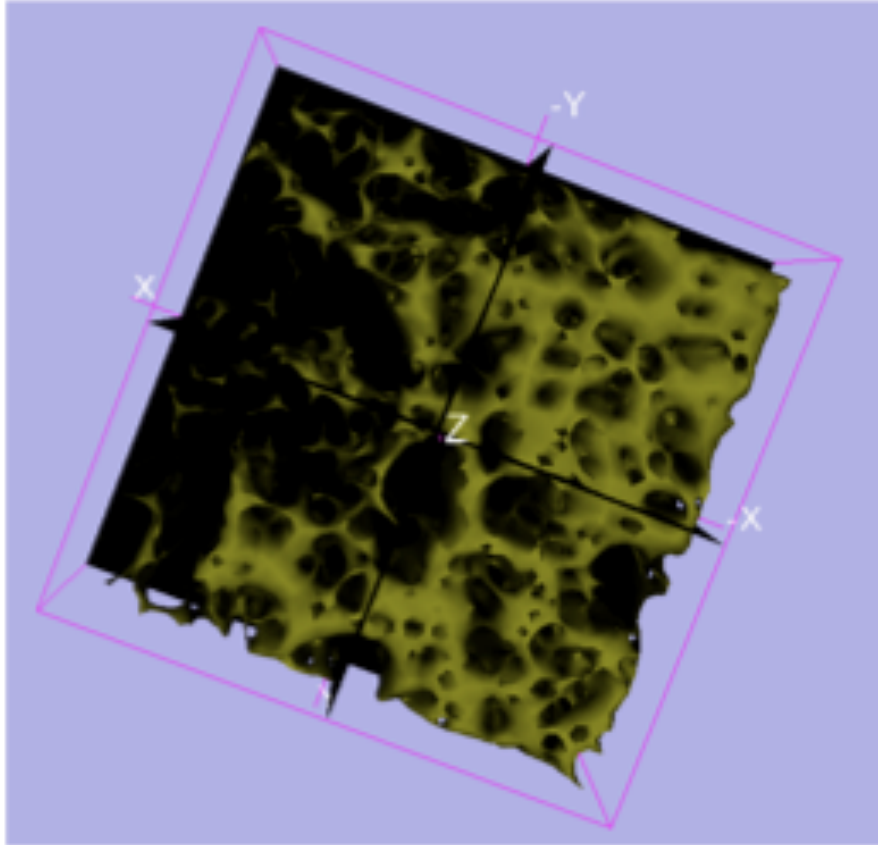
ToF-SIMS image of the surface area ($1600\mu\text{m}^2$; $X=400\mu\text{m}$, $Y=400\mu\text{m}$) of a chrysotile fiber found in a suspended sediment sample taken from the Bridge sampling location in the Sumas River watershed. Green = Mg, Blue = Si, and Red = Al.



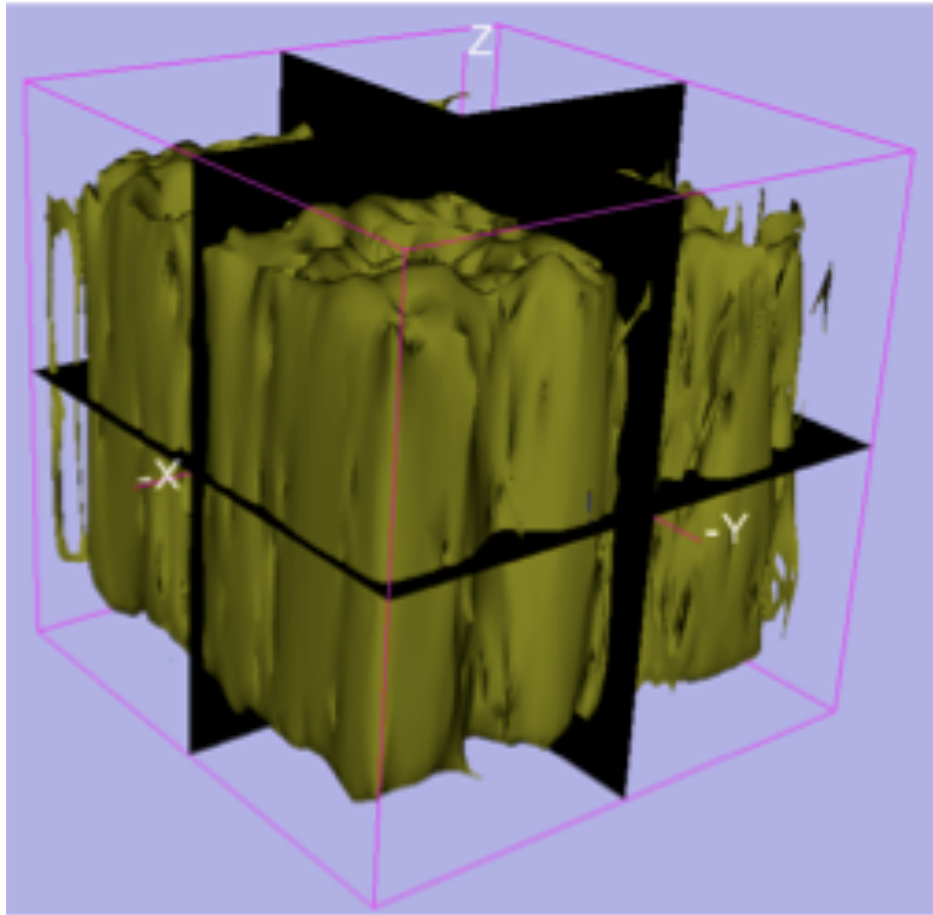
ToF SIMS image of the depth view of a chrysotile fiber found in the 14-1 mine tailing sample taken from Cassiar mine, BC. Surface area = $1600\mu\text{m}^2$ (X=400 μm , Y=400 μm) and depth of analysis, Z, is 2nm. Green = Mg, Blue = Si, Red = Al.



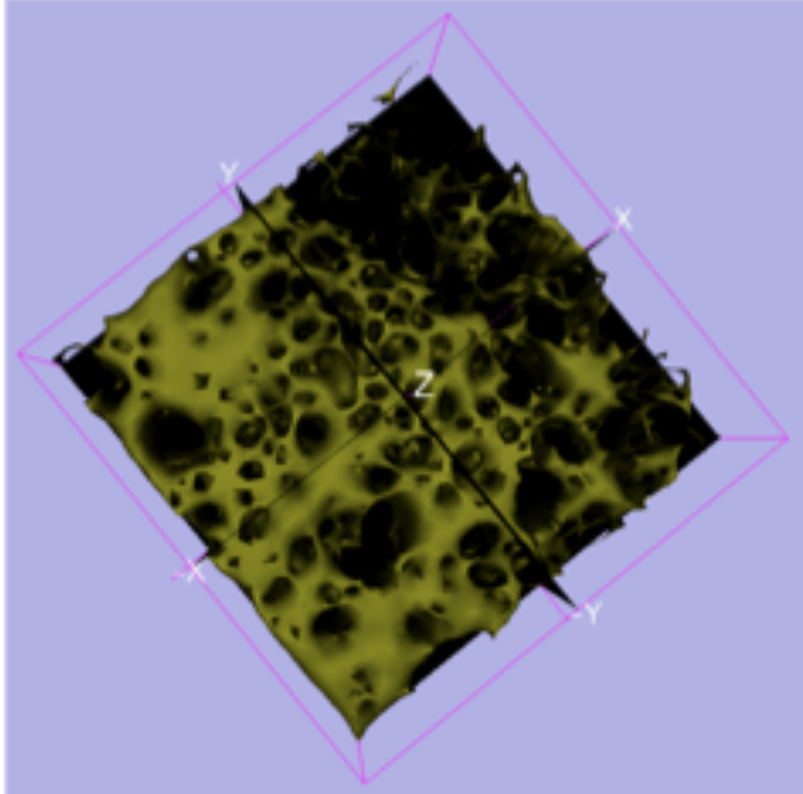
ToF-SIMS image of the surface area ($1600\mu\text{m}^2$; $X=400\mu\text{m}$, $Y=400\mu\text{m}$) of a chrysotile fiber found in the 14-1 mine tailing sample taken from Cassiar mine, BC. Green = Mg, Blue = Si, and Red = Al.



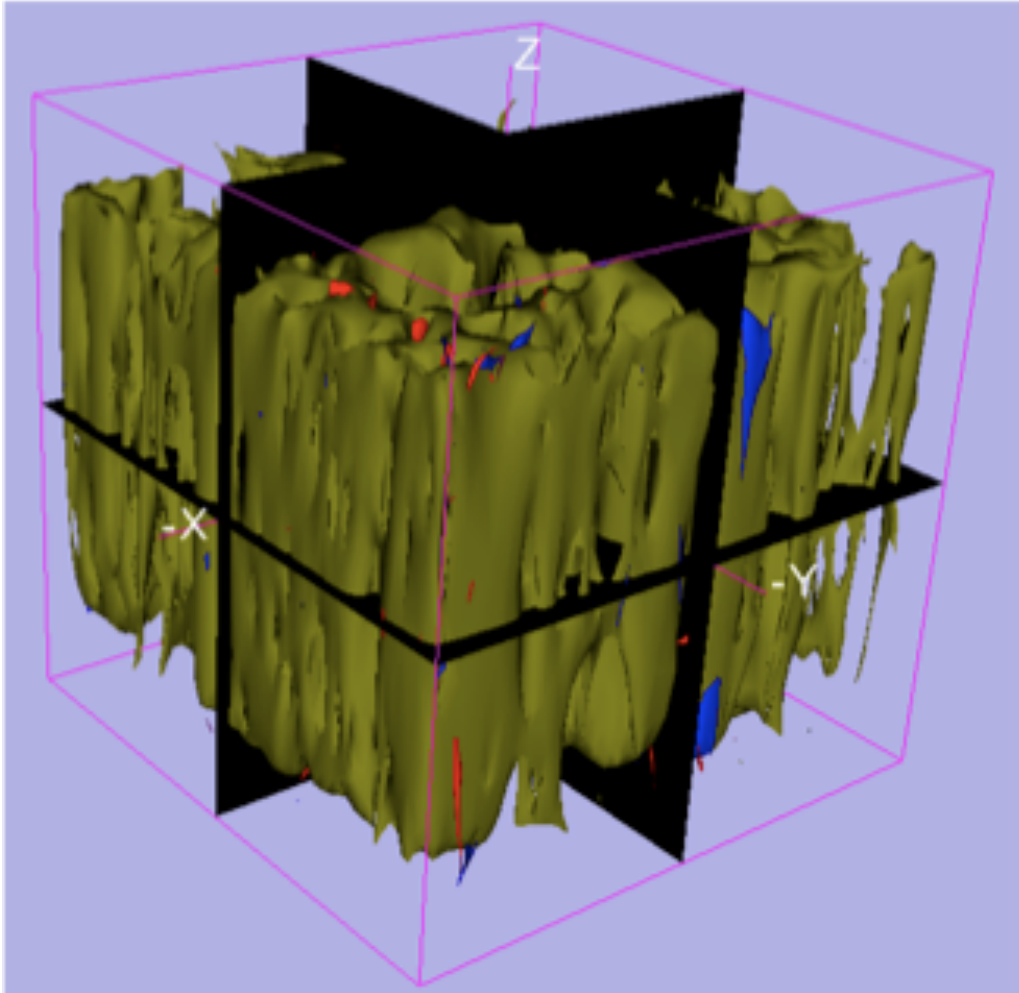
ToF SIMS image of the depth view of a chrysotile fiber found in the 16-1 mine tailing sample taken from Cassiar mine, BC. Surface area = $1600\mu\text{m}^2$ (X=400 μm , Y=400 μm) and depth of analysis, Z, is 2nm. Green = Mg, Blue = Si, Red = Al.



ToF-SIMS image of the surface area ($1600\mu\text{m}^2$; $X=400\mu\text{m}$, $Y=400\mu\text{m}$) of a chrysotile fiber found in the 16-1 mine tailing sample taken from Cassiar mine, BC. Green = Mg, Blue =Si, and Red = Al.



ToF SIMS image of the depth view of a chrysotile fiber found in the 17-1 mine tailing sample taken from Cassiar mine, BC. Surface area = $1600\mu\text{m}^2$ ($X=400\mu\text{m}$, $Y=400\mu\text{m}$) and depth of analysis, Z , is 2nm. Green = Mg, Blue = Si, Red = Al.



ToF-SIMS image of the surface area ($1600\mu\text{m}^2$; $X=400\mu\text{m}$, $Y=400\mu\text{m}$) of a chrysotile fiber found in the 17-1 mine tailing sample taken from Cassiar mine, BC. Green = Mg, Blue = Si, and Red = Al.

